# SUPPORTED POLY(ETHYLENEIMINE) ADSORBENTS FOR CO$_2$ REMOVAL FROM AIR

A Dissertation
Presented to
The Academic Faculty

by

Miles Sakwa-Novak

In Partial Fulfillment
of the Requirements for the Degree
Doctor of Philosophy in the
School of Chemical & Biomolecular Engineering

Georgia Institute of Technology
December 2015

# SUPPORTED POLY(ETHYLENEIMINE) ADSORBENTS FOR CO$_2$ REMOVAL FROM AIR

Approved by:

Dr. Christopher W.Jones, Advisor
School of Chemical & Biomolecular
Engineering
*Georgia Institute of Technology*

Dr. David S. Sholl
School of Chemical & Biomolecular
Engineering
*Georgia Institute of Technology*

Dr. Krista S. Walton
School of Chemical & Biomolecular
Engineering
*Georgia Institute of Technology*

Dr. Michael A. Filler
School of Chemical & Biomolecular
Engineering
*Georgia Institute of Technology*

Dr. Andrei G. Fedorov
The George W. Woodruff School of
Mechanical Engineering
*Georgia Institute of Technology*

Date Approved:  Sept.17 2015

"The majority of men are not intellectual initiators or originators… It is not that they don't think; it is that they don't sustain their thinking consistently, as a way of life…"

-Ayn Rand

# ACKNOWLEDGEMENTS

# TABLE OF CONTENTS

Page

# LIST OF TABLES

# LIST OF FIGURES

# SUMMARY

The simultaneous desire for global economic growth and the threat of climate change poses a unique challenge to mankind. Despite warnings from the scientific community, the decarbonization of the energy and transportation sectors continues to progress at too slow a pace for complete mitigation of the risk of climate change. As such, strategies to geoengineer the climate to mitigate such risks have been proposed. One of these is direct $CO_2$ capture from air using engineering chemicals, or 'air capture'. Air capture is a particularly challenging technical problem due to the ultra-dilute nature of $CO_2$ in air, currently at a concentration of ~400 parts per million (ppm). Any technology intended to separate $CO_2$ from air at a scale relevant to global climate change must perform the separation with with near infinite selectivity for $CO_2$, and have the capacity to process enormous volumes of air rapidly and at low cost.

Amine based solid adsorbents are excellent potential candidates for this application, most notably due to their advantageous interaction thermodynamics with $CO_2$. These 'supported amines adsorbents' are able to selectively concentrate $CO_2$ from air, and rapidly liberate it upon a temperature increase to ~100 $^{o}$C. Our research group has worked in the development of these materials for air capture and other applications, partnering with Global Thermostat, LLC and Corning, Inc to that end. Global Thermostat has proposed a temperature swing adsorption process for $CO_2$ extraction from air that utilizes supported amine adsorbents dispersed in a honeycomb monolith structure, and steam to drive desorption. This particular technology is the subject of this dissertation,

where the goal was to progress the materials development. The specific areas addressed were i) sorbent stability, ii) tuning of oxide properties, iii) tuning of organic properties, and iii) amine incorporation into honeycomb monoliths.

The operating lifetime of any technology is essential to its economic viability, meaning that the performance of adsorbents should last for many thousands of cycles. An understanding of the mechanisms of degradation of target adsorbents under relevant operating conditions is thus very important. In chapter 2, the hydrothermal stability of alumina/poly(ethyleneimine) (PEI) adsorbents are studied in detail. It is shown that under relevant timescales of steam exposure, the adsorbents partially hydrate from $\gamma$-alumina to boehmite. It is further shown that his hydration does not affect the porosity or efficiency of impregnated PEI to adsorb $CO_2$, the most important properties of the adsorbent. This firm understanding of degradation and its relation to performance provides confidence in the alumina/PEI composition as a practical choice for commercial deployment.

Supported amines have a high degree of tunability in their materials design. These include the properties of the host oxide, as well as those of the active organic amine. In chapter 3, the relative importance of oxide surface properties in improving the amine efficiency of PEI are studied in relation to altered textural properties. It is shown that changes to the pore size, particle size and pore surface texture have a more substantial effect on the amine efficiency of PEI than the acid/base properties of the surface. In chapter 4, the effect of various additive/PEI mixtures are assessed in the context of their improvement in the amine efficiency of air capture sorbents. Low molecular weight poly(ethyleneglycol) (PEG) is shown to be particularly effective, and target PEG/PEI

contents that have improved kinetic and thermodynamic performance are identified. These studies both provide insight into the efficacy of particular material design levers in improving adsorption performance.

Finally, in order to utilize performance levers such as those studied in chapters 3 and 4 in honeycomb monoliths, a firm understanding of how to prepare such monoliths and how their performance compares with analogous powders is necessary. In chapter 5, PEI functionalized alumina powders, small monolith pieces, and a large monolith are prepared, characterized and assessed relative to one another in $CO_2$ adsorption experiments. Despite differences in the deposition of PEI in particular pore size regimes observed in monoliths compared to powders, their adsorption performance at each scale was similar. A lone exception was the equilibration rate of the large monolith sample, suggesting that a study of transport phenomena in such a structure will be an important research topic in the near future.

# CHAPTER 1

# INTRODUCTION TO $CO_2$ CAPTURE AND SUPPORTED AMINES

Parts of this chapter are adapted from 'Sakwa-Novak, Miles A. and Jones, Christopher W. (2014). Supported amine materials for CO2 capture. In *AccessScience*. McGraw-Hill Education. http://dx.doi.org/10.1036/1097-8542.YB150578' with permission of McGraw-Hill.

## 1.1 Introduction & Motivation

The development of clean technologies to produce energy while reducing global $CO_2$ emissions has emerged as a generational challenge.[1–3] The removal of $CO_2$ from the emissions mixture of power plants is necessary, as cheap and abundant fossil fuels will likely continue to be used to produce electricity on a global scale.[4–6] One practical approach to this is retrofitting current power plants with separation units to remove the $CO_2$ from the plant's exhaust flue gas, and subsequently sequestering the $CO_2$ in underground reservoirs. This process is referred to as post combustion $CO_2$ capture and sequestration (PC-CCS). A schematic of this process is depicted in figure 1.1. Currently this is practiced in a limited capacity using aqueous amine gas scrubbers at the demonstration, or in some cases commercial, scale at several facilities.[7–10] Here, flue gas leaving the plant, containing ~10-15% $CO_2$ by volume, is contacted with the amine solution, where the mildly acidic $CO_2$ molecules interact with the basic amines. When the solution saturates with $CO_2$, it is heated to regenerate the sorbent and concentrate the $CO_2$

for downstream sequestration or use. While these amine solutions effectively remove $CO_2$ from the flue gas, the process requires high energy input due to the large thermal mass of aqueous solution that must be heated during regeneration. This ultimately results in a parasitic loss of ~20-30% of the power generation of the facility, a loss that would be reflected in a higher price of electricity if widely implemented.[11,12]
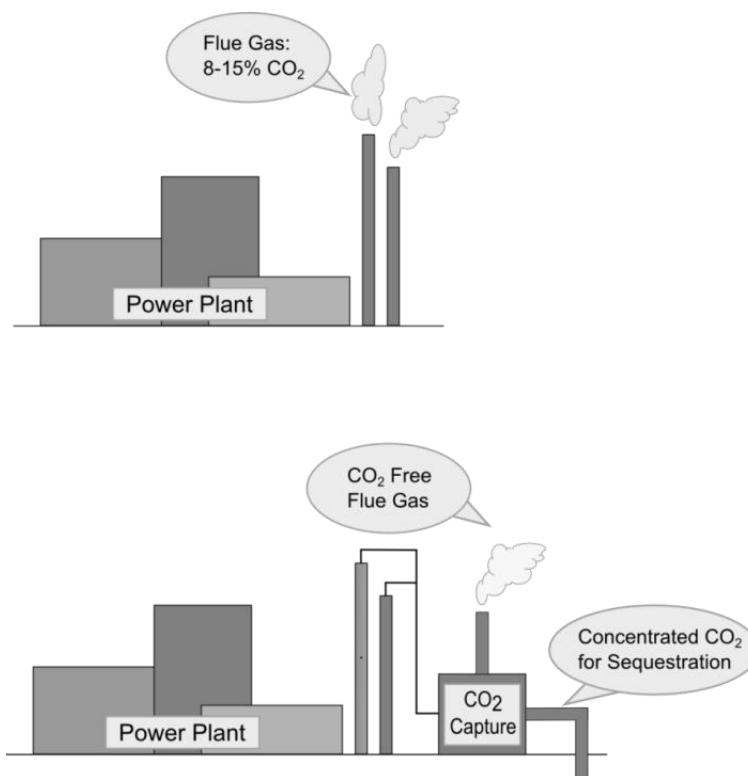


Figure 1.1 Schematic of Post Combustion $CO_2$ Capture

Due in part to these limitations, the scale up and deployment of like technologies for CCS has progressed slowly.[4,13] Thus, it has been suggested by some that CCS may not be deployed widely enough and soon enough to stabilize the concentration of $CO_2$ in the atmosphere at acceptable levels.[14,15] Additionally, one-third to one-half of global $CO_2$ emissions do not originate from electricity generating power plants that would be

retrofitted for PC-CCS.[16] The remainder of emissions, those from highly dispersed sources such as automobiles, airplanes, and residential fuel combustion, remain unaccounted for in scenarios where $CO_2$ is only removed from power plant flue gas. Given these considerations, processes that result in a net reduction of $CO_2$ in the ambient environment, sometimes referred to as carbon dioxide removal or negative emissions technologies, have been increasingly regarded as having a role to play in future emissions control strategies.[3,14,15,17] Such processes include increased land afforestation, ocean fertilization, bioenergy with carbon capture and sequestration (BECCS), and direct removal of $CO_2$ from air with chemicals (DAC).[17–19]

## 1.2    Direct Air Capture

Along with land afforestation and BECCS, DAC does not involve the potentially irreversible modification of the atmosphere or ocean, but rather aims to reduce pollution emitted at an earlier time. While the environmental benefits of such a process are self-evident, suitable technologies to provide such a service do not exist commercially at a scale relevant to global climate alteration. Several processes have been proposed, and cost estimates have ranged from 20-1000 $/ton of $CO_2$ captured, depending on the technology type and estimation methodology employed.[14,18,20–24] While it is anticipated that the cost to remove $CO_2$ from air will be more expensive than the cost to remove it from flue gas, the magnitude of this difference remains to be conclusively demonstrated. Lackner has suggested 50 $/ton $CO_2$ as a reasonable target price,[14] and has shown that at such a price $CO_2$ could be provided as an input to produce select fuels.[22]

Keith and Zeman have suggested use of alkaline NaOH solutions that react with $CO_2$ to form $Na_2CO_3$.[23,25] In this process, the NaOH is regenerated by caustization of the $Na_2CO_3$ with $Ca(OH)_2$ to from $CaCO_3$ and NaOH. The solid $CaCO_3$ is then separated from the liquid and decomposed at 900 $^\circ$C to form CaO and $CO_2$ where the $CO_2$ can be compressed for sequestration or use. Finally, the $Ca(OH)_2$ is regenerated by reaction of CaO with $H_2O$. This technology is being pursued commercially for air capture by Carbon Engineering LTD, which was started by Keith. The most recently published literature estimates a cost of ~300$ / ton $CO_2$ removed from air using this process, including the cost of capital.[23] The primary cost drivers reported for the process were the high cost of capital, the cost of fugitive $CO_2$ emissions (those generated in the production of electricity and heat from fossil resources to drive the process) and the cost of heating during the $CaCO_3$ regeneration step. While high compared to the expected costs of flue gas capture, these estimates are nearly half of those previously estimated for a similar process.[18,24]

Lackner proposed a different process for air capture that offers the potential for dramatically reduced heating demands.[26,27] Here, a $CO_2$ separation cycle using a hydroxide or water treated quaternary amine ion exchange resin is driven by a moisture swing. The resin cycles between bicarbonate (dry, 2 mol $CO_2$ / mol OH resin site) and carbonate (wet, 1 mol $CO_2$ / mol OH resin site) states in the presence of $CO_2$, thereby adsorbing $CO_2$ from (relatively) dry air and desorbing $CO_2$ upon the introduction of (additional) water vapor or liquid water to the resin surface. The performance of the technology is necessarily dependent on the relative humidity of the feed air containing

$CO_2$. Relative humidities below 50% (at ~20-30 $^{\circ}$C) are required for high swing capacities,[26] thus necessitating relatively dry air need be fed to the separation unit. Due to the low energy requirement for regeneration the authors have suggested costs as low as 20-30 \$/ton $CO_2$, though these were not derived from rigorous chemical engineering based methodologies.

Supported amines adsorbents, described in greater detail in the section below, are another promising technology candidate for air capture applications. These materials differ from the quaternary amines suggested by Lackner in that they are primarily composed of primary and secondary amines, and tend to form carbamates instead of carbonates upon contact with $CO_2$. Additionally, they can function efficiently at a wide range of relative humidities. Several academic groups have explored the use of supported amine materials for air capture. Steinfeld has proposed a temperature/vacuum swing adsorption process using amine functionalized nanocellulose,[28–32] and Climeworks AG, is pursuing a similar technology commercially. Drage estimated ~150 \$/ton $CO_2$ for a temperature swing adsorption processes utilizing a fluidized bed of supported amine functionalized porous silica.[33] Others have focused predominantly on improving materials design for air capture applications.[34–43] Our research group has explored the use of supported amine adsorbents for air capture in collaboration with Global Thermostat LLC and Corning Inc.[44–53] Polymeric amines, such as poly(ethyleneimine) (PEI), are proposed to be dispersed in a honeycomb monolith structure, and utilized in a cyclic adsorption process as depicted in figure 1.2. Here, $CO_2$ in air adsorbs onto the amines in the monolith and is subsequently liberated by contact with steam, which provides a swing

in temperature and pressure to drive the desorption. A process level model by Kulkarni et al found the operational cost of this process to be as low as ~100 \$/ton $CO_2$.[21] In that study, a base 50 m$^3$ adsorption unit was estimated to have throughputs of 100-600 ton $CO_2$ / year, depending on the process cycle dynamics. No capital costs or heat integration methods were included in the study, both of which are likely to significant impact process economics, though in opposite directions. The potential for concomitant increases in $CO_2$ throughput and decreases in marginal costs were clearly illustrated for adsorbents with improved thermodynamics (increased working capacity / unit volume adsorbent) and kinetics (cycles / day).
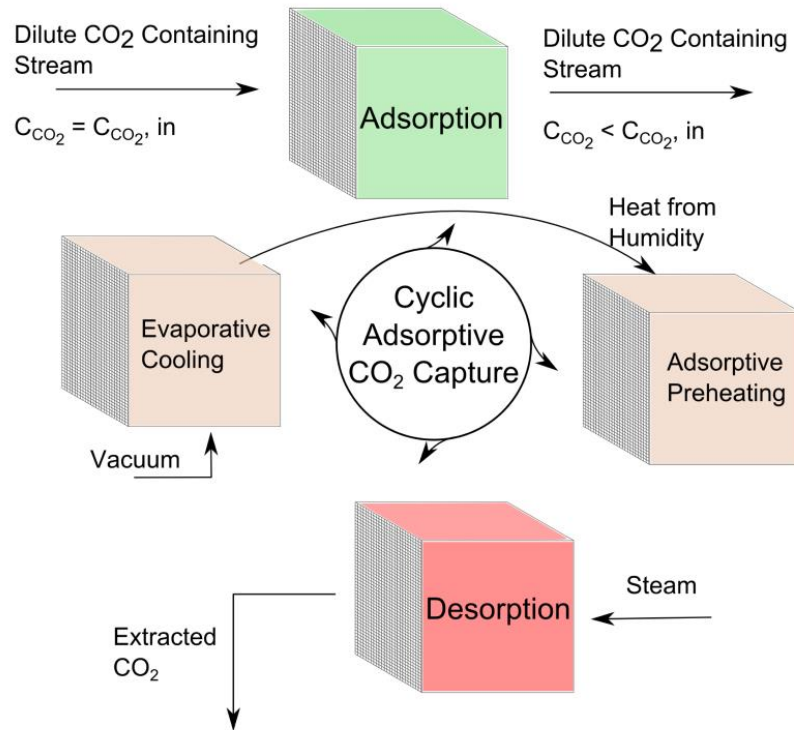


Figure 1.2 Schematic describing the process proposed to be used with amine functionalized monoliths for $CO_2$ capture from air

## 1.3    Adsorbents for $CO_2$ Capture

The supported amine adsorbents that are at the core of the technology described by Kulkarni are part of a broad array of adsorbents that have been suggested for both CCS and DAC applications. Solids are advantageous over liquid absorbents in that their heat capacities are, in general, much lower, so the thermal energy required for regeneration is potentially less. Adsorbents are typically porous materials with high specific surface areas (100- >2000 $m^2$/g) and are generally characterized by their pore size and interaction strength with the adsorbate of interest, in this case $CO_2$. Many solid adsorbents have been proposed for PC-CCS, including zeolites, carbons, aluminas, metal organic frameworks (MOFs), and supported amine materials.[54] For several of these, predominantly carbons, MOFs and supported amines, the materials can be specifically designed for efficient interaction with $CO_2$. For supported amines, the basic premise in the design of the materials is to utilize the effective acid/base chemistry of the aqueous amine system while also taking advantage of the potential of reduced thermal regeneration requirements of a solid. When properly engineered, these materials can be effective in both CCS and DAC applications.

### 1.3.1   Supported Amine Materials

Supported amines are composite materials comprised of a high surface area support and amine containing organic moieties that are distributed along its surface. The mesoporous supports are often metal oxides, most often amorphous silica, or carbons, and typically possess pores with diameters in the mesopore range of 4-40 nanometers. A

wide variety of amine moieties have been incorporated into mesoporous supports and evaluated as potential $CO_2$ capture adsorbents. In describing the materials, it is instructive to classify them based on the method used to incorporate the amine molecule into the support material, as is pictorially demonstrated in figure 1.3. Class 1 materials are prepared via the physical impregnation of amines into the pores of the support. Most commonly, amine containing oligomers and low molecular weight polymers such as PEI are incorporated into supports using this method. Class 1 adsorbents are broadly characterized as having high amine loadings, a relative ease of preparation, and weak physical interactions between amine molecules and the support surface. Class 2 materials are prepared via the covalent tethering of amines to the support surface, often via aminosilane grafting. These materials typically contain lower amine loadings than class 1 materials, but provide a strong covalent amine-support interaction. Importantly, these materials are conceptually simple, and have provided an excellent model for studying fundamental phenomena. Finally, class 3 materials are prepared via the *in-situ* polymerization of amine containing monomers directly from the support surface. Class 3 materials combine the high amine densities of class 1 materials and covalent amine tethering of class 2, but typically at the expense of a lower degree of control of the structure of amine moiety and relatively difficult laboratory preparation.
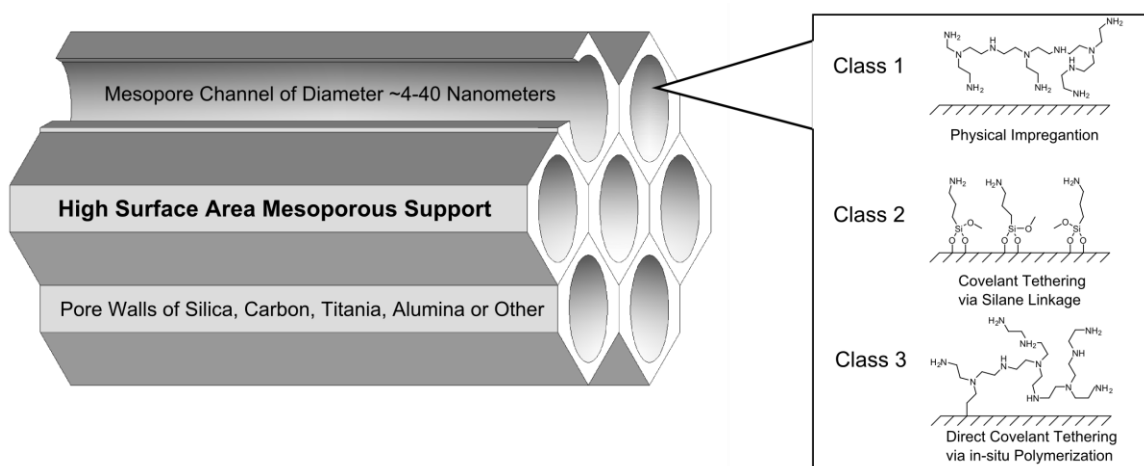
Figure 1.3 Pictorial description of supported amine materials

Supported amine materials are chemisorbents for $CO_2$, meaning that the $CO_2$-amine interaction is relatively strong and often forms a covalent bond. A precise understanding of the chemical bond that is formed is both fundamentally and practically important. To approach this, the established $CO_2$-amine chemistry from liquid solutions[55] has been extrapolated to the solid system, and has been supplemented by spectroscopic investigation.[44,56–58] A reaction schematic is shown in figure 1.4, where it is currently believed that ammonium carbamate ion pairs are the primary reaction product, and are formed via a zwitterionic mechanism. This mechanism requires two base molecules in the immobilization of one $CO_2$ molecule. In the absence of water, two amines are required to capture one $CO_2$, yielding a maximum amine efficiency (moles of $CO_2$ / moles of amine), of one half at the saturation limit of the material. However, when water is present and can act as a free base, the theoretical efficiency increases to one.
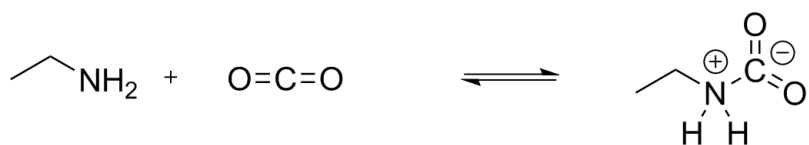
Step 1: Formation of zwitterionic species from primary amine and $CO_2$
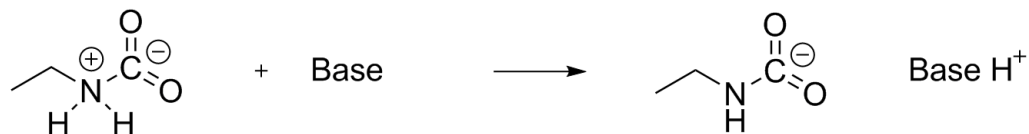


Step 2: Formation of alkyl carbamate ion pair via deprotonation of zwitterion by a free base (either an additional amine or water, if present)

Figure 1.4 Proposed reaction chemistry between $CO_2$ and primary or secondary amines

1.3.1.1 Performance as $CO_2$ Adsorbents

The success of any material as a $CO_2$ separation agent requires superior $CO_2$ uptake and adsorption rate under relevant process conditions, as well as adequate stability under those conditions. The strong $CO_2$-amine interaction lends these materials very steep $CO_2$ adsorption isotherms, offering them their promise in the proposed applications. The majority of research on supported amine materials has been aimed at developing structure property relationships and novel material compositions that provide improved $CO_2$ capacities at relevant $CO_2$ partial pressures. In general, high $CO_2$ capacities are reported for materials with large pore volumes, small amine molecules, and optimal loadings of amines in the support. Further modifications such as support surface composition and additive incorporation have been shown to enhance $CO_2$ capacities of class 1 materials to varying degrees. The rates of $CO_2$ uptake on supported amine materials are generally very rapid, as the $CO_2$ molecules can diffuse freely through the mesopores of the material to adsorption sites. Data obtained in laboratory testing

10

generally reflects these rapid uptake dynamics, except when the materials are highly loaded with amines and a restriction on $CO_2$ diffusion is incurred.

An understanding of how process conditions such as temperature, humidity, contaminants and regeneration method affect the $CO_2$ capacity of the material is practically important. The effect of adsorption temperature on $CO_2$ capacity of a material is dependent on the material composition. Highly loaded materials tend to show an optimum capacity at an elevated adsorption temperature due to competing kinetic and thermodynamic effects. Moderately loaded materials tend to show decreasing $CO_2$ capacities with increasing temperature, as would be thermodynamically expected. As described above, water can increase the amine efficiency of a material. Laboratory testing of the materials in the presence of humidity tends to reflect this expected increase, though rarely by the theoretical factor of two. However, this demonstrated ability to retain high $CO_2$ uptakes in the presence of humidity is a significant practical advantage of these materials compared to other adsorbents such as zeolites and MOFs. Oxygen does not competitively adsorb on these materials, and thus does not impede the $CO_2$ capacity except when oxidative degradation occurs, while $SO_x$ and $NO_x$ tend to degrade the material performance by irreversible binding to amines.[59–61]

1.3.1.2 <u>Process Considerations</u>

Due to the strong, chemisorptive nature of the $CO_2$/amine interaction, the sorbents typically require a temperature swing for regeneration. Several regeneration strategies have been proposed including combined temperature vacuum swing adsorption (TVSA),[29–31,62] temperature swing adsorption (TSA) using a concentrated $CO_2$ purge

stream,[63–69] and steam stripping.[51,70] Steam stripping has been proposed as the desorption method for the process utilizing amine functionalized monoliths described above. Such may be advantageous compared to the other proposed options because steam may be available as waste heat from industry, does not necessarily require external equipment such as large vacuum pumps, and provides both thermal and concentration driving forces for $CO_2$ desorption from the adsorption sites. Furthermore, a concentrated $CO_2$ product stream can easily be obtained by compression of the effluent steam/$CO_2$ mixture that would result from such a process. Ultimately, the success of a particular regeneration method will also depend on the stability of the materials to the conditions imposed during the regeneration. This is particularly important for supported amine materials, as degradation under some relevant operating conditions remains a primary drawback to their commercial implementation. In particular, material degradation at regeneration temperatures (~100 $^o$C) under relevant partial pressures of oxygen,[69,71–73] $CO_2$,[66,67,74] and steam[75] have been reported. Exposure to oxygen and $CO_2$ has resulted in degradation of the amine moieties while steam exposure has resulted in degradation of the support material, depending in both cases on the chemical composition of the sorbent. Structure property relationships have been developed for sorbent stability under these different environments, though the engineering of stable and high performing materials remains a critical challenge.
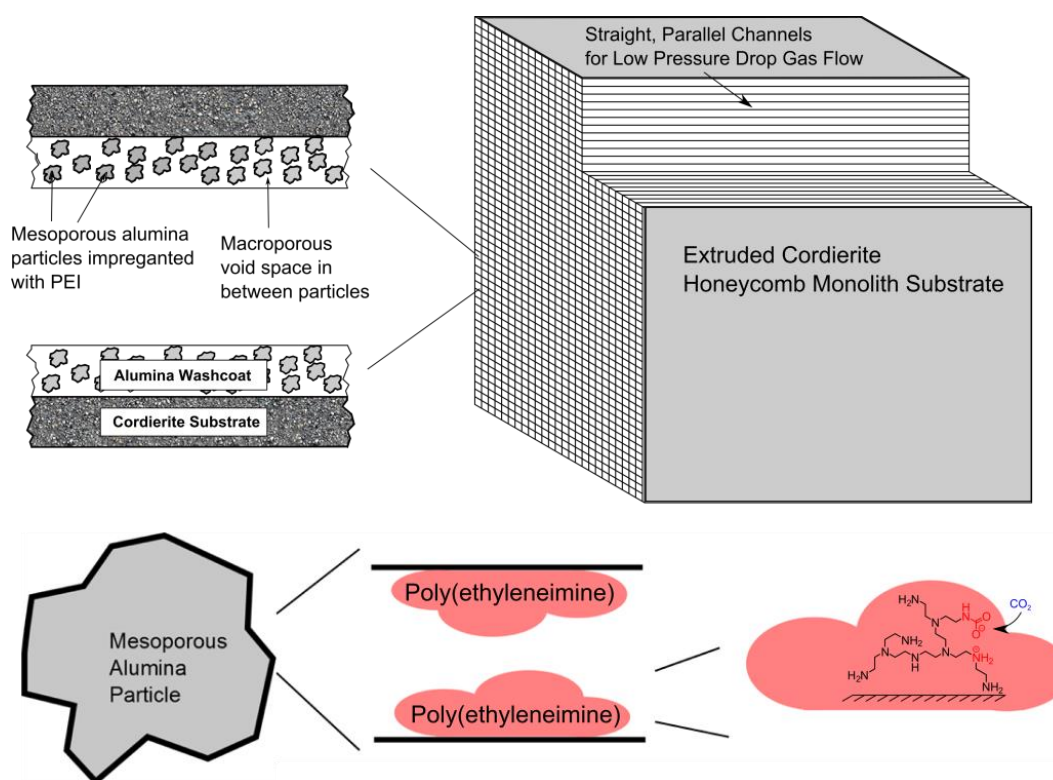
Figure 1.5 Schematic describing amine functionalized monolith. In this configuration, a washcoat of poly(ethyleneimine) functionalized porous alumina is washcoated on a cordierite honeycomb monolith substrate.

An additional factor to be considered in the process design is the form of adsorbent contactor to be utilized. Traditional packed beds,[76] fluidized beds,[77,78] hollow fibers[79,80] and monoliths[81,82] have been suggested for use, depending on the particular application. Each option offers different volumetric packing capacities and transport characteristics of the contacting gas. The extruded honeycomb monolith, with an array of straight, parallel channels, offers the lowest pressure drop of each of the aforementioned options. For DAC processes this is essential, as enormous volumes of air are required to be processed economically. A schematic of a PEI functionalized honeycomb monolith is given in figure 1.5, where a washcoat of porous alumina is supported on a substrate of

13

cordierite and hosts the aminopolymer PEI. However, an optimized air capture technology may differ from this picture in the properties of the substrate, washcoat, and amine that are utilized.

## 1.4 Outlook

Supported amine materials are a promising candidate technology for post combustion $CO_2$ capture and direct air capture due to their high $CO_2$ uptakes and potential for reduced operating cost compared to conventional liquid amine or alkali absorbents. However, several barriers must be overcome prior to their large scale deployment. Process and material development must continue to progress in parallel to reduce the degradation of the materials so as to provide them with adequate commercial lifetimes. Furthermore, process development and scale up of the materials will provide better means to estimate the process cost savings over the existing technology. Finally, a comprehensive fundamental understanding of the molecular level phenomena occurring in these materials, including adsorption, diffusion, and chemical interactions, will provide the means for further material development and optimization.

Specific to the amine functionalized honeycomb monolith technology of interest here, links between material design, stability, and performance along thermodynamic and kinetic axes are of critical importance. Structure-property relationships between such metrics and individual components of the monolith, such as the oxide and organic, will lead to the conceptual design of an improved or optimized structure. To move from conceptual design to practical demonstration, the development of effective preparation

methods is necessary. These issues have been, in part, addressed and are reported in the subsequent text of this dissertation.

## 1.5 References

(1)     Chu, S.; Majumdar, A. Opportunities and Challenges for a Sustainable Energy Future. *Nature* **2012**, *488*, 294–303.

(2)     Friedlingstein, P.; Andrew, R. M.; Rogelj, J.; Peters, G. P.; Canadell, J. G.; Knutti, R.; Luderer, G.; Raupach, M. R.; Schaeffer, M.; van Vuuren, D. P.; et al. Persistent Growth of $CO_2$ Emissions and Implications for Reaching Climate Targets. *Nat. Geosci.* **2014**, *7* (10), 709–715.

(3)     IPCC, 2014: Summary for Policymakers. In: Climate Change 2014: Mitigation of Climate Change. Contribution of Working Group III to the Fifth Assessment Report of the Intergovernmental Panel on Climate Change [Edenhofer, O., R. Pichs-Madruga, Y. Sokona, E. Farahani, S. Kadner, K. Seyboth, A. Adler, I. Baum, S. Brunner, P. Eickemeier, B. Kriemann, J. Savolainen, S. Schlömer, C. von Stechow, T. Zwickel and J.C. Minx (eds.)]. Cambridge University Press, Cambridge, United Kingdom and New York, NY, USA

(4)     Haszeldine, R. S. Carbon Capture and Storage: How Green Can Black Be? *Science* **2009**, *325*, 1647–1652.

(5)     D'Alessandro, D. M.; Smit, B.; Long, J. R. Carbon Dioxide Capture: Prospects for New Materials. *Angew. Chem. Int. Ed. Engl.* **2010**, *49* (35), 6058–6082.

(6)     Boot-Handford, M. E.; Abanades, J. C.; Anthony, E. J.; Blunt, M. J.; Brandani, S.; Mac Dowell, N.; Fernández, J. R.; Ferrari, M.-C.; Gross, R.; Hallett, J. P.; et al. Carbon Capture and Storage Update. *Energy Environ. Sci.* **2014**, *7* (1), 130–189.

(7)     Wang, M.; Lawal, a.; Stephenson, P.; Sidders, J.; Ramshaw, C. Post-Combustion $CO_2$ Capture with Chemical Absorption: A State-of-the-Art Review. *Chem. Eng. Res. Des.* **2011**, *89* (9), 1609–1624.

(8)     Clark, V. R.; Herzog, H. J. Assessment of the US EPA's Determination of the Role for $CO_2$ Capture and Storage in New Fossil Fuel-Fired Power Plants. *Environ. Sci. Technol.* **2014**, *48* (14), 7723–7729.

(9)     Kishimoto, S.; Hirata, T.; Iijima, M.; Ohishi, T.; Higaki, K.; Mitchell, R. Current Status of MHI's CO 2 Recovery Technology and Optimization of CO 2 Recovery Plant with a PC Fired Power Plant. *Energy Procedia* **2009**, *1* (1), 1091–1098.

(10)    Iijima, M.; Nagayasu, T.; Kamijyo, T.; Kishimoto, S.; Nakatani, S. Large-Scale Carbon Dioxide Capture Demonstration Project at a Coal-Fired Power Plant in the USA. *Mitsubishi Heavy Ind. Tech. Rev.* **2012**, *49* (1), 37–43.

(11)   Goto, K.; Yogo, K.; Higashii, T. A Review of Efficiency Penalty in a Coal-Fired Power Plant with Post-Combustion $CO_2$ Capture. *Appl. Energy* **2013**, *111*, 710–720.

(12)   Ahn, H.; Luberti, M.; Liu, Z.; Brandani, S. Process Configuration Studies of the Amine Capture Process for Coal-Fired Power Plants. *Int. J. Greenh. Gas Control* **2013**, *16*, 29–40.

(13)   Herzog, H. J. Scaling up Carbon Dioxide Capture and Storage: From Megatons to Gigatons. *Energy Econ.* **2011**, *33* (4), 597–604.

(14)   Lackner, K. S.; Brennan, S.; Matter, J. M.; Park, H. A.; Wright, A.; van der Zwaan, B. The Urgency of the Development of $CO_2$ Capture from Ambient Air. *Proc. Natl. Acad. Sci. U. S. A.* **2012**, *109* (33), 13156–13162.

(15)   Keith, D. W. Why Capture $CO_2$ from the Atmosphere? *Science* **2009**, *325* (5948), 1654–1655.

(16)   IPCC, 2014: Summary for Policymakers. In: Climate Change 2014: Mitigation of Climate Change. Contribution of Working Group III to the Fifth Assessment Report of the Intergovernmental Panel on Climate Change [Edenhofer, O., R. Pichs-Madruga, Y. Sokona, E. Farahani, S. Kadner, K. Seyboth, A. Adler, I. Baum, S. Brunner, P. Eickemeier, B. Kriemann, J. Savolainen, S. Schlömer, C. von Stechow, T. Zwickel and J.C. Minx (eds.)]. Cambridge University Press, Cambridge, United Kingdom and New York, NY, USA

(17)  Socolow, R. Direct Air Capture of $CO_2$ with Chemicals: A Technology Assessment for the APS Panel on Public Affairs; The American Physical Society. College Park, MD. 2011.

(18)  Socolow, R. Direct Air Capture of $CO_2$ with Chemicals: A Technology Assessment for the APS Panel on Public Affairs; The American Physical Society. College Park, MD. 2011.

(19)  Shepherd, J. Geoengineering the Climate; The Royal Society: London, U.K., 2009.

(20)  House, K. Z.; Baclig, A. C.; Ranjan, M.; van Nierop, E. a; Wilcox, J.; Herzog, H. J. Economic and Energetic Analysis of Capturing $CO_2$ from Ambient Air. *Proc. Natl. Acad. Sci. U. S. A.* **2011**, *108* (51), 20428–20433.

(21)  Kulkarni, A. R.; Sholl, D. S. Analysis of Equilibrium-Based TSA Processes for Direct Capture of $CO_2$ from Air. *Ind. Eng. Chem. Res.* **2012**, *51* (25), 8631–8645.

(22)  Goldberg, D. S.; Lackner, K. S.; Han, P.; Slagle, A. L.; Wang, T. Co-Location of Air Capture, Subseafloor $CO_2$ Sequestration, and Energy Production on the Kerguelen Plateau. *Environ. Sci. Technol.* **2013**, *47* (13), 7521–7529.

(23)  Zeman, F. Reducing the Cost of Ca-Based Direct Air Capture of $CO_2$. *Environ. Sci. Technol.* **2014**, *48*, 11730–11735.

(24)  Mazzotti, M.; Baciocchi, R.; Desmond, M. J.; Socolow, R. H. Direct Air Capture of $CO_2$ with Chemicals: Optimization of a Two-Loop Hydroxide Carbonate

System Using a Countercurrent Air-Liquid Contactor. *Clim. Change* **2013**, *118* (1), 119–135.

(25)   Zeman, F. Energy and Material Balance of $CO_2$ Capture from Ambient Air. *Environ. Sci. Technol.* **2007**, *41* (21), 7558–7563.

(26)   Wang, T.; Lackner, K. S.; Wright, A. B. Moisture-Swing Sorption for Carbon Dioxide Capture from Ambient Air: A Thermodynamic Analysis. *Phys. Chem. Chem. Phys.* **2013**, *15* (2), 504–514.

(27)   Lackner, K. S. Capture of Carbon Dioxide from Ambient Air. *Eur. Phys. J. Spec. Top.* **2009**, *176* (1), 93–106.

(28)   Gebald, C.; Wurzbacher, J. A.; Borgschulte, A.; Zimmermann, T.; Steinfeld, A. Adsorption of Amine-Functionalized Cellulose Single-Component and Binary $CO_2$ and $H_2O$ Adsorption of Amine-Functionalized Cellulose. *Environ. Sci. Technol.* **2014**, *48*, 2497–2504.

(29)   Gebald, C.; Wurzbacher, J. a; Tingaut, P.; Steinfeld, A. Stability of Amine-Functionalized Cellulose during Temperature-Vacuum-Swing Cycling for $CO_2$ Capture from Air. *Environ. Sci. Technol.* **2013**, *47* (17), 10063–10070.

(30)   Wurzbacher, J. A.; Gebald, C.; Piatkowski, N.; Steinfeld, A. Concurrent Separation of $CO_2$ and $H_2O$ from Air by a Temperature-Vacuum Swing Adsorption/desorption Cycle. *Environ. Sci. Technol.* **2012**, *46* (16), 9191–9198.

(31)    Wurzbacher, J. A.; Gebald, C.; Steinfeld, A. Separation of $CO_2$ from Air by Temperature-Vacuum Swing Adsorption Using Diamine-Functionalized Silica Gel. *Energy Environ. Sci.* **2011**, *4* (9), 3584–3592.

(32)    Sehaqui, H.; Gálvez, M. E.; Becatinni, V.; cheng Ng, Y.; Steinfeld, A.; Zimmermann, T.; Tingaut, P. Fast and Reversible Direct $CO_2$ Capture from Air onto All-Polymer Nanofibrillated Cellulose—Polyethylenimine Foams. *Environ. Sci. Technol.* **2015**, DOI: 150211062437002.

(33)    Zhang, W.; Liu, H.; Sun, C.; Drage, T. C.; Snape, C. E. Capturing $CO_2$ from Ambient Air Using a Polyethyleneimine-Silica Adsorbent in Fluidized Beds. *Chem. Eng. Sci.* **2014**, *116*, 306–316.

(34)    Goeppert, A.; Meth, S.; Prakash, G. K. S.; Olah, G. A. Nanostructured Silica as a Support for Regenerable High-Capacity Organoamine-Based $CO_2$ Sorbents. *Energy Environ. Sci.* **2010**, *3* (12), 1949–1960.

(35)    Zhang, H.; Goeppert, A.; Czaun, M.; Prakash, G. K. S.; Olah, G. A. $CO_2$ Capture on Easily Regenerable Hybrid Adsorbents Based on Polyamines and Mesocellular Silica Foam. Effect of Pore Volume of the Support and Polyamine Molecular Weight. *RSC Adv.* **2014**, *4* (37), 19403–19417.

(36)    Zhang, H.; Goeppert, A.; Surya Prakash, G. K.; Olah, G. A. Applicability of Linear Polyethylenimine Supported on Nano-Silica for the Adsorption of $CO_2$ from Various Sources Including Dry Air. *RSC Adv.* **2015**, *5*, 52550–52562.

(37)   Goeppert, A.; Czaun, M.; May, R. B.; Prakash, G. K. S.; Olah, G. A.; Narayanan, S. R. Carbon Dioxide Capture from the Air Using a Polyamine Based. *J. Am. Chem. Soc.* **2011**, *113*, 20164–20167.

(38)   Wang, J.; Wang, M.; Li, W.; Qiao, W.; Long, D.; Ling, L. Application of Polyethyleneimine-Impregnated Solid Adsorbents for Direct Capture of Low-Concentration CO2. *AIChE J.* **2015**, *61* (3), 972–980.

(39)   Wang, J.; Huang, H.; Wang, M.; Yao, L.; Qiao, W.; Long, D.; Ling, L. Direct Capture of Low-Concentration $CO_2$ on Mesoporous Carbon-Supported Solid Amine Adsorbents at Ambient Temperature. *Ind. Eng. Chem. Res.* **2015**, *54* (19), 5319–5327.

(40)   Rahaman, M. S. A.; Zhang, L.; Cheng, L.-H.; Xu, X.-H.; Chen, H.-L. Capturing Carbon Dioxide from Air Using a Fixed Carrier Facilitated Transport Membrane. *RSC Adv.* **2012**, *2* (24), 9165–9172.

(41)   Chen, Z.; Deng, S.; Wei, H.; Wang, B.; Huang, J.; Yu, G. Polyethylenimine-Impregnated Resin for High $CO_2$ Adsorption : An E Ffi Cient Adsorbent for $CO_2$ Capture from Simulated Flue Gas and Ambient Air. *ACS Appl. Mater. Interfaces* **2013**, *5* (15), 6937–6945.

(42)   He, L.; Fan, M.; Dutcher, B.; Cui, S.; Shen, X. D.; Kong, Y.; Russell, A. G.; McCurdy, P. Dynamic Separation of Ultradilute $CO_2$ with a Nanoporous Amine-Based Sorbent. *Chem. Eng. J.* **2012**, *189-190*, 13–23.

(43)  Belmabkhout, Y.; Serna-Guerrero, R.; Sayari, A. Amine-Bearing Mesoporous Silica for $CO_2$ Removal from Dry and Humid Air. *Chem. Eng. Sci.* **2010**, *65* (11), 3695–3698.

(44)  Didas, S. A.; Sakwa-Novak, M. A.; Foo, G. S.; Sievers, C.; Jones, C. W. Effect of Amine Surface Coverage on the Co-Adsorption of $CO_2$ and Water: Spectral Deconvolution of Adsorbed Species. *J. Phys. Chem. Lett.* **2014**, *5*, 4194–4200.

(45)  Kuwahara, Y.; Kang, D.-Y.; Copeland, J. R.; Bollini, P.; Sievers, C.; Kamegawa, T.; Yamashita, H.; Jones, C. W. Enhanced $CO_2$ Adsorption over Polymeric Amines Supported on Heteroatom-Incorporated SBA-15 Silica: Impact of Heteroatom Type and Loading on Sorbent Structure and Adsorption Performance. *Chem. Eur. J.* **2012**, *18* (52), 16649–16664.

(46)  Didas, S. A.; Kulkarni, A. R.; Sholl, D. S.; Jones, C. W. Role of Amine Structure on Carbon Dioxide Adsorption from Ultradilute Gas Streams such as Ambient Air. *ChemSusChem* **2012**, *5* (10), 2058–2064.

(47)  Kuwahara, Y.; Kang, D.-Y.; Copeland, J. R.; Brunelli, N. A.; Didas, S. A.; Bollini, P.; Sievers, C.; Kamegawa, T.; Yamashita, H.; Jones, C. W. Dramatic Enhancement of $CO_2$ Uptake by Poly(ethyleneimine) Using Zirconosilicate Supports. *J. Am. Chem. Soc.* **2012**, *134* (26), 10757–10760.

(48)    Choi, S.; Drese, J. H.; Eisenberger, P. M.; Jones, C. W. Application of Amine-Tethered Solid Sorbents for Direct CO2 Capture from the Ambient Air. *Environ. Sci. Technol.* **2011**, *45* (6), 2420–2427.

(49)    Chaikittisilp, W.; Khunsupat, R.; Chen, T. T.; Jones, C. W. Poly ( Allylamine ) ÀMesoporous Silica Composite Materials for $CO_2$ Capture from Simulated Flue Gas or Ambient Air. *Ind. Eng. Chem. Res.* **2011**, 14203–14210.

(50)    Choi, S.; Gray, M. L.; Jones, C. W. Amine-Tethered Solid Adsorbents Coupling High Adsorption Capacity and Regenerability for $CO_2$ Capture from Ambient Air. *ChemSusChem* **2011**, *4* (5), 628–635.

(51)    Li, W.; Choi, S.; Drese, J. H.; Hornbostel, M.; Krishnan, G.; Eisenberger, P. M.; Jones, C. W. Steam-Stripping for Regeneration of Supported Amine-Based $CO_2$ Adsorbents. *ChemSusChem* **2010**, *3* (8), 899–903.

(52)    Hicks, J. C.; Drese, J. H.; Fauth, D. J.; Gray, M. L.; Qi, G. G.; Jones, C. W. Designing Adsorbents for $CO_2$ Capture from Flue Gas-Hyperbranched Aminosilicas Capable of Capturing $CO_2$ Reversibly. *J. Am. Chem. Soc.* **2008**, *130* (10), 2902–2903.

(53)    Chaikittisilp, W.; Kim, H.-J.; Jones, C. W. Mesoporous Alumina-Supported Amines as Potential Steam-Stable Adsorbents for Capturing $CO_2$ from Simulated Flue Gas and Ambient Air. *Energy & Fuels* **2011**, *25*, 5528–5537.

(54)   Choi, S.; Drese, J. H.; Jones, C. W. Adsorbent Materials for Carbon Dioxide Capture from Large Anthropogenic Point Sources. *ChemSusChem* **2009**, *2* (9), 796–854.

(55)   Donaldson, T. L.; Nguyen, Y. N. Carbon Dioxide Reaction Kinetics and Transport in Aqueous Amine Membranes. *Ind. Eng. Chem. Fundam.* **1980**, *19* (2), 260–266.

(56)   Pinto, L.; Mafra, L.; Guil, M. Adsorption and Activation of $CO_2$ by Amine-Modified Nanoporous Materials Studied by Solid-State NMR and $^{13}CO_2$ Adsorption. *Chem. Mater.* **2011**, *23*, 1387–1395.

(57)   Danon, A.; Stair, P. C.; Weitz, E. FTIR Study of $CO_2$ Adsorption on Amine-Grafted SBA-15: Elucidation of Adsorbed Species. *J. Phys. Chem. C* **2011**, *115* (23), 11540–11549.

(58)   Bacsik, Z.; Ahlsten, N.; Ziadi, A.; Zhao, G.; Garcia-Bennett, A. E.; Martín-Matute, B.; Hedin, N. Mechanisms and Kinetics for Sorption of $CO_2$ on Bicontinuous Mesoporous Silica Modified with N-Propylamine. *Langmuir* **2011**, *27* (17), 11118–11128.

(59)   Xu, X.; Song, C.; Miller, B. G.; Scaroni, A. W. Adsorption Separation of Carbon Dioxide from Flue Gas of Natural Gas-Fired Boiler by a Novel Nanoporous "Molecular Basket" Adsorbent. *Fuel Process. Technol.* **2005**, *86* (14-15), 1457–1472.

(60)  Co, P.; Adsorption, C. S.; Rezaei, F.; Jones, C. W. Stability of Supported Amine Adsorbents to $SO_2$ and $NO_x$ in Postcombustion $CO_2$ Capture. 1. Single-Component Adsorption. *Ind. Eng. Chem. Res.* **2013**, *52* (x), 12192–12201.

(61)  Co, P.; Adsorption, C. S.; Rezaei, F.; Jones, C. W. Stability of Supported Amine Adsorbents to $SO_2$ and $NO_x$ in Postcombustion $CO_2$ Capture. 2. Multicomponent Adsorption. *Ind. Eng. Chem. Res.* **2014**, *53*, 12103–12110.

(62)  Stuckert, N. R.; Yang, R. T. $CO_2$ Capture from the Atmosphere and Simultaneous Concentration Using Zeolites and Amine-Grafted SBA-15. *Environ. Sci. Technol.* **2011**, *45* (23), 10257–10264.

(63)  Drage, T. C.; Arenillas, a.; Smith, K. M.; Snape, C. E. Thermal Stability of Polyethylenimine Based Carbon Dioxide Adsorbents and Its Influence on Selection of Regeneration Strategies. *Microporous Mesoporous Mater.* **2008**, *116* (1-3), 504–512.

(64)  Kim, S.; Ida, J.; Guliants, V. V; Lin, J. Y. S. Tailoring Pore Properties of MCM-48 Silica for Selective Adsorption of $CO_2$. *J. Phys. Chem. B* **2005**, *109* (13), 6287–6293.

(65)  Gray, M. L.; Hoffman, J. S.; Hreha, D. C.; Fauth, D. J.; Hedges, S. W.; Champagne, K. J.; Pennline, H. W. Parametric Study of Solid Amine Sorbents for the Capture of Carbon Dioxide. *Energy & Fuels* **2009**, *23* (10), 4840–4844.

(66)    Sayari, A.; Heydari-Gorji, A.; Yang, Y. $CO_2$-Induced Degradation of Amine-Containing Adsorbents: Reaction Products and Pathways. *J. Am. Chem. Soc.* **2012**, *134* (33), 13834–13842.

(67)    Sayari, A.; Belmabkhout, Y.; Da'na, E. $CO_2$ Deactivation of Supported Amines: Does the Nature of Amine Matter? *Langmuir* **2012**, *28* (9), 4241–4247.

(68)    Zhao, W.; Zhang, Z.; Li, Z.; Cai, N. Investigation of Thermal Stability and Continuous $CO_2$ Capture from Flue Gases with Supported Amine Sorbent. *Ind. Eng. Chem. Res.* **2013**, *52*, 2084–2093.

(69)    Heydari-Gorji, A.; Sayari, A. Thermal , Oxidative , and $CO_2$ -Induced Degradation of Supported Polyethylenimine Adsorbents. *Ind. Eng. Chem. Res.* **2012**, *51*, 6887–6894.

(70)    Hammache, S.; Hoffman, J. S.; Gray, M. L.; Fauth, D. J.; Howard, B. H.; Pennline, H. W. Comprehensive Study of the Impact of Steam on Polyethyleneimine on Silica for $CO_2$ Capture. *Energy & Fuels* **2013**, *27*, 6899–6905.

(71)    Heydari-Gorji, A.; Belmabkhout, Y.; Sayari, A. Degradation of Amine-Supported $CO_2$ Adsorbents in the Presence of Oxygen-Containing Gases. *Microporous Mesoporous Mater.* **2011**, *145* (1-3), 146–149.

(72) Calleja, G.; Sanz, R.; Arencibia, a.; Sanz-Pérez, E. S. Influence of Drying Conditions on Amine-Functionalized SBA-15 as Adsorbent of $CO_2$. *Top. Catal.* **2011**, *54* (1-4), 135–145.

(73) Bali, S.; Chen, T. T.; Chaikittisilp, W.; Jones, C. W. Oxidative Stability of Amino Polymer–Alumina Hybrid Adsorbents for Carbon Dioxide Capture. *Energy & Fuels* **2013**, *27* (3), 1547–1554.

(74) Sayari, A.; Belmabkhout, Y. Stabilization of Amine-Containing $CO_2$ Adsorbents: Dramatic Effect of Water Vapor. *J. Am. Chem. Soc.* **2010**, *132* (18), 6312–6314.

(75) Li, W.; Bollini, P.; Didas, S. A.; Choi, S.; Drese, J. H.; Jones, C. W. Structural Changes of Silica Mesocellular Foam Supported Amine-Functionalized $CO_2$ Adsorbents upon Exposure to Steam. *ACS Appl. Mater. Interfaces* **2010**, *2* (11), 3363–3372.

(76) Ebner, A. D.; Gray, M. L.; Chisholm, N. G.; Black, Q. T.; Mumford, D. D.; Nicholson, M. A.; Ritter, J. A. Suitability of a Solid Amine Sorbent for $CO_2$ Capture by Pressure Swing Adsorption. *Ind. Eng. Chem. Res.* **2011**, *50*, 5634–5641.

(77) Zhang, W.; Liu, H.; Sun, C.; Drage, T. C.; Snape, C. E. Performance of Polyethyleneimine-Silica Adsorbent for Post-Combustion $CO_2$ Capture in a Bubbling Fluidized Bed. *Chem. Eng. J.* **2014**, *251*, 293–303.

(78)    Meth, S.; Goeppert, A.; Prakash, G. K. S.; Olah, G. A. Silica Nanoparticles as Supports for Regenerable $CO_2$ Sorbents. *Energy* **2012**.

(79)    Fan, Y.; Labreche, Y.; Lively, R. P.; Jones, C. W.; Koros, W. J. Dynamic $CO_2$ Adsorption Performance of Intertnally Cooled Silica-Supported Poly(ethyleneimine) Hollow Fiber Sorbents. *AIChE J.* **2014**, *60* (11), 3878–3887.

(80)    Fan, Y.; Kalyanaraman, J.; Labreche, Y.; Rezaei, F.; Lively, R. P.; Real, M. J.; Koros, W. J.; Jones, C. W.; Kawajiri, Y. $CO_2$ Sorption Performance of Composite Polymer / Aminosilica Hollow Fiber Sorbents : An Experimental and Modeling Study. *Ind. Eng. Chem. Res.* **2015**, *54*, 1783–1795.

(81)    Rezaei, F.; Mosca, A.; Webley, P.; Hedlund, J.; Xiao, P. Comparison of Traditional and Structured Adsorbents for $CO_2$ Separation by Vacuum-Swing Adsorption. *Adsorpt. J. Int. Adsorpt. Soc.* **2010**, 4832–4841.

(82)    Mosca, A.; Hedlund, J.; Webley, P. A.; Grahn, M.; Rezaei, F. Structured Zeolite NaX Coatings on Ceramic Cordierite Monolith Supports for PSA Applications. *Microporous Mesoporous Mater.* **2010**, *130* (1-3), 38–48.

# CHAPTER 2

# HYDROTHERMAL STABILITY OF PEI/ALUMINA ADSORBENTS

Parts of this chapter are adapted from 'Sakwa-Novak, M. A.; Jones, C. W. Steam Induced Structural Changes of a Poly(ethylenimine) Impregnated γ - Alumina Sorbent for $CO_2$ Extraction from Ambient Air. *ACS Appl. Mater. Interfaces* **2014**, *6*, 9245–9255' with permission of The American Chemical Society.

## 2.1    Introduction & Motivation

Our research group and others have recently demonstrated the use of steam stripping to regenerate several representative supported amine materials. Li *et al*[1] studied the steam regeneration of all three classes[2] of amines supported on a commercial mesoporous silica. In that study, a packed bed of sorbent was subjected to three cycles of $CO_2$ adsorption followed by exposure to flowing steam for regeneration.  Class 1 and 3 sorbents, incorporating poly(ethyleneimine) (PEI) into the pores of the support material by physical impregnation or *in-situ* polymerization, respectively, adsorbed as much or more $CO_2$ in cycles 2 and 3 as in cycle 1, indicating that the exposure to flowing steam fully regenerated the $CO_2$ adsorption sites on the material. On the other hand, a class 2 sorbent, grafted with 3-(aminopropyl)trimethoxysilane (APS), showed slight reduction in $CO_2$ capacity in the second two cycles, relative to the first. However, it was not elucidated whether this was due to incomplete regeneration of $CO_2$ adsorption sites in the material or due to degradation of the material induced by exposure to steam. Recently,

Hammache *et al*[3] extended similar analysis to 8 cycles of $CO_2$ adsorption followed by steam exposure on both a class 1 PEI impregnated, and a hybrid (class 2 and class 1) APS grafted and PEI impregnated commercial mesoporous silica. The authors found that both materials retained at least 88% of their initial $CO_2$ capacity from simulated flue gas at 10% $CO_2$, with the capacities on the 8th cycle being 2.8 mmol/g and 2.7 mmol/g, respectively. Importantly, the authors suggest that no significant structural changes occurred to the sorbent as a result of the steam cycling. The materials were also subjected to continuous exposure to steam for 5 hours, as well as $CO_2$ free cycling, where the sorbent was exposed to cycles of steam for 30-40 minutes followed by drying under helium flow. The sorbent exposed to $CO_2$ free cycling showed greater reduction in $CO_2$ capacity than that exposed to steam continuously, even though the total steam time during cycling was 3.5 hours (1.5 hours less than for the continuous sample). Importantly, the authors report that no significant structural changes occurred in the sorbent in these experiments as well. The authors do suggest, however, that PEI may reagglomerate in the pores of the sorbent as a result of steam exposure, which may slightly reduce the surface area, pore volume and $CO_2$ capacity of the material. Nonetheless, while these studies demonstrate the feasibility of steam to regenerate adsorption sites on supported amine sorbents, they do not provide thorough insight into the stability of such materials over the very long timescales of industrial operation.

To this end, longer accelerated steam exposure studies have been performed to investigate the possibility of long term steam induced structural changes to representative sorbents. Li *et al*[4] found that that exposure to steam for 24 hours on sorbents comprised

of all 3 classes of amines supported on mesocellular foam (MCF), an extra-large pore, thin walled mesoporous silica, caused significant collapse of the silica pore structure, which in turn caused significant loss of $CO_2$ capacity. Similarly, Chaikittislip *et al*[5] found that when PEI was supported on SBA-15 mesoporous silica, and the material exposed to steam for 24 hours, that a significant loss of the mesopore structure occurred, causing similarly large reductions in $CO_2$ capacity. However, when PEI was supported a mesoporous $\gamma$-alumina, and the material subjected to the same 24 hours of steam exposure, there was much less change in the pore structure observed in the $N_2$ physisorption data, and the material retained a much greater fraction of its initial $CO_2$ capacity than did the SBA-15 silica analog.[5] Important to note, however, is that in both of these reports the steam treatment was performed under a static environment in an apparatus similar to a batch reactor. Noteworthy is that the SBA-15 silica, containing much thicker silica walls between pores than the MCF, retained much of its mesopore structure after steam treatment when amines were not present in the pores of the material. Thus, one may surmise that the presence of amines in the silica pore network significantly enhances the degradation of the pore structure, likely due to Si-O-Si bond hydrolysis, which would be catalyzed by the amines. Nonetheless, both of these studies suggest that mesoporous silica, the most common metal-oxide material reported in the literature for use as a support in $CO_2$ capture sorbent preparation, may be susceptible to hydrolysis in the presence of steam over very long timescales when amine groups are present on the surface. As a result, oxides such as crystalline $\gamma$-alumina, which may be

less susceptible to hydrolysis and pore collapse, may be more practical supports for sorbents used in a process employing steam stripping as a regeneration technique.[5]

However, greater resolution into any steam induced structural changes to $\gamma$-alumina supported amine sorbents is necessary prior to their large scale deployment. Furthermore, study of such materials under the more practical environment of flowing steam (as opposed to static), similar to the Hammache study, is desired. Here, we report on the findings of an accelerated degradation study of a PEI impregnated (class 1) mesoporous $\gamma$-alumina under such conditions. This sorbent is shown to have a high $CO_2$ capacity under simulated air capture conditions, and retains over 90% of this capacity after continuous exposure to steam for up to 12 hours. The material was characterized in detail following exposure to flowing steam for various times. It is found that after exposure to steam for times of 90 minutes and greater, that the $\gamma$-alumina partially hydrates to form boehmite, an aluminum oxyhydroxide. The effect of the presence of boehmite in the sorbent on the efficiency of PEI adsorbing $CO_2$ under simulated air conditions was probed, and the results suggest that the partial phase transition does not significantly affect the PEI amine efficiency. Further subtle structural changes to the sorbent observed in the $N_2$ physisorption profiles, which suggest possible PEI rearrangement, are discussed as well.

## 2.2 Experimental

### 2.2.1 Materials

The following materials were used as received from the supplier: methanol (ACS Grade, BDH), branched poly(ethyleneimine) (PEI) ($M_W$ ~ 800, $M_n$ ~ 600, Sigma-Aldrich), Versal-250 (V-250) pseudoboehmite (UOP). Nitrogen (UHP), helium (UHP) and a premixed cylinder of 5% $CO_2$ in helium were purchased from Airgas Inc. A specialty gas mixture of 400 ppm $CO_2$ in helium, used in gravimetric $CO_2$ uptake experiments, was purchased from Matheson Tri-Gas.

### 2.2.2 Preparation of Poly(ethyleneimine) Sorbents

The $\gamma$-alumina support used throughout the study was prepared by calcination of the V-250 mesoporous pseudoboehmite. Calcination was performed by increasing the oven temperature from ambient to 550 $^o$C at 5 $^o$C/min and then holding at 550 $^o$C for 12 h, under static air, before cooling to room temperature. Prior to PEI incorporation, the $\gamma$-alumina was dried at 110 $^o$C under vacuum (~ 20 mTorr) overnight. The dried $\gamma$-alumina was then dispersed in methanol in a ratio of 15 mL methanol to 1 g dried $\gamma$-alumina. Separately, a given amount of PEI was dissolved in 20 mL of methanol. The separate mixtures were equilibrated by stirring for at least 1 h, and then were combined by dropwise addition of the PEI/methanol mixture into the $\gamma$-alumina/methanol dispersion. The mixtures were then stirred at room temperature for 24 hours, before the solvent was removed by rotary evaporation, followed by drying under high vacuum (~20 mTorr) at 100 $^o$C overnight. Prior to testing, sorbents were pelletized by loading 0.5 grams of dried

sorbent into a cylindrical pellet die of diameter 13 mm and pressing to a pressure between 2500-3000 psi. The cylindrical pellets were then crushed and sieved between 150 and 800 microns.

### 2.2.3 Material Characterization

Organic loadings of the freshly prepared sorbents were determined by thermogravimetric analysis using a Netzsch STA409PG TGA. The organic loading was calculated from the measured weight loss between the temperatures of 120 $^{o}$C and 900 $^{o}$C. For samples containing boehmite, contents of C, H, N, and Al were estimated by elemental analysis performed by Galbraith Laboratories (Knoxville, TN), and the amine loading was determined accordingly. Surface areas and total pore volumes of the sample were estimated from $N_2$ physisorption data  obtained by measurements performed on a Micromeritics Tristar II 3020 apparatus at 77 K. Prior to physisorption analysis, the samples were degassed at 110 $^{o}$C for at least 10 hours. Surface areas were estimated by the BET equation, while total pore volumes were taken to be equal to the total amount of $N_2$ adsorbed at a $P/P_0$ of 0.99.  Powder XRD patters were obtained by use of a PANalytical X'pert diffractometer with a Cu-K-alpha X-ray source. FT-IR experiments were performed on a Bruker Vertex 80v optical bench. FT-Raman experiments were performed on an attached Ram II module on the same bench. For FT-IR measurements, ~1 mg of sample was mixed with ~100 mg KBr and pressed to pellets for analysis. $^{27}$Al solid state NMR experiments were performed on a Bruker DSC 400 spectrometer. 2400 scans were taken for each sample with a spinning speed of 12 kHz.

### 2.2.4 $CO_2$ Adsorption

Humid $CO_2$ adsorption capacities were measured in packed bed experiments while dry capacities were measured gravimetrically on a TGA. All $CO_2$ capacities reported in this chapter were measured at a $CO_2$ concentration of 400 ppm. Packed bed experiments were performed in a flow adsorption system (see figure A.1 in appendix A for schematic) using 1 g of pelletized sorbent. A Li-COR Li-840A $CO_2/H_2O$ IR gas analyzer was used to follow real time $CO_2$ and $H_2O$ gas phase concentrations. Prior to $CO_2$ adsorption experiments the samples were pretreated under flowing $N_2$ and heated to 110 $^o$C until less than 0.01 mmol/min of $H_2O$ and $CO_2$ minute was observed in the effluent downstream of the sorbent bed. $CO_2$ adsorption was then performed by exposing the sample bed to a flow of simulated air at 30 $^o$C, 400 ppm $CO_2$ balanced by $N_2$ and 50% relative humidity (at 30 $^o$C). Humidity was controlled by passing the $CO_2/N_2$ mixture through a sparger containing DI $H_2O$ immersed in a temperature controlled fluid bath. $CO_2$ adsorption experiments were terminated when the concentration of $CO_2$ in the effluent stream was at least 99% of that in the inlet stream. In this way, the reported $CO_2$ capacities are pseudoequilibrium values. Adsorption capacities were estimated by integrating the resulting $CO_2$ breakthrough curves, and were measured both before and after steam exposure.

Dry adsorption capacities were measured gravimetrically on a TA Instruments Q500 TGA. The samples were pretreated by heating to 110 $^o$C and holding at this temperature for 3 h under helium flow. The samples were then cooled to 30 $^o$C and allowed to thermally equilibrate at this temperature for 60 minutes. Subsequently, the gas

flow was switched from helium to a premixed gas containing 400 ppm $CO_2$/He and allowed to equilibrate for 12 hours.

### 2.2.5 Steam Exposure

To investigate steam induced structural changes to the $\gamma$-alumina supported PEI sorbents, samples were exposed to flowing steam for various times. Steam exposure experiments were performed in the same flow adsorption system as was used to measure humid $CO_2$ capacities. A schematic of the system is reported in Fig A.1 of appendix A. Samples were exposed to steam following an initial measurement of equilibrium adsorption capacity (see above). Prior to steam treatment, the samples were pretreated under $N_2$ flow at 110 $^o$C, during which upstream lines and the packed bed reactor jacket were heated to ~115 $^o$C. Steam was then introduced at ~5 g/min and allowed to contact the samples continuously for times of 5 min, 90 min, 12 h and 24 h in distinct experiments. In a separate experiment, one sample was exposed to steam flow in a cyclic fashion. Here, the sorbent was exposed to cycles of preheating to 110 $^o$C under $N_2$ flow, followed by exposure to flowing steam for 5 min, and then finally to partial cooling and drying under $N_2$ flow. During the cooling/drying step $N_2$ was immediately introduced into the packed bed after the steam was turned off. Heating of the reactor jacket and upstream system lines were turned off and $N_2$ was allowed to flow until the packed bed reached a temperature of 30 $^o$C. A total of 18 cycles of these three steps were completed, such that the total steam exposure time was 90 min. Preceding and following all steam exposure experiments, pseudoequilibrium $CO_2$ capacities of the materials were estimated

by flowing simulated air over the sample and subsequently integrating the resulting breakthrough curve, as described above.

## 2.3  Results and Discussion

### 2.3.1  Fresh Sorbent Characterization

Figures 2.1 and 2.2 show the XRD patterns and $N_2$ physisorption profiles of the calcined $\gamma$-alumina support before and after impregnation with 30 wt% of poly(ethyleneimine) (PEI). The diffraction patterns of the bare support and impregnated sorbent show characteristic $\gamma$-alumina peaks[6] at $2\theta$ of 37, 46.5 and 66.5 as well as a broad peak between $2\theta$ of 15-30 that is attributed to diffraction arising from average intermolecular distances of Al and O atoms in amorphous regions of the alumina sample[7]. $\gamma$-Alumina is poorly crystalline and so it may be expected that such regions would exist in the sample. The amorphous peak is more prominent and slightly shifted to higher $2\theta$ in the PEI impregnated sample. This change, while subtle, may be due to coordination of aminopolymer to surface atoms, slightly disrupting the $\gamma$-alumina structure at this interface. Nonetheless, the prominence of the $\gamma$-alumina peaks in the diffraction pattern before and after PEI impregnation suggest the alumina remained predominantly in $\gamma$ form. Table 1 shows the BET surface area ($m^2$/g) and total pore volume ($cm^3$/g) of the materials, calculated by total adsorbed $N_2$ at a partial pressure of 0.99. The values here are normalized by the mass of $Al_2O_3$. The physisorption profiles of the bare $\gamma$-alumina show significant $N_2$ uptake at partial pressures greater than 0.8, indicative of large mesopores and macropores. The existence of hysteresis on the desorption branch of the

isotherm confirms the presence of mesopores in the material. After impregnation with PEI, the surface area and total pore volume of the material decreased substantially. The reduction in pore volume between the bare $\gamma$-alumina support and that impregnated with PEI was calculated to be 0.50 $cm^3$/g $Al_2O_3$, which is very close to the expected occupied volume of PEI of 0.49 $cm^3$/g $Al_2O_3$ (calculated assuming a liquid density of 1.05 g/mL for PEI), indicating successful impregnation of the PEI into the pores of the $\gamma$-alumina[8]. Since samples exposed to steam were in the form of pellets, the BET surface area and pore volume of the pelletized material are reported in Table 1 as well. The surface area of bare $\gamma$-alumina remained unchanged after pelletization, but the total pore volume decreased significantly, by 0.35 $cm^3$/g $Al_2O_3$. After pelletization of the PEI impregnated sorbents a reduction of 39 $m^2$/g $Al_2O_3$ and 0.27 $cm^3$/g $Al_2O_3$ was observed in the BET surface area and total pore volume, respectively.
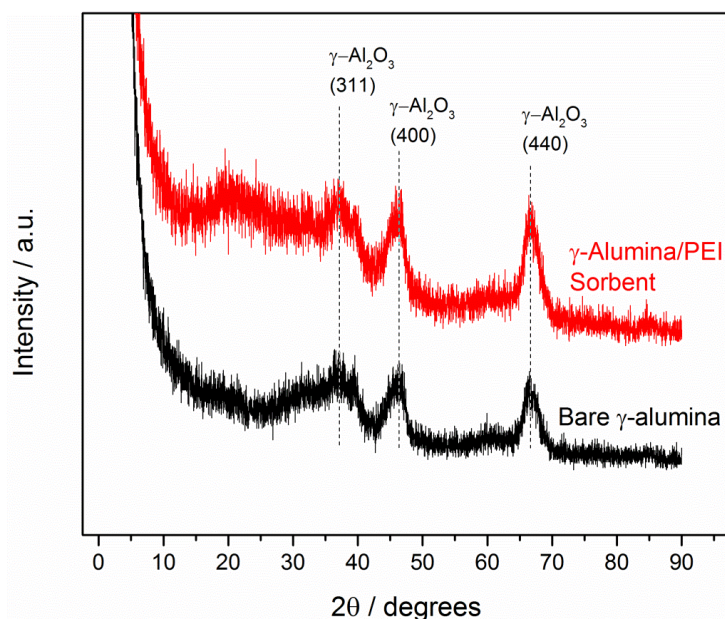


Figure 2.1 XRD patterns of $\gamma$-alumina support before and after PEI incorporation.
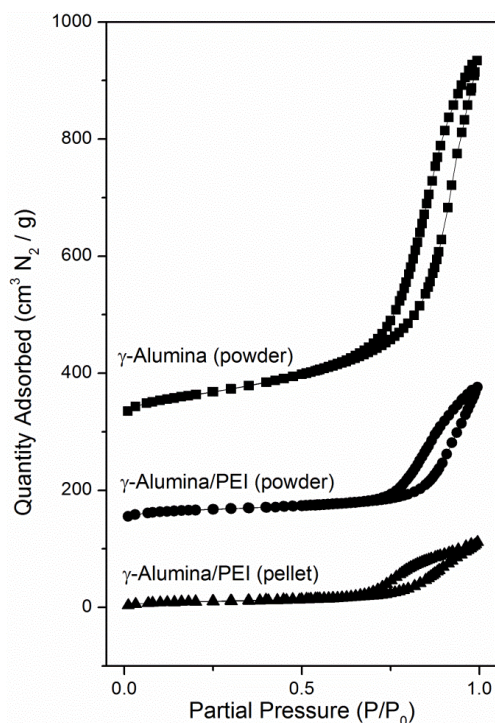
Figure 2.2 $N_2$ physisorption profiles at 77 K of $\gamma$-alumina before and after PEI incorporation in powder and pellet form. Profiles are offset by 150 cm$^3$/g

Table 2.1 Physical characteristics of $\boldsymbol{\gamma}$-alumina support before and after PEI incorporation in powder and pellet form.

| Sample | BET SA | Total PV[a] | Amine Loading[b] |
|---|---|---|---|
| | (per g Al$_2$O$_3$) | | (per g sorbent) |
| | m2/g | cm3/g | mmol N/g |
| $\gamma$-Alumina | 243 | 1.04 | n/a |
| $\gamma$-Alumina Pellets | 244 | 0.69 | n/a |
| PEI Impregnated Sorbent | 97 | 0.53 | 8.4 |
| Pelletized Sorbent | 58 | 0.26 | 8.5 |

## 2.3.2 Effect of steam exposure on CO$_2$ capacity

Table 2.2 and Figure 2.3 show the results of the steam exposure experiments.

Figure 2.3 shows pseudoequilibrium CO$_2$ capacities and amine efficiencies of the

materials as a function of time exposed to steam. The data points furthest to left on the plot, and containing error bars, correspond to the capacity and efficiency of the material prior to steam exposure, measured to be 1.71 mmol/g and 0.22 mol N/ mol $CO_2$, respectively. The shortest steam exposure time was 5 minutes, chosen to represent a typical exposure time of one desorption cycle in a hypothetical large scale process. After exposure to steam flow for 5 minutes, the $CO_2$ capacity of the material increased to 1.96 mmol/g. Because the sample was thoroughly dried following exposure to steam, and adsorption experiments were performed at 50% relative humidity, differences in the amount of physisorbed water left from steaming between experiments are likely negligible and hence are likely not responsible for this observed increase in capacity. While we have not thoroughly investigated the nature of this increase, we hypothesize that it may be due to the combined effect of a reduction in surface acidity as a result of surface hydration via steam treatment *prior* to re-agglomeration of PEI inside the sorbent pores. As discussed below, the $N_2$ physisorption data suggest that PEI shifts inside the pores of the support at steam times of 90 minutes and greater, but not after the 5 minute exposure. However, the $^{27}$Al NMR data suggest a reduction in tetrahedral aluminum sites after 5 minutes of steaming, which may indicate a decrease in surface acidity.[9] These two combined phenomena may lead to the increase in capacity that is observed. After 90 minutes of continuous steam exposure the capacity of the material was nearly unchanged compared to that of the fresh sample. The sorbent was also exposed to steam in a cyclic fashion, where the material was subjected to 18 cycles of 5 minutes steam exposure followed by partial drying under inert $N_2$ flow (for a total of 90 minutes of cumulative

steam time). The capacity of the material after this cyclic treatment was slightly higher than that of the fresh sample, though within the expected experimental error limits of the adsorption system. The slight increase in surface area and decrease in amine loading, as evidenced in table 2, suggests that a small degree of amine leaching may have occurred during this testing, though a reduction in $CO_2$ capacity was not observed. Further decreases in the capacity after exposure to steam for 12 hours (1.62 mmol/g) and 24 hours (0.66 mmol/g) were observed. The significant decrease in $CO_2$ capacity of the sample exposed to steam for 24 hours is attributed to leaching of PEI out of the pores of the $\gamma$-alumina support. As can be seen from the data in Table 2, the amine loading of the sample decreased from ~ 8 mmol N/g to ~ 2 mmol N/g after this extensive steam treatment. Each of the other samples did not show such a decrease in amine loading. The amine efficiency of each of the samples ranged between 0.21 to 0.28 mol $CO_2$/mol N, with the highest value being that of the sample exposed to steam for 24 hours. This result is somewhat unexpected, since at moderate amine loadings amine efficiency typically increases with amine loading.[2] The slight increase here may be due to a reduction in surface acidity associated with hydration and subsequent formation of boehmite on the $\gamma$-alumina surface, as discussed in detail below.

Hammache *et al*[3] reported that PEI leaching did not occur in their similar studies using mesoporous silica as a support, though the longest steam exposure time tested was 5 hours in that study. Nonetheless, our data suggest that PEI leaching can occur over significantly longer timescales of steam exposure to $\gamma$-alumina supported PEI. Worth noting, however, is that it is difficult to extrapolate degrees of amine leaching from these

laboratory studies to what might occur in industrial scale operation of a sorbent. Factors such as contactor configuration, sorbent cycle steps, and steam flowrate and quality remain unexplored and may play an important role in promoting or reducing PEI leaching. Furthermore, extended continuous steam exposure is clearly impractical in a large scale operation, and is meant here to accelerate degradative mechanisms.

Table 2.2 Textural properties and $CO_2$ capacities of samples after exposure to steam.

| Sample | BET SA | Total PV[a] | Amine Loading[b] | $CO_2$ Capacity[c] | Amine Efficiency |
|---|---|---|---|---|---|
| | | | (per gram sorbent) | | |
| | $m^2/g$ | $cm^3/g$ | mmol N/g | mmol $CO_2$/g | mol $CO_2$/mol N |
| Fresh Sorbent | 38 | 0.17 | 7.81 | 1.71 | 0.22 |
| 5 Minute Steam | 37 | 0.17 | 7.95 | 1.96 | 0.25 |
| 1.5 Hour Steam | 46 | 0.17 | 8.33 | 1.73 | 0.21 |
| 1.5 Hour Steam - Cycled | 70 | 0.21 | 7.13 | 1.79 | 0.25 |
| 12 Hour Steam | 53 | 0.19 | 7.61 | 1.5 | 0.20 |
| 24 Hour Steam | 177 | 0.45 | 2.34 | 0.66 | 0.28 |

[a]Values estimated from total $N_2$ sorption at $p/p_0 = 0.99$. [b] Values estimated from elemental analysis. [c]Values estimated from humid adsorption experiments in the flow adsorption system at 50% RH, 30 $^{\circ}$C and 400 ppm $CO_2$.
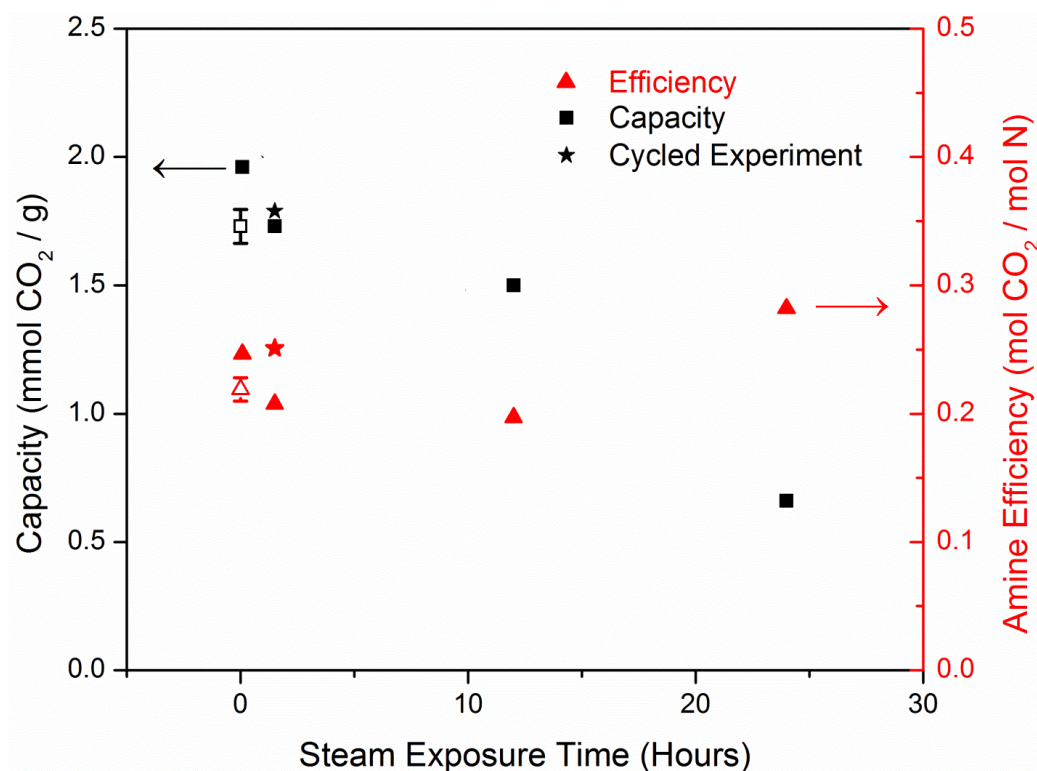
Figure 2.3 CO$_2$ capacities of sorbents after exposure to steam for various times. Capacities measured in the flow adsorption system at 30 $^o$C, 50% RH and 400 ppm CO$_2$/N$_2$. Open symbols are fresh sorbent capacity and efficiency values, while closed symbols are those after exposure to steam. Error bars on fresh sample capacity and efficiency are standard deviations calculated from initial capacity measurements on all samples.

### 2.3.3   XRD Experiments

To probe the potential for structural changes to the $\gamma$-alumina itself as a result of steaming, the materials were characterized with XRD following steam treatment. Mixtures of aluminum oxides, such as $\gamma$-alumina, and water at elevated temperatures are known to be thermodynamically unstable,[10–12] though the dynamics of phase transition are reported to be on the order of hours[12] for liquid water, and days[11] for water vapor. Figure 2.4 shows the XRD patterns of the materials after the steam exposure experiments,

as well as the pattern of the V250 pseudoboehmite precursor that was used in the preparation of the $\gamma$-alumina support used in this study. Relatively intense X-ray peaks associated with boehmite at $2\theta$ of 14.5, 28.2, 38.3, and 49 degrees are observed on the samples exposed to steam for 90 minutes or longer, while additional less intense peaks at $2\theta$ of 51.5, 55, 65, 72 degrees can be observed in the samples exposed to steam for 12 and 24 hours. The boehmite peaks in the patterns of the samples exposed to steam for 12 and 24 hours are quite intense compared to those on the samples exposed to steam for 90 minutes, indicating that further boehmite crystallization occurred with increasing steam exposure time. In each of the samples, the peaks at 46.5 and 66.5 degrees associated with $\gamma$-alumina are still present, indicating that on these timescales, full phase transition of the materials did not occur. This is further confirmed by $^{27}$Al MAS NMR experiments as discussed below. Notable is that the patterns of the samples exposed to steam for 90 minutes continuously and in cyclic fashion are nearly identical, in terms of relative intensities and the presence of boehmite peaks. This indicates that the cycling did not significantly change the dynamics or extent of boehmite formation on these materials compared to continuous exposure.
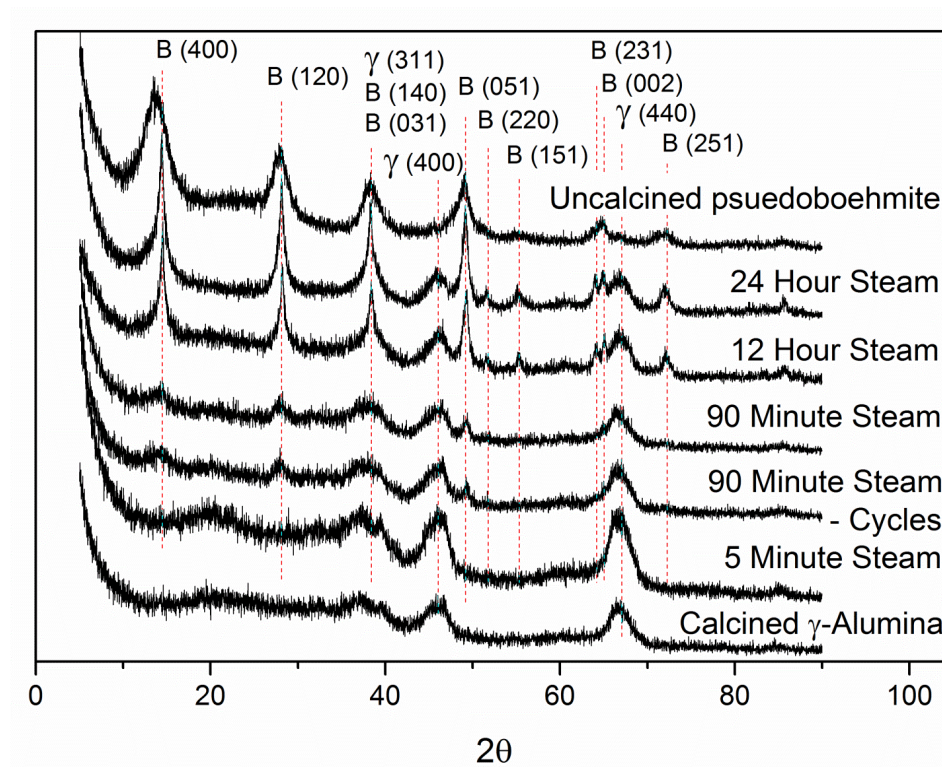
Figure 2.4 XRD patterns of the sorbents after exposure to steam for various times. Diffraction peaks are labeled according to species (B for boehmite and $\gamma$ for $\gamma$-alumina) with the corresponding species Miller index.

## 2.3.4 $^{27}$Al MAS NMR Experiments

To further investigate and quantify the phase transition from $\gamma$-alumina to boehmite during steam treatment, $^{27}$Al MAS NMR experiments were performed to probe the nature of aluminum atoms present in the samples. It is well established that $\gamma$-alumina contains aluminum atoms that are both tetrahedrally and octahedrally coordinated, with ~30% of the Al atoms present in tetrahedral form.[13,14] Boehmite, on the other hand, does not contain tetrahedral Al atoms.[14] By comparing relative amounts of tetrahedral and octahedral atoms, as determined by peak integration of $^{27}$Al NMR results, it is possible to estimate the amount of boehmite present in a sample.[12] Figure 2.5 shows the $^{27}$Al MAS

45

NMR results for each of the samples. For all of the samples, both the tetrahedral peak (67 ppm) and octahedral peak (6.6 ppm) are observed, though in different relative intensities. It is clear that the relative intensity of the tetrahedral peak decreases for samples exposed to steam for 90 minutes or longer compared to the fresh sample, consistent with the results from the XRD experiments.
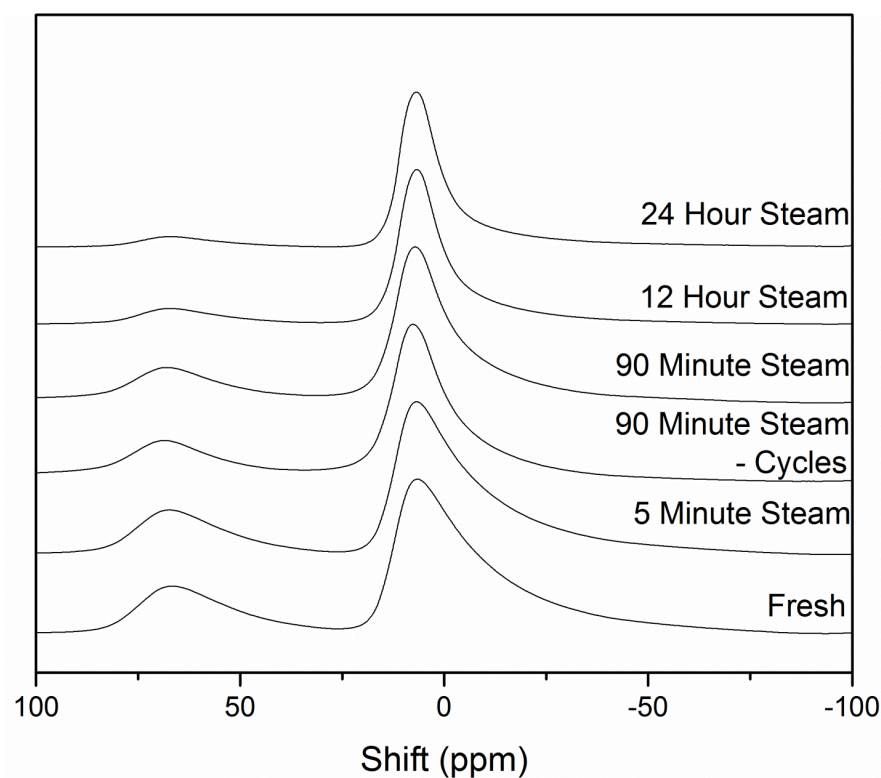


Figure 2.5 $^{27}$Al NMR spectra of samples after exposure to steam for various times. Tetrahedral aluminum peak at ~67 ppm and octahedral aluminum peak at ~7 ppm.

The peaks corresponding to tetrahedral and octahedral aluminum were integrated, and the ratio of the integrated area of the tetrahedral peak to those of the tetrahedral plus the octahedral peaks (percentage tetrahedral atoms) are shown in figure 2.6.
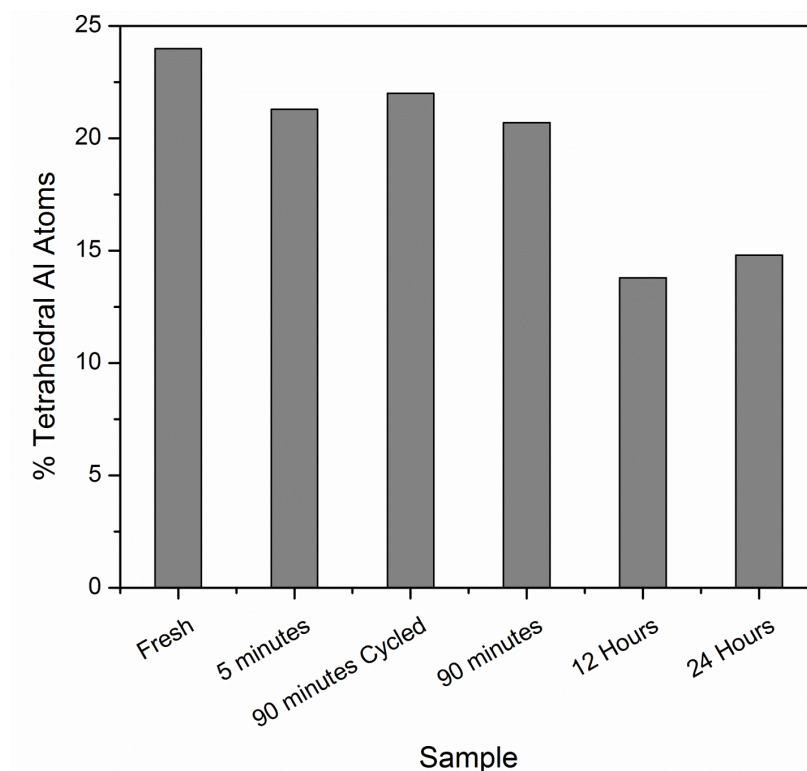
Figure 2.6 Percentage tetrahedral atoms; estimated by integration of $^{27}$Al NMR peaks associated with tetrahedral and octahedral atoms and taking the ratio of tetrahedral to total aluminum.

The fresh sample contained 24% tetrahedral atoms, slightly less than the ~30% that is normally reported. The samples exposed to steam for times between 5 minutes and 90 minutes, including the cycled experiment, appear to show a reduction in the relative amount of tetrahedral aluminum present in the samples. Interestingly, the sample exposed to steam for 5 minutes shows this reduction in tetrahedral aluminum content, but no peaks associated with boehmite are observed in the XRD patterns of the sample. This may be due to isolated tetrahedral aluminum atoms that are converted to octahedral coordination upon hydration,[15] but that have not been able to form large enough boehmite crystals to be observed in the XRD pattern. Further reduction in the tetrahedral aluminum

content is observed for the samples exposed to steam for 12 and 24 hours. Importantly, both of these samples show essentially equal quantities of tetrahedral aluminum atoms, which suggests that significant additional boehmite formation may not occur in hours 12-24 of steam treatment. Again, this is consistent with the XRD patterns of the samples, where the relative intensities of boehmite peaks are very similar for the 12 hour and 24 hour steamed samples. These data suggest a nonlinear dependence of steam exposure time on the rate of boehmite formation under the steam conditions and timescales tested, with significant boehmite formation occurring between hours 1.5 and 12 of steam treatment and very little boehmite formation occurring after 12 hours of steam treatment. It is hypothesized that this could be due to a difference in the rate of boehmite formation of surface aluminum atoms compared to those buried deeper inside the walls of the pore structure of the material. Aluminum atoms at the surface may undergo a rapid phase transition to boehmite at timescales between 1.5 and 12 hours, while those inside the pore walls take much longer to form crystalline boehmite under the conditions tested.

### 2.3.5 Sorbent Textural Properties

To probe changes to the textural properties of the sorbents, the $N_2$ physisorption profiles of the sorbents after exposure to steam were measured and are shown in Figure 2.7, while the total pore volumes and BET surface areas are reported in Table 2.2. The BET surface areas and total pore volumes of each of the samples remain nearly unchanged, aside from the 24 hour steamed sample, which showed an increase in both due to PEI leaching. The physisorption profiles for fresh sample and that exposed to steam for 5 minutes are nearly identical, suggesting that short exposure times do not

significantly change the porous characteristics of the sample. The profiles for the samples exposed to steam for 90 minutes, including the sample exposed to cyclic steam treatment, and 12 hours show qualitative differences in the hysteresis region of the isotherm, which is associated with capillary condensation and evaporation from mesopores.
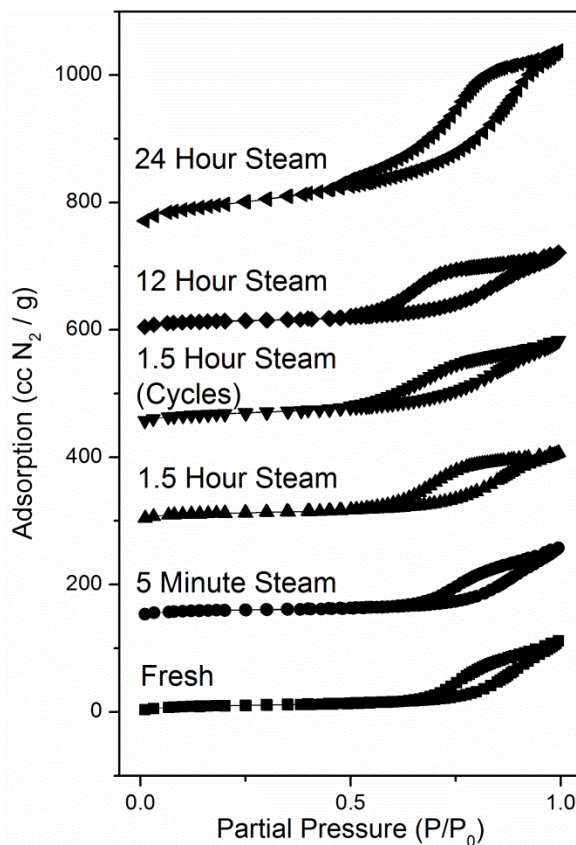


Figure 2.7 $N_2$ physisorption profiles at 77 K of samples exposed to steam for various times. Profiles offset by 150 $cm^3$/g.

The changes to the isotherms for the two 90 minute samples and the 12 hour sample in the hysteresis region suggest some change to the mesoporous character of these samples, induced by steam exposure. To clearly illustrate these qualitative observations, Figure 2.8 (top) shows the physisorption profiles of the fresh and 90 minute samples

overlaid. In the profiles for each of these samples, relative to the profile of the fresh sample, the $N_2$ adsorption at a given partial pressure in the region of capillary condensation is higher. This may be indicative of an effective decrease in the mesopore size. On the desorption branch of the isotherm, the onset of significant $N_2$ evaporation occurs at lower partial pressures for the steamed samples compared to the fresh sample. While it is much more difficult to draw direct inferences in qualitative changes to the desorption branch of a $N_2$ physisorption isotherm to a material property (as compared to changes in the adsorption branch), the desorption branch is thought of as being controlled by network characteristics of the mesoporous material.[16] However, it is unclear whether these changes are due to rearrangement of the aminopolymer in the pores of the support as a result of extended exposure to steam, or if the changes are a result of the phase change to boehmite that is observed in each of these samples.

Figure 2.8 (bottom) shows the physisorption profiles of the bare alumina before and after exposure to steam for 24 hours. The surface area of the material increased slightly after exposure to steam while the pore volume of the sample exposed to steam decreased. The increase in surface area is expected to be due to formation of small boehmite particles on the large $\gamma$-alumina surface.[12] The XRD pattern of the material, shown in Figure A.2 (Appendix A), confirms that boehmite did begin to form. Interestingly, the intensity of the boehmite peaks in the bare $\gamma$-alumina sample exposed to steam for 24 hours are less intense than those of the PEI impregnated sorbent exposed to steam for the same amount of time, and even are less intense than the PEI impregnated sample exposed to steam for 12 hours. This suggests that the presence of the PEI on the

50

surface may facilitate the phase transition in some manner. The hysteresis region of the two samples are qualitatively very similar, and do not appear to show the differences observed in the PEI impregnated sorbents discussed above. It is suggested, then, that the changes observed in the profiles of the composite sorbents are likely not due to the formation of boehmite, but are more likely attributable to physical rearrangement of the aminopolymer due to exposure to steam. Worth noting is that Hammache *et al*[3] suggested a steam induced polymer rearrangement as well, though they invoked this due to their observed reductions in surface areas and pore volumes of the sorbents after steam treatment.
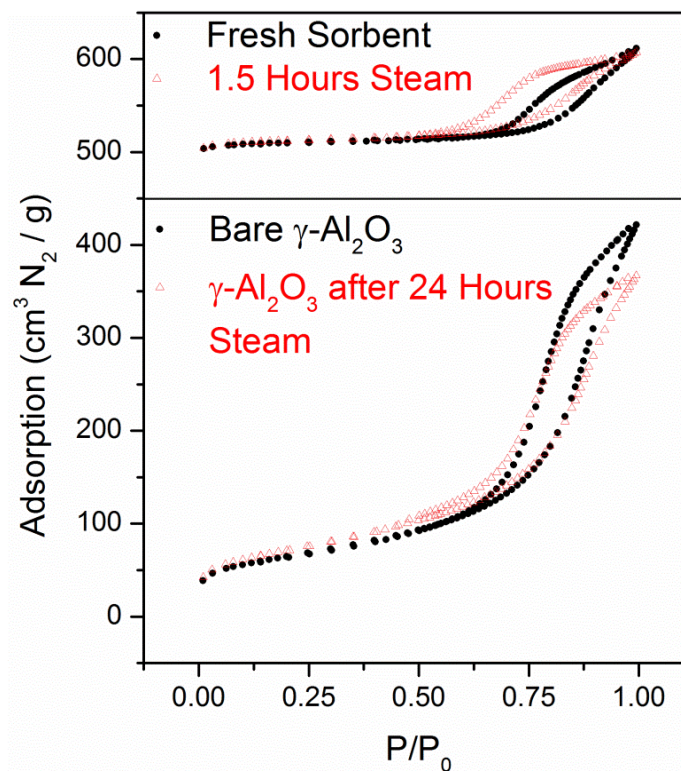


Figure 2.8 $N_2$ physisorption profiles of PEI containing sorbent (top) and bare $\gamma$-alumina support (bottom) before and after steam treatment. Sorbent profiles offset 500 $cm^3$/g.

### 2.3.6   FT-IR and FT-Raman Spectra

To probe whether the steam treatment induced any chemical change to the PEI, FT-IR and FT-Raman spectra were collected and are reported here in Figures 2.9 and 2.10, respectively. Previous studies on steam treatment of all three classes amines supported on silica, and exposed to an environment of static steam for 24 hours, showed no change in the FT-IR or FT-Raman spectra when oxygen was not present in the system.[4] As such, since oxygen was not expected to be present in the experiments reported here, no change was expected to be observed in the spectra for peaks associated with PEI.
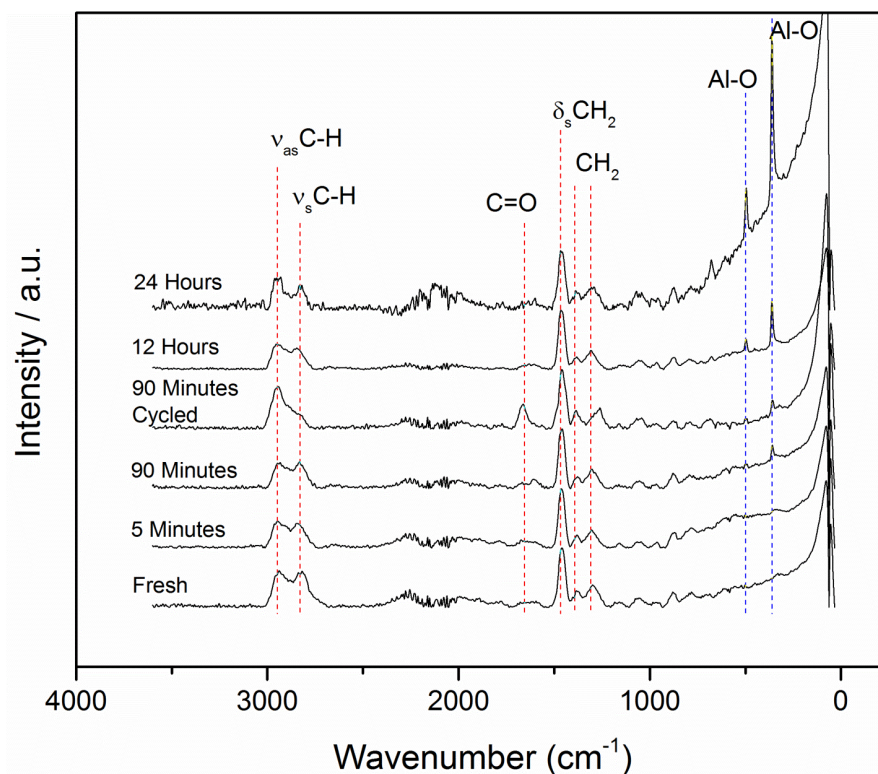


Figure 2.9 FT-Raman spectra of samples exposed to steam for various times. Red assignments are associated with organic moieties while blue assignments are associated with boehmite.
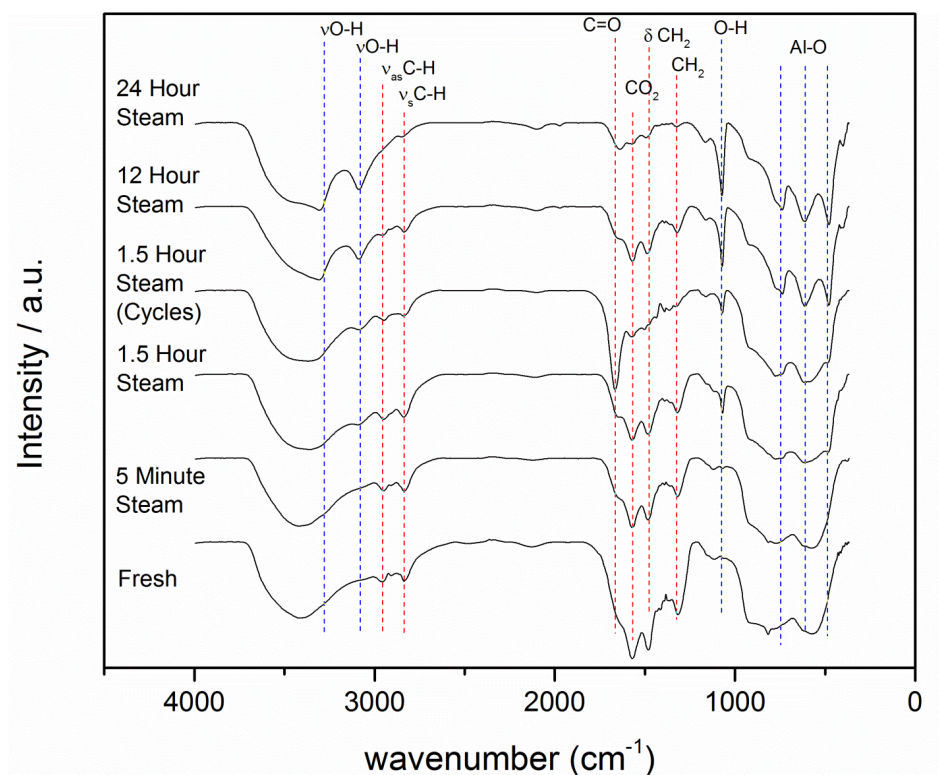
Figure 2.10 FT-IR spectra of samples exposed to steam for various times. Red assignments are associated with organic moieties while blue are associated with boehmite.

Both the FT-Raman and FT-IR spectra for each sample show the expected peaks associated with PEI, as well as the emergence of some new peaks associated with boehmite. The cycled sample shows a strong peak in both the FT-IR and the FT-Raman at 1667 cm$^{-1}$ associated with the carbonyl stretch of an amide group, which is likely due to oxidation of the PEI. This oxidation is attributed to an error in sample handling after completion of testing and not to the steam treatment itself, as the sample was left in the heated reactor overnight in the absence of an inert purge flow passing over it. This is explained further in the section A.3 of appendix A. In the FT-Raman spectra, peaks observed at 1460, 1390 and 1300 cm$^{-1}$ are associated with methylene motions.[17] In the

FT-IR spectra, peaks associated with methylene motions are observed at 1480 and 1310 $cm^{-1}$. An additional strong peak in the IR spectra at 1565 $cm^{-1}$ is due to chemisorbed $CO_2$ from the ambient environment.[18–22] Symmetric and antisymmetric C-H stretches from PEI are observed at 2950 and 2830 $cm^{-1}$ in both the FT-Raman and FT-IR spectra.[17] At steam times of 90 minutes and greater, peaks in the FT-Raman at 495 and 360 $cm^{-1}$ associated with Al-O stretches in boehmite begin become observable. Similarly, in the FT-IR spectra, an O-H stretching peak at 1070 $cm^{-1}$ is observed for steam times of 90 minutes and greater. At steam times of 12 and 24 hours, O-H stretches associated with boehmite at 3300 and 3080 $cm^{-1}$ are observed in the FT-IR spectra and the low wavenumber ($< 1000$ $cm^{-1}$) fingerprint region of the spectra shows the characteristic shape of boehmite.[6] As expected, there is no evidence in the spectra to suggest any degradation of the PEI, aside from the oxidation observed due to improper handling of the cycled sample. Small changes in the FT-Raman spectrum of the cycled sample in the region of the symmetric C-H stretch (2830 $cm^{-1}$) and one methylene motion (1460 $cm^{-1}$) have been observed in the spectra of other oxidized PEI samples supported on $\gamma$-alumina as well.[23]

## 2.3.7   Effect of Boehmite on $CO_2$ Adsorption Capacity

Since significant boehmite formation appears to occur in early timescales of steam treatment (relative to hundreds or thousands of hours of exposure in a large scale operation), and since boehmite formation is observed in the sample exposed to cyclic steam exposure, it can be inferred that a partial phase transition to boehmite may occur during large scale operation of the sorbents. Furthermore, it has recently been shown that

the composition of the mesoporous oxide support can have significant effects on the amine efficiency of PEI in $CO_2$ adsorption applications.[24,25] Thus, it is important to understand any impact this partial phase change may have on the properties of the sorbent, and its $CO_2$ capture performance.

To this end, the effect of the presence of boehmite on the mesoporous support of the sorbent on the amine efficiency of PEI was directly probed. Two analogous sets of materials were prepared at 4 weight loadings of PEI: 10%, 20%, 30% and 40%. In one set, PEI was impregnated into freshly calcined $\gamma$-alumina, similar to the sorbents discussed previously. In the other set, PEI was impregnated into $\gamma$-alumina that had been previously exposed to steam for 24 hours and had partially hydrated to boehmite. By preparing the samples in this fashion, the textural properties of each sorbent at a given weight loading were very similar. Worth noting is that the pore volume of the boehmite/alumina sample was completely filled at 40 wt% PEI while a small pore volume remained for the alumina sample at 40 wt% of PEI. The BET surface areas and total pore volumes of all the samples are shown in Table 2.3 and the physisorption profiles of the PEI impregnated materials are reported in Figure A.4 (appendix A). Because the textural properties of the sample sets were very similar at each PEI loading, it is expected that the primary difference between each sample set is the presence of boehmite on one and not the other. Pseudoequilibrium adsorption capacities were estimated for these samples by use of a TGA, using dry $CO_2$ adsorption at 400 ppm $CO_2$ in helium. The results of the study are shown in Figure 2.11, in which the calculated

amine efficiency of the PEI is plotted as a function of the weight percent of PEI in the

sorbent.
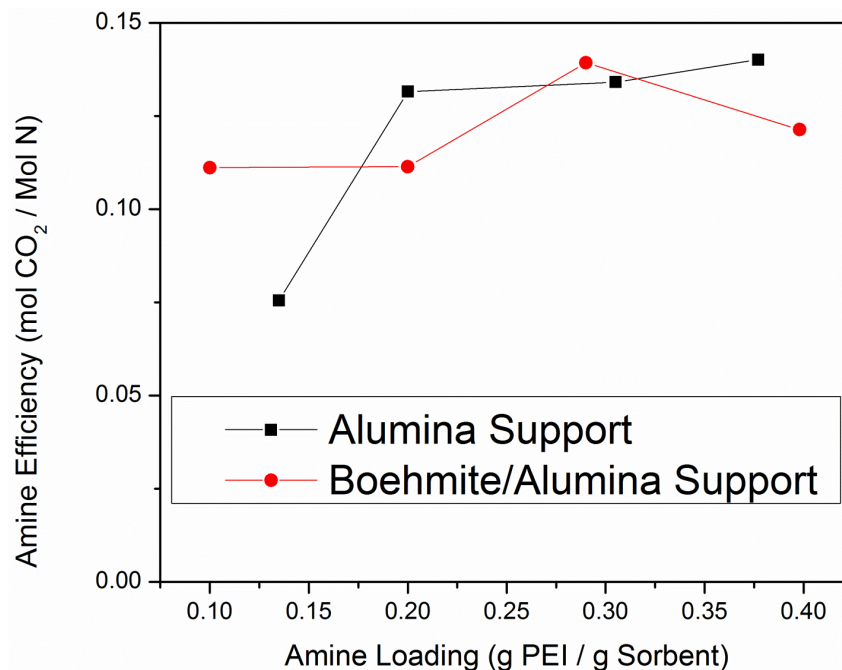


Figure 2.11 Amine efficiency as a function of amine loading of sorbents comprised of PEI supported on either pure γ-alumina or γ-alumina partially hydrated to boehmite.

Table 2.3 Textural properties, $CO_2$ capacities and amine efficiencies of materials used to evaluate the effect of boehmite on the amine efficiency of PEI.

| Sample | BET SA | Total PV[a] | Amine Loading[b] | CO$_2$ Capacity[c] | Amine Efficiency |
|---|---|---|---|---|---|
| | (per g sorbent) | | (per g sorbent) | | |
| | m$^2$/g | cm$^3$/g | mmol N/g | mmol CO$_2$/g | mol CO$_2$/mol N |
| Alumina 10 % | 131 | 0.39 | 3.1 | 0.24 | 0.08 |
| Alumina 20 % | 73 | 0.27 | 4.7 | 0.61 | 0.13 |
| Alumina 30 % | 19 | 0.12 | 7.1 | 0.95 | 0.13 |
| Alumina 40 % | 4.7 | 0.04 | 8.8 | 1.23 | 0.14 |
| Boehmite/Alumina 10 % | 138 | 0.43 | 2.3 | 0.26 | 0.11 |
| Boehmite/Alumina 20 % | 80 | 0.34 | 4.7 | 0.47 | 0.11 |
| Boehmite/Alumina 30 % | 27 | 0.16 | 6.7 | 0.89 | 0.14 |
| Boehmite/Alumina 40 % | 0.1 | 0.01 | 9.3 | 1.12 | 0.12 |

Both sample sets show a general trend of increasing amine efficiency with increasing weight loading of PEI, a trend that is expected at moderate levels of PEI incorporation and is typically associated with an increased amine proximity,[2] which is thought to be a necessary condition for CO2 adsorption in the absence of water. The slight decrease of amine efficiency at 40 wt% for the boehmite/alumina sample is likely due to complete pore filling with PEI, which induces severe CO2 diffusion limitation. No other obvious trend is evident from these data, leading to the conclusion that the presence of boehmite on the support does not significantly alter the ability of the PEI to adsorb CO2, at least from a thermodynamic standpoint. Worth noting is that at 30 weight % of PEI, the amine efficiencies of the samples are nearly identical. Because the sorbents discussed previously in the study were prepared at a weight loading of 30 wt% PEI, these data suggests that the formation of boehmite may not have played a direct role in altering the CO2 capacity of the material in the steam treatment experiments.

## 2.4    Conclusions

The $CO_2$ adsorption properties of PEI-impregnated alumina sorbents after exposure to flowing steam for various times were evaluated here. The as-synthesized sorbent was shown to have a high equilibrium $CO_2$ capacity of ~1.7 mmol/g at simulated air conditions. It was found that the $\gamma$-alumina support partially hydrated to form boehmite, an aluminum oxyhydroxide, at steam exposure times of 90 minutes and greater, including

in a sample exposed to cyclic steam exposure. XRD and $^{27}$Al NMR, experiments suggested that significant boehmite formation occurred between 90 minutes and 12 hours of steam exposure, but then the phase transformation slowed after 12 hours of steam exposure. It was shown that the presence of boehmite in the sorbent did not significantly affect the equilibrium $CO_2$ capacity of the PEI at simulated air capture conditions. Significant PEI leaching occurred in only the sample exposed to flowing steam for 24 continuous hours, and was primarily responsible for the observed reduction of $CO_2$ capacity for that sample, whereas the PEI content of the other sorbents remained unchanged. Subtle changes observed in the $N_2$ physisorption data for samples exposed to steam for times of 90 minutes and 12 hours were attributed to PEI rearrangement inside the pores of the support material during steam cycling.

## 2.5    References

(1)    Li, W.; Choi, S.; Drese, J. H.; Hornbostel, M.; Krishnan, G.; Eisenberger, P. M.; Jones, C. W. Steam-Stripping for Regeneration of Supported Amine-Based $CO_2$ Adsorbents. *ChemSusChem* **2010**, *3* (8), 899–903.

(2)    Bollini, P.; Didas, S. A.; Jones, C. W. Amine-Oxide Hybrid Materials for Acid Gas Separations. *J. Mater. Chem.* **2011**, *21* (39), 15100–15120.

(3)    Hammache, S.; Hoffman, J. S.; Gray, M. L.; Fauth, D. J.; Howard, B. H.; Pennline, H. W. Comprehensive Study of the Impact of Steam on Polyethyleneimine on Silica for $CO_2$ Capture. *Energy & Fuels* **2013**, *27*, 6899–6905.

(4)    Li, W.; Bollini, P.; Didas, S. A.; Choi, S.; Drese, J. H.; Jones, C. W. Structural Changes of Silica Mesocellular Foam Supported Amine-Functionalized $CO_2$ Adsorbents upon Exposure to Steam. *ACS Appl. Mater. Interfaces* **2010**, *2* (11), 3363–3372.

(5)    Chaikittisilp, W.; Kim, H.-J.; Jones, C. W. Mesoporous Alumina-Supported Amines as Potential Steam-Stable Adsorbents for Capturing $CO_2$ from Simulated Flue Gas and Ambient Air. *Energy & Fuels* **2011**, *25*, 5528–5537.

(6)    Wefers, K.; Misra, C. *Oxides and Hydroxides of Aluminum: Alcoa Laboratories Technical Report*; 1987.

(7)     Warren, B. E. X-Ray Determination of the Structure of Glass. *J. Am. Ceram. Soc.* **1934**, *17*, 249–254.

(8)     Drese, J. H.; Choi, S.; Lively, R. P.; Koros, W. J.; Fauth, D. J.; Gray, M. L.; Jones, C. W. Synthesis-Structure-Property Relationships for Hyperbranched Aminosilica $CO_2$ Adsorbents. *Adv. Funct. Mater.* **2009**, *19* (23), 3821–3832.

(9)     Coster, D.; Blumenfeld, A. L.; Fripiat, J. J. Lewis Acid Sites and Surface Aluminum in Aluminas and Zeolites: A High-Resolution NMR Study. *J. Phys. Chem.* **1994**, *98* (24), 6201–6211.

(10)    Laiti, E.; Persson, P.; Öhman, L.-O. Balance between Surface Complexation and Surface Phase Transformation at the Alumina/Water Interface. *Langmuir* **1998**, *14* (4), 825–831.

(11)    Laubengayer, A. W.; Weisz, R. S. A Hydrothermal Study of Equilibria in the System Alumina-Water. *J. Am. Chem. Soc.* **1943**, *65* (2), 247–250.

(12)    Ravenelle, R. M.; Copeland, J. R.; Kim, W.; Crittenden, J. C.; Sievers, C.; Peachtree, W.; Nw, S.; States, U. Structural Changes of Γ-Al2O3 -Supported Catalysts in Hot Liquid Water. *ACS Catal.* **2011**, *1*, 552–561.

(13)    John, C. S.; Alma, N. C. M.; Hays, G. R. Characterization of Transitional Alumina by Solid-State Magic Angle Spinning Aluminum NMR. *Appl. Catal.* **1983**, *6*, 341–346.

(14)   Zhou, R. S.; Snyder, R. L. Structures and Transformation Mechanisms of the Η, Γ and Θ Transition Aluminas. *Acta Crystallogr. Sect. B Struct. Sci.* **1991**, *47* (5), 617–630.

(15)   Wouters, B. H.; Chen, T.; Grobet, P. J. Reversible Tetrahedral-Octahedral Framework Aluminum Transformation in Zeolite Y. *J. Am. Chem. Soc.* **1998**, *120* (10), 11419–11425.

(16)   Thommes, M. Physical Adsorption Characterization of Nanoporous Materials. *Chemie Ing. Tech.* **2010**, *82* (7), 1059–1073.

(17)   Sanchez-Cortes, S.; Berenguel, R. M.; Madejón, A.; Pérez-Méndez, M. Adsorption of Polyethyleneimine on Silver Nanoparticles and Its Interaction with a Plasmid DNA: A Surface-Enhanced Raman Scattering Study. *Biomacromolecules* **2002**, *3* (4), 655–660.

(18)   Srikanth, C. S.; Chuang, S. S. C. Spectroscopic Investigation into Oxidative Degradation of Silica-Supported Amine Sorbents for $CO_2$ Capture. *ChemSusChem* **2012**, *5*, 1435–1442.

(19)   Khatri, R. A.; Chuang, S. S. C.; Soong, Y.; Gray, M. Thermal and Chemical Stability of Regenerable Solid Amine Sorbent for $CO_2$ Capture. *Energy & Fuels* **2006**, *196* (17), 1514–1520.

(20)    Ii, J. C.F.; Tanthana, J.; Chuang, S. S. C. Oxide-Supported Tetraethylenepentamine for $CO_2$ Capture. *Environ. Prog. Sustain. Energy* **2009**, *28* (4), 589–598.

(21)    Bacsik, Z.; Ahlsten, N.; Ziadi, A.; Zhao, G.; Garcia-Bennett, A. E.; Martín-Matute, B.; Hedin, N. Mechanisms and Kinetics for Sorption of $CO_2$ on Bicontinuous Mesoporous Silica Modified with N-Propylamine. *Langmuir* **2011**, *27* (17), 11118–11128.

(22)    Knofel, C.; Martin, C.; Hornebecq, V.; Llewellyn, P. L. Study of Carbon Dioxide Adsorption on Mesoporous Aminopropylsilane-Functionalized Silica and Titania Combining Microcalorimetry and in Situ Infrared Spectroscopy. *J. Phys. Chem. C* **2009**, *113*, 21726–21734.

(23)    Bali, S.; Chen, T. T.; Chaikittisilp, W.; Jones, C. W. Oxidative Stability of Amino Polymer–Alumina Hybrid Adsorbents for Carbon Dioxide Capture. *Energy & Fuels* **2013**, *27* (3), 1547–1554.

(24)    Kuwahara, Y.; Kang, D.-Y.; Copeland, J. R.; Bollini, P.; Sievers, C.; Kamegawa, T.; Yamashita, H.; Jones, C. W. Enhanced $CO_2$ Adsorption over Polymeric Amines Supported on Heteroatom-Incorporated SBA-15 Silica: Impact of Heteroatom Type and Loading on Sorbent Structure and Adsorption Performance. *Chem. Eur. J.* **2012**, *18* (52), 16649–16664.

(25)    Kuwahara, Y.; Kang, D.-Y.; Copeland, J. R.; Brunelli, N. A.; Didas, S. A.; Bollini, P.; Sievers, C.; Kamegawa, T.; Yamashita, H.; Jones, C. W. Dramatic

Enhancement of $CO_2$ Uptake by Poly(ethyleneimine) Using Zirconosilicate Supports. *J. Am. Chem. Soc.* **2012**, *134* (26), 10757–10760.

# CHAPTER 3

# INFLUENCE OF SUPPORT PROPERTIES ON AMINE

# EFFICIENCY OF SUPPORTED PEI

Parts of this chapter are adapted from 'Sakwa-Novak, M. A.; Holewinski, A.; Hoyt, C. B.; Yoo, C.-J.; Chai, S.; Dai, S.; Jones, C. W. Probing the Role of Zr Addition vs. Textural Properties in Enhancement of $CO_2$ Adsorption Performance in Silica/PEI Composite Sorbents. *Langmuir* **2015**, *31* (34), pp 9356–9365' with permission of The American Chemical Society.

## 3.1    Introduction & Motivation

Along with porous alumina, mesoporous silicas are regarded as particularly promising supports for creation of adsorbents for $CO_2$ capture applications when organic amine groups are incorporated into the pore space or onto the pore surface.[11,12] Mesoporous silicas with ordered pore structures, namely SBA-15 and MCM-41, have proven to be excellent model supports for amine groups, permitting controlled experiments to derive physical understanding of underlying phenomena governing the adsorption process.[13–19]

More broadly, ordered mesoporous oxides are an important class of porous materials that have shown promise in catalytic, adsorptive, drug delivery and other applications.[1,2] In particular, hexagonally ordered mesoporous silicas such as MCM-41 and SBA-15 have been extensively explored for use in such applications, as their textural

and morphological properties can be altered with a relatively high degree of control.[3–5] These materials can be tailored with a wide variety of functional moieties to tune the material activity and selectivity towards a desired result through a variety of synthetic strategies.[6–8] Additionally, these structured mesoporous materials have been extensively characterized and thus provide a well-defined model platform to study fundamental surface phenomena relevant to their suggested applications.[9,10]

In the case of physically impregnated amines, the textural and morphological nature of the host mesoporous silica is known to have an effect on the efficiency of the guest polyamines impregnated into the pore structure during $CO_2$ adsorption processes. In general, larger pore diameters, larger pore volumes and a higher degree of interconnectivity between pores are properties of the silica that have been shown to enhance such efficiencies. However, the underlying phenomena governing these observations are not fully understood. In 2008, Ahn and coworkers[20] prepared a set of materials with varying textural properties and compared the $CO_2$ capacities of the materials at 50 wt% PEI. Improvement in the capacity and kinetics of the materials correlated with the pore diameter of the bare oxide and not with the pore volume of the materials. Noteworthy is that some of the oxide materials in their study contained 2D pore systems while others contained 3D pore systems. This finding was corroborated by a recent study by Fan et al,[21] who reported adsorption-breakthrough experiments on materials comprised of PEI at 50 wt% supported on mesoporous silica of varying pore size but similar pore volume. Here, breakthrough capacities were higher for the materials with the larger pore size, and qualitative differences in the shapes of the breakthrough

65

curves of the materials with different pore sizes were observed. Both observations suggested that a smaller pore size induced kinetic limitations on $CO_2$ diffusion and adsorption into the impregnated PEI.

In contrast to these results, Yan et al[22] found that when tuning the synthesis of SBA-15 through an increased hydrothermal aging time and temperature to alter the pore size, pore volume and intrawall pores, increased $CO_2$ capacity was correlated with increased pore volume and not with increased pore size for adsorbents prepared with 50 wt% PEI. A similar conclusion was reached by Olah[23] and Rodrigues-Castellon[24], whereby in both studies a series of siliceous materials was prepared with systematically varying textural properties and, when impregnated with PEI, those with the highest pore volumes had higher $CO_2$ capacities at higher PEI loadings.

Supplementing these studies was a comprehensive report by Song[25] that showed that PEI impregnated into oxide supports with pores connected in a 3D network led to higher capacities (~20-100% improvement, depending on the specific materials and conditions) than those with 2D pore networks, especially at higher PEI loadings. Noteworthy is that this trend held true even when an oxide with a 2D network had larger pores and higher pore volume than an oxide with a 3D network. Additionally, in this report, SBA-15 was assumed to have a 2D pore network, though it is known that SBA-15 has intrawall micropores that create a 3D pore network of hierarchal pore size when synthesized using many recipes.[26,27] The effect of these intrawall micropores in SBA-15 on the efficiency of impregnated PEI was directly addressed by Yan et al,[28] who tuned the amount of intrawall porosity in SBA-15 by the systematic addition of NaCl to the

synthesis. Their data suggested that when PEI was impregnated at 6 mmol N / g, (~25 wt%) increases in $CO_2$ capacities correlated with decreased micropore volume of the oxide, and not with mesopore size or total pore volume. Additionally, the authors concluded that $CO_2$ uptake on the PEI impregnated material was correlated with the surface areas of the materials after PEI impregnation, suggesting perhaps that materials with less microporosity led to an improved dispersion of impregnated PEI. Finally, adding yet another dimension of importance, Sayari[29] showed that the pore length of SBA-15 was important in determining observed amine efficiencies of impregnated PEI, with shorter pores leading to more efficient $CO_2$ adsorption with impregnated PEI compared to longer pores.

The nature of the oxide surface has also been implicated to affect impregnated PEI. Sayari showed that hydrophobizing the surface of pore expanded MCM-41 resulted in increased adsorption efficiencies of impregnated PEI,[30,31] while Zhu et al showed a similar result for SBA-15.[32] It was demonstrated by our group that the incorporation of heteroatoms, such as zirconium, as isolated species in the siliceous framework of an SBA-15 silica induced significant increases in the efficiency of a physically impregnated PEI to adsorb $CO_2$ from dilute streams.[33,34] These heteroatoms increased the number of acidic and basic sites on the silica surface, and it was hypothesized that this change in surface chemistry may have caused the PEI to deposit differently on the surface in such a way as to more efficiently interact with $CO_2$. In that study, care was taken to ensure that the textural properties of the samples, specifically the surface area, pore volume, and mesopore size, were comparable across all heteroatom-incorporated and bare SBA-15

67

samples. Jaroniec also recently found that $CO_2$ capacities of zirconia-alumina-organosilica composites increased with the content of zirconia, though in that study amines were not utilized and $CO_2$ adsorption occurred on the oxide structure itself.[35]

In this contribution we have extended our analysis of doped SBA-15 / PEI composites as $CO_2$ adsorbents to include post-synthetic Zr incorporation and Zr incorporation onto an SBA-15 silica with improved textural and morphological properties. The incorporation of Zr by either synthetic (during the SBA-15 synthesis) or post-synthetic (on premade SBA-15) methods improved the amine efficiency of PEI when using an SBA-15 prepared by a 'standard' synthesis method, which included hydrothermal aging at 100 $^{\circ}$C. However, when an optimized SBA-15 silica was used as a support no enhancement in $CO_2$ capacity was observed when Zr was incorporated by either method. The optimized silica was prepared by careful choice of initial temperature, stirring conditions,[5] and a hydrothermal aging step at 130 $^{\circ}$C. The resulting material showed increased pore volume, pore size and primary particle size, reduced microporosity, and large, well defined particle morphology. Thus, previously reported improvements in $CO_2$ capacity for the Zr-doped SBA-15 aged at 100 $^{\circ}$C were, in part, due to alterations in the textural and morphological nature of the materials (induced by Zr incorporation) rather than surface properties. The enhancements were magnified in the standard SBA-15 but not in the SBA-15 with improved textural and morphological properties. This suggests that subtle textural properties play a more decisive role than the acid/base properties of the silicate surface in controlling PEI/$CO_2$ interactions.

## 3.2    Experimental

### 3.2.1    Materials

All chemicals were used as received from the supplier. Pluronics P123, tetraethyleorthosilicate (TEOS), poly(ethyleneimine) (PEI) aluminum chloride hexahydrate (AlCl$_3$ 8H$_2$O, 99%) were purchased from Sigma-Aldrich. Zirconyl chloride octahydrate was purchased from Acros. Sodium chloride (ACS grade) was purchased from EMD. Methanol (ACS grade) and HCl (fuming, ACS grade) were purchased from BDH chemicals. Tetramethylammonium hydroxide (TMAOH, 25 %wt aqueous solution, electronic grade) was purchased from Alfa Aesar.

### 3.2.2    SBA-15 Synthesis

SBA-15 was prepared according to two procedures, denoted in the text by the temperature of the hydrothermal treatment (100 $^o$C or 130 $^o$C), though there were other differences in the preparation as described below. *SBA15-100* was prepared in a similar manner to other reports from our group. Here, in a 2000 mL Erlenmeyer flask equipped with a stirring rod, 24 g of P123 was dissolved in an acidic mixture containing 636 g DI H$_2$O and 120 mL of concentrated HCl (37%) by allowing to stir at room temperature for 3h. Subsequently, 46.26 g of TEOS was added to the mixture by pipette and the flask was placed in an oil bath. A glass funnel was placed loosely over the top of the flask to act as a condenser. The temperature was increased to 40 $^o$C and the mixture was stirred at this temperature for 20h. Subsequently, the stir bar was removed and the temperature of the oil bath was raised to 100 $^o$C and maintained at that temperature for 24 hours. Finally, the

material was filtered, washed with copious amounts of DI $H_2O$ and dried overnight at 75 $^o$C. The template was removed by calcination of the material at 550 $^o$C for 10 h, using a ramp rate of 1.2 $^o$C/min, with an intermediate soak at 200 $^o$C for 1 h to remove residual water. *SBA15-130* was prepared in a 700 mL Berghof synthesis reactor equipped with an impeller to accommodate sealing the container during the 130 $^o$C hydrothermal treatment. Due to the volume limitation of the container, the synthesis was scaled down relative to SBA15-100. Here, 4 g of P123 was dissolved in an acidic mixture containing 129.4 g $H_2O$ and 20.57 g HCl (37%) at 35 $^o$C for 3h under stirring at 600 rpm (set by the impeller controller). Next, 8.5 g of TEOS was rapidly poured into the container and stirring was allowed to continue for 5 minutes, before the impeller controller was turned off. The container was then sealed shut, and the material was statically aged at 35 $^o$C for 20 h, followed by 130 $^o$C for 48 h. Finally, the material was filtered, washed, dried and calcined in the same manner as the SBA15-100 described above. All samples were stored in glass jars under ambient conditions prior to use.

### 3.2.3  Heteroatom Incorporation

Zirconia was incorporated into the SBA-15 via two methods; a 'synthetic' method, where zirconium chloride octahydrate ($ZrOCl_2$ $8H_2O$) was added during the synthesis just prior to the addition of TEOS and a 'post-synthetic' method, where Zr was deposited on pre-formed SBA-15 through an impregnation of $ZrOCl_2$ $8H_2O$. Additionally, aluminum was doped onto the SBA-15 post-synthetically via the same procedure but with aluminum chloride hexahydrate ($AlCl_3$ $6H_2O$) as the aluminum precursor. The synthetic Zr doping method was adapted to the different synthesis

procedures of SBA15-100 and SBA15-130; the synthetic Zr-SBA15-100 was prepared according to the procedure of SBA15-100 and synthetic Zr-SBA15-130 was prepared according to the procedure of SBA15-130.

"Synthetic" Zr Incorporation was adapted from previous reports from our group[46,47] but developed elsewhere.[49] Zr-SBA15-100 syntheses were carried in a 250 mL Erlenmeyer flask equipped with a stirring rod and loosely capped with a glass funnel to act as a condenser. In a given synthesis 3.0 g P123 and 1.77 g NaCl were dissolved in 120 mL DI $H_2O$ and stirred for 3h. Next, a given amount of zirconium chloride octahydrate ($ZrOCl_2$ $8H_2O$) was added, and subsequently 6.44 g TEOS was added by pipette. Zr was added according to expected Zr/Si molar ratios of 0.05, 0.10, 0.15 or 0.20, which corresponded to 0.5 g, 1 g, 1.5 g or 2 g of $ZrOCl_2$ $8H_2O$ in the synthesis. Zr-SBA15-130 syntheses were carried out in the same vessel as used for the parent SBA15-130 synthesis (700 mL Berghof reactor with impeller). Here, the quantity of materials used in the synthesis was the same as the synthetic Zr-SBA15-100 but the synthesis procedure was the same as the parent SBA15-130. The P123 (3g), NaCl (1.77g) and DI $H_2O$ (120g) were equilibrated at 35 $^{\circ}$C under stirring for 3h. Subsequently, $ZrOCl_2$ $8H_2O$ (0.5g or 1g) and TEOS (6.44g) were added and the solution stirred for 5m before the stirring was stopped and the solution allowed to age at 35 $^{\circ}$C for 20 h, followed by 130 $^{\circ}$C for 48 h. Finally, the material was filtered, washed, dried and calcined in the same manner as the SBA15-100 described above.

"Post Synthetic" Al and Zr Incorporation of Al and Zr onto SBA-15 was adapted from the procedure Auroux et al. for grafting of Al onto SBA-15.[50] SBA-15 was dried at 110

$^o$C overnight under high vacuum prior to use. A solution was prepared containing 10 mL of DI $H_2O$ and a given amount $AlCl_3$ $6H_2O$ or $ZrOCl_2$ $8H_2O$. To this solution, 2 molar equivalents of TMAOH solution were added (mol TMAOH / mol Al or Zr = 2). This solution was then placed in an oil bath at 70 $^o$C and stirred for 3h. Then, 1 g of dry SBA-15 was added to the solution and the resultant slurry mixed for 3h at 70 $^o$C. Then, the solution was filtered, washed with 100 mL DI $H_2O$ and dried overnight in a 75 $^o$C oven. Finally, the material was calcined at 500 $^o$C for 10h, with a 2.5 $^o$C/min ramp rate.

### 3.2.4 Adsorbent Preparation

Prior to PEI impregnation, all support materials (SBA-15) were dried at ~20 mtorr at ~100 $^o$C for 12-16 h. All adsorbents here were prepared at 30 wt% PEI. In a given adsorbent preparation, 0.25 g of SBA-15 was dispersed in 20 mL of MeOH. In a separate container, 0.107 g of PEI was dissolved in 10 mL of MeOH. The two mixtures were allowed to stir for 1 h to completely dissolve the PEI and fill the pores of the SBA-15 with MeOH. Then, the PEI containing solution was added by pipette to the SBA-15 containing solution and the mixture was allowed to stir for 3h. The solvent was then removed with rotary evaporation at ~50 $^o$C. Finally, the resulting adsorbent was dried under vacuum at ~20 mtorr and ~60 $^o$C for 12-16 h to remove adsorbed solvent. Samples were stored in vials under ambient conditions prior to use.

### 3.2.5 Characterization

<u>Organic Content of Materials</u> – TGA experiments were performed using a Netzch STA409PG and a flow of diluted air as the oxygen source. Organic content of the

materials was determined from weight loss in the 120 $^o$C – 900 $^o$C region of the TGA experiment. ~10-15 mg of material were used in a typical TGA experiment.

<u>CO$_2$ Adsorption</u> – Dry CO$_2$ capacities were estimated using TGA analysis under a flow of 400 ppm CO$_2$/N$_2$ using a TA Instruments Q500 instrument. In a given experiment, ~14 +/- 0.2 mg of sample was used. Samples were first pretreated under He flow at 110 $^o$C for 3h before cooling to 30 $^o$C under He and subsequently thermally equilibrating for 1h. Then, the gas flow (90 mL/min) was switched to 400 ppm CO$_2$/He and the sample was allowed to equilibrate for 12h.

<u>Elemental Analysis</u> – Zr and Si contents were measured at Galbraith Laboratories (Knoxville, TN) using the ME-70 procedure.

<u>SEM</u> – SEM images were taken on two microscopes. Figures 3.4 a-c and C.2 were taken on a Hitachi SU8010 at an accelerating voltage of 5 kV. Samples were prepared by depositing the sample on carbon tape and subsequently coating with gold sputter using a sputtering time of 60 s (Quorum Q150T). Figures 3.4d and S3 and S4 were recorded on a Zeiss Auriga Crossbeam, also at an acceleration voltage of 5 kV.

<u>TEM</u> – TEM images were acquired on an FEI Tecnai F30 field emission gun microscope. The accelerating voltage was 300keV. Samples were prepared by suspending the various silica powders in methanol at 5mg/mL via sonication and pipetting a droplet onto a formvar-coated Cu grid.

<u>N$_2$ Physisorption</u> – Nitrogen isotherms were collected at 77K on a Micromeritics Tristar II 3020. Samples were degassed at 110 $^o$C for 10-12h prior to each measurement. The BET method was applied for the calculation of surface areas using the MicroActive

software package while for pore size analysis the NLDFT equilibrium kernel for $N_2$ adsorption onto silica was employed via the Quantachrome VersaWin software package..

## 3.3     Results and Discussion

### 3.3.1    Impact of Zirconium Incorporation on SBA-15 Properties

SBA-15 was prepared according to two different synthesis procedures in order to generate materials of differing textural and morphological properties. The syntheses differed in several ways, including the containers and stirring devices that were used, the stirring time after the addition of TEOS to the P123 micelle template solution, and the hydrothermal aging treatment, where the material was either aged at 100 $^{\circ}$C for 24h or 130 $^{\circ}$C for 48h. Alteration of the hydrothermal treatment to longer time (48 h) and higher temperature (130 $^{\circ}$C) has been shown to reduce the intrawall porosity of the resultant material, by dehydrating the hydrophilic PEO corona of the surfactant micelles.[39] Control of the initial stirring conditions also tunes the morphology of the SBA-15 particles, with faster stirring generally resulting in larger particles (~10 fold increase) for a given temperature and micelle concentration.[5] For simplicity, materials prepared by the two methods are referred to throughout the text with reference to their hydrothermal aging temperature, as either SBA15-100 or SBA15-130. Figure 3.1 shows the $N_2$ physisorption profiles of SBA-15 prepared by both methods, as well as the resulting pore size distributions derived from the NLDFT equilibrium model for $N_2$ adsorption onto cylindrical pores of silica.

74
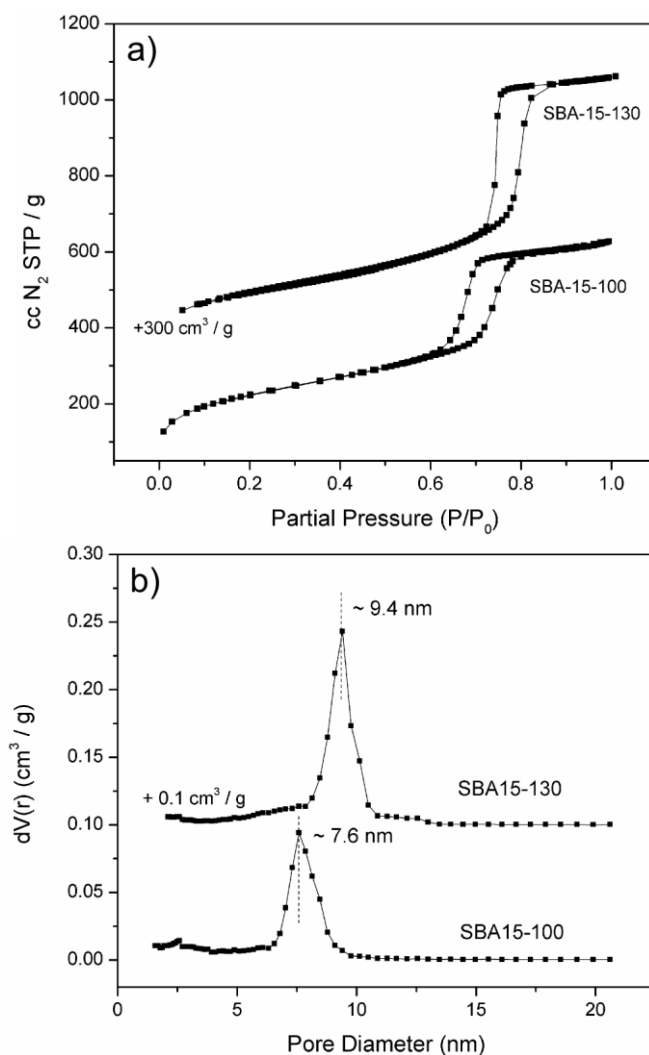
Figure 3.1 $N_2$ physisorption (a) and NLDFT pore size distributions (b) for parent SBA-15.

The SBA15-130 showed a higher pore volume and larger pore size (1.18 cm$^3$/g and 9.4 nm, respectively) compared to the SBA15-100 (0.97 cm$^3$/g and 7.6 nm). The surface area of the SBA15-130 was less than that of the SBA15-100, with corresponding values of 675 m$^2$/g and 804 m$^2$/g. Each of these differences are consistent with the expected dehydration of PEO chains in the P123 micelle, which has been shown to result

75

in materials with larger, but less numerous intrawall pores, compared to the SBA15-100.[9,39,40,51]

The incorporation of zirconium onto the different SBA-15 supports led to materials of differing textural properties, depending on the incorporation method utilized. Figure 3.2 shows the $N_2$ physisorption isotherms, NLDFT pore size distributions, and the corresponding cumulative pore size distributions, while table 3.1 contains the tabulated Zr content and textural properties of the resultant families of SBA15-100 and SBA15-130. The two incorporation methods are distinguished throughout the text as either 'synthetic' where Zr was added during the SBA-15 synthesis, or 'post-synthetic' where Zr was added to pre-synthesized SBA-15. In the synthetic method, the zirconium precursor, zirconium chloride octahydrate ($ZrOCl_2$ $8H_2O$), was added just prior to the addition of TEOS during the SBA-15 synthesis. This method of Zr incorporation was that used in prior studies from our group,[46,47] and is a 'self-acidifying' method, meaning that the pH of the P123/$H_2O$ solution is reduced only upon addition of the Zr precursor.[49] Both techniques were used to incorporate Zr onto SBA-15 prepared via the 100 $^o$C and 130 $^o$C synthesis methods, and each at two similar loadings of Zr. The synthetic Zr-SBA15-100 was prepared at four Zr loadings to reproduce the results of our previous studies.[46,47] Additionally, aluminum was post-synthetically added to SBA15-100, with the characterization presented in appendix B table B.1 and figure B.3. Such Al-SBA15 has been thoroughly characterized for acid/base properties in the literature and thus was chosen as a control material for this study. [50]
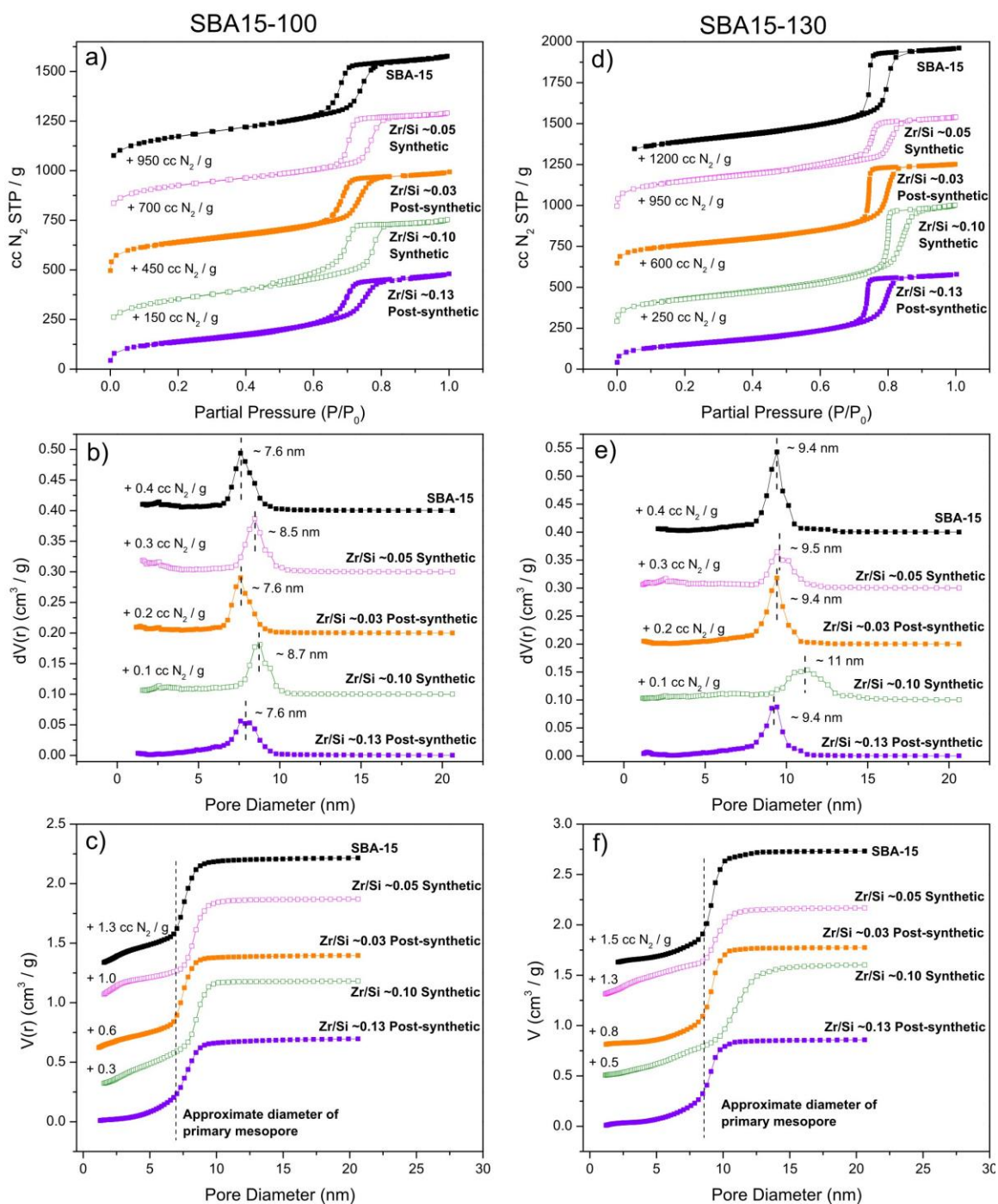
Figure 3.2. N$_2$ physisorption isotherms, NLDFT pore size distributions, and NLDFT cumulative pore size distributions of SBA15-100 (a-c) or SBA15-130 (d-f) during the synthesis and Zr-SBA-15 prepared by the synthetic (open squares) or post-synthetic (closed squares) methods.

The textural properties of the Zr-SBA15 materials differed relative to those of the parent SBA-15 to varying degrees for both the SBA15-100 and SBA15-130 families. Importantly, the nature of the changes in the textural properties of the Zr-SBA15 was dependent on the method of Zr incorporation used. Compared to the parent SBA-15 materials, synthetic Zr incorporation led to materials with very similar surface areas and pore volumes but slightly different mesopore sizes, as evident in the NLDFT PSDs shown in figures 3.2b and 3.2e. Conversely, post synthetic Zr incorporation led to materials with reduced surface areas and pore volumes, but unaltered mesopore sizes relative to the parent SBA-15. Additionally, the nature of the pores with diameters smaller than the primary mesopores (those running through the walls of the silica) was altered by the method of Zr incorporation as well as SBA-15 synthesis procedure, as noted above. Figure 3.2c shows the cumulative pore volume as a function of pore size for the family of SBA15-100 materials. There was significant pore volume resulting from these smaller pores, especially for the parent SBA15-100 and the synthetic Zr-SBA15-100's. Figure 3.2f shows the same data for the SBA15-130 set of samples. Here, the parent SBA15-130 had less pore volume resulting from pores with diameter below its primary mesopore size compared to the parent SBA15-100. For the both the synthetic Zr-SBA15-100 and Zr-SBA15-130, there were increases in the amount of intrawall pore volume relative to the parent SBA-15 samples, perhaps induced by the NaCl utilized in the synthesis. Conversely, for the post-synthetic Zr-SBA-15-100 and Zr-SBA15-130, there was a reduction in the intrawall pore volume. This was most pronounced for the Zr-SBA15-100 with Zr/Si ~ 0.1. It is hypothesized that this was due to filling of the smaller

pores and smoothing of the corrugated SBA-15 surface from the impregnation and

deposition of the Zr species during the post-synthetic procedure.

Table 3.1 Textural properties of SBA-15 samples with and without incorporated zirconium.

| Sample Name | Zr Incorporation Method | Synthesis Method 100/130 | Zr/Si Gel[a] mol/mol | Zr/Si[b] mol/mol | Surface Area[c] $m^2/g$ | Pore Volume[d] $cm^3/g$ | Pore Size[e] nm |
|---|---|---|---|---|---|---|---|
| *SBA15-100 Family of Supports* | | | | | | | |
| SBA15-100 | - | 100 | 0 | 0 | 804 | 0.97 | 7.6 |
| Zr05-SBA15-100-S | Synthetic | 100 | 0.05 | 0.05 | 804 | 0.92 | 8.5 |
| Zr10-SBA15-100-S | Synthetic | 100 | 0.10 | 0.10 | 736 | 0.93 | 8.7 |
| Zr15-SBA15-100-S | Synthetic | 100 | 0.15 | 0.15 | 608 | 0.47 | 5.1 |
| Zr20-SBA15-100-S | Synthetic | 100 | 0.20 | 0.20 | 520 | 0.35 | 5.1 |
| Zr03-SBA15-100-PS | Post Synthetic | 100 | 0.03 | 0.03 | 661 | 0.84 | 7.6 |
| Zr13-SBA15-100-PS | Post Synthetic | 100 | 0.13 | 0.13 | 489 | 0.74 | 7.6 |
| | | | | | | | |
| *SBA15-130 Family of Supports* | | | | | | | |
| SBA15-130 | - | 130 | 0 | 0 | 675 | 1.18 | 9.4 |
| Zr05-SBA15-130-S | Synthetic | 130 | 0.05 | 0.05 | 698 | 0.91 | 9.5 |
| Zr10-SBA15-130-S | Synthetic | 130 | 0.10 | 0.10 | 632 | 1.17 | 11.0 |
| Zr03-SBA15-130-PS | Post Synthetic | 130 | 0.03 | 0.03 | 563 | 1.01 | 9.4 |
| Zr13-SBA15-130-PS | Post Synthetic | 130 | 0.13 | 0.14 | 527 | 0.89 | 9.4 |

[a]Based on content of $ZrOCl_2$ and TEOS (or expected Si content of SBA-15) added during synthesis; [b]Measured by elemental analysis; [c]Estimated using BET method from $N_2$ physisorption data; [d]Estimated using total $N_2$ adsorption at $p/p_0 = 0.99$; [e]Derived from NLDFT equilibrium model for $N_2$ adsorption onto cylindrical silica pores

TEM images are shown in figure 3.3 for samples prepared by both SBA-15 synthesis methods and both Zr incorporation methods at a Zr/Si content of ~ 0.1. In all cases, the straight, parallel pores of SBA-15 can be observed. In the case of post-synthetic Zr-SBA15, dark spots were observed on the particles that were not present in the images of the synthetic Zr-SBA15 or the parent SBA15. These spots are attributed to agglomerates of $ZrO_2$ that precipitated during the synthesis and remained on the particle surface. The presence of agglomerates on the post-synthetic Zr-SBA15 materials is consistent with the deposition/pore filling hypothesis posed above, as smaller $ZrO_2$ particles may deposit into the small intrawall pores.
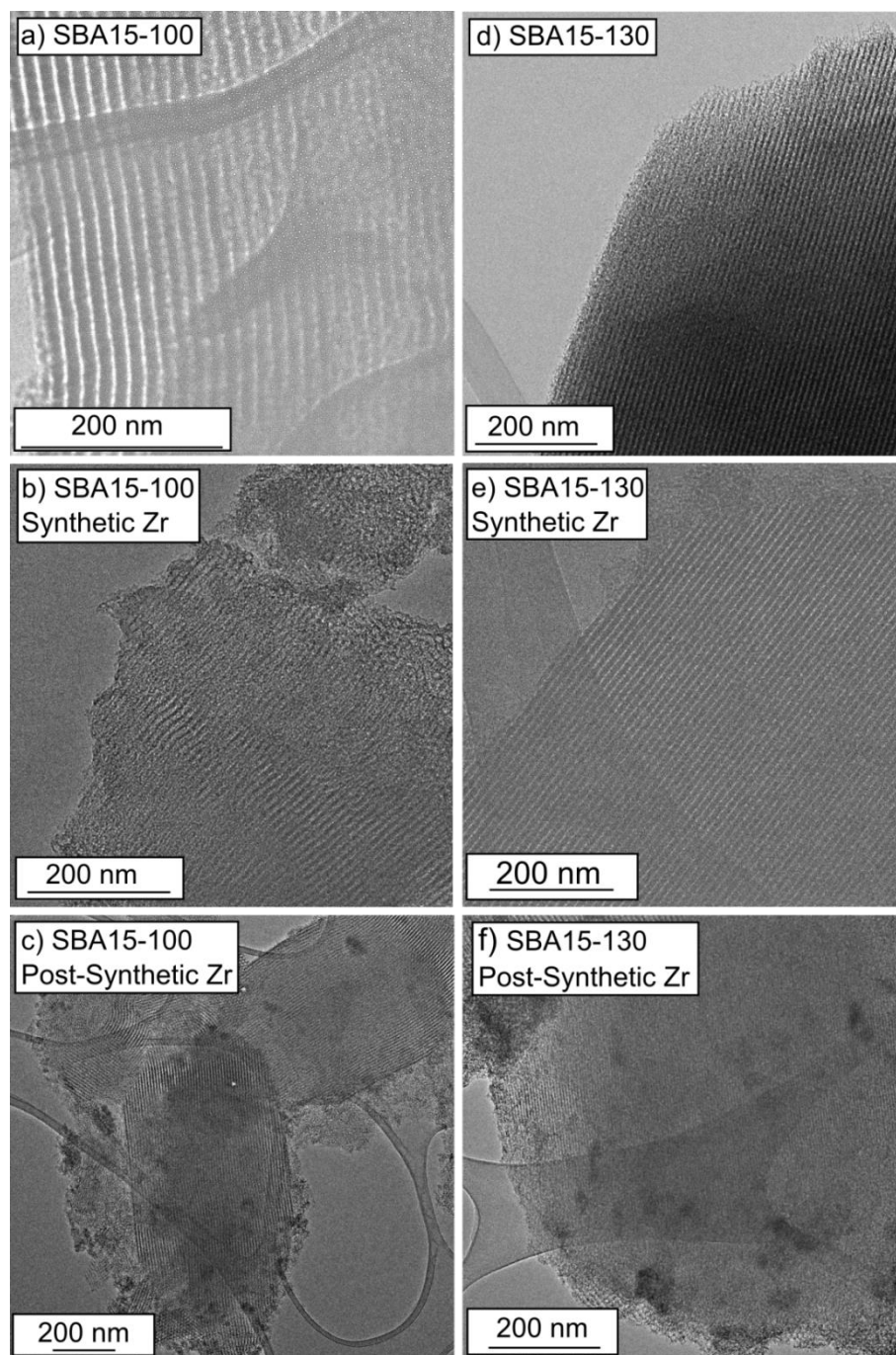
Figure 3.3 TEM images of materials prepared with the 100 $^{\circ}$C SBA-15 synthesis (a-c) and 130 $^{\circ}$C synthesis (d-f). Zr-SBA-15 materials are each at the ~0.1 Zr content for both the synthetic (middle row) and post-synthetic (bottom row) incorporation methods.

The various synthetic methods also impacted the macroscopic particle morphology of the SBA-15 materials. SEM images of the parent SBA-15 samples and synthetic Zr-SBA15 samples at Zr/Si ~ 0.1 are shown in figure 3.4. The images illustrate morphological differences both between the parent silicas and between each synthetic Zr-SBA15 derivative. The SBA15-100 had oval shaped particles that were less than a micron in diameter, while the SBA15-130 had much larger particles, with diameters of ~1-2 microns, most of which were hexagonal in shape. Unlike the pure SBA15-100, the synthetic Zr-SBA15-100 particles had a platelet-like morphology of high aspect ratio, with the diameter of the particles being ~ 1-4 micron and the thickness less than 1 micron. Such a morphology of SBA-15 has been previous observed upon the incorporation of Zr in synthesis,[52] though the Zr-SBA15 synthesis in that study differed by the presence of HCl in the P123 micelle template solution. The Zr-SBA15-130 also showed a deviation in morphology from the parent SBA15-130, clearly losing the distinct hexagonal features of the particles. However, the particles did not show as dramatic of a change to platelet like morphology like their SBA15-100 counterparts, instead taking on a more ill-defined shape with roughness on the particle surface—possibly due to agglomeration and sintering of smaller primary SBA-15 particles. As expected, post-synthetic Zr incorporation did not alter the morphology of the parent SBA-15. SEM images of synthetic Zr-SBA15-100 at Zr/Si ~0.05 and post-synthetic Zr-SBA15-100 at Zr/Si ~0.1 are shown in figures B.1 and B.2 of appendix B, respectively.
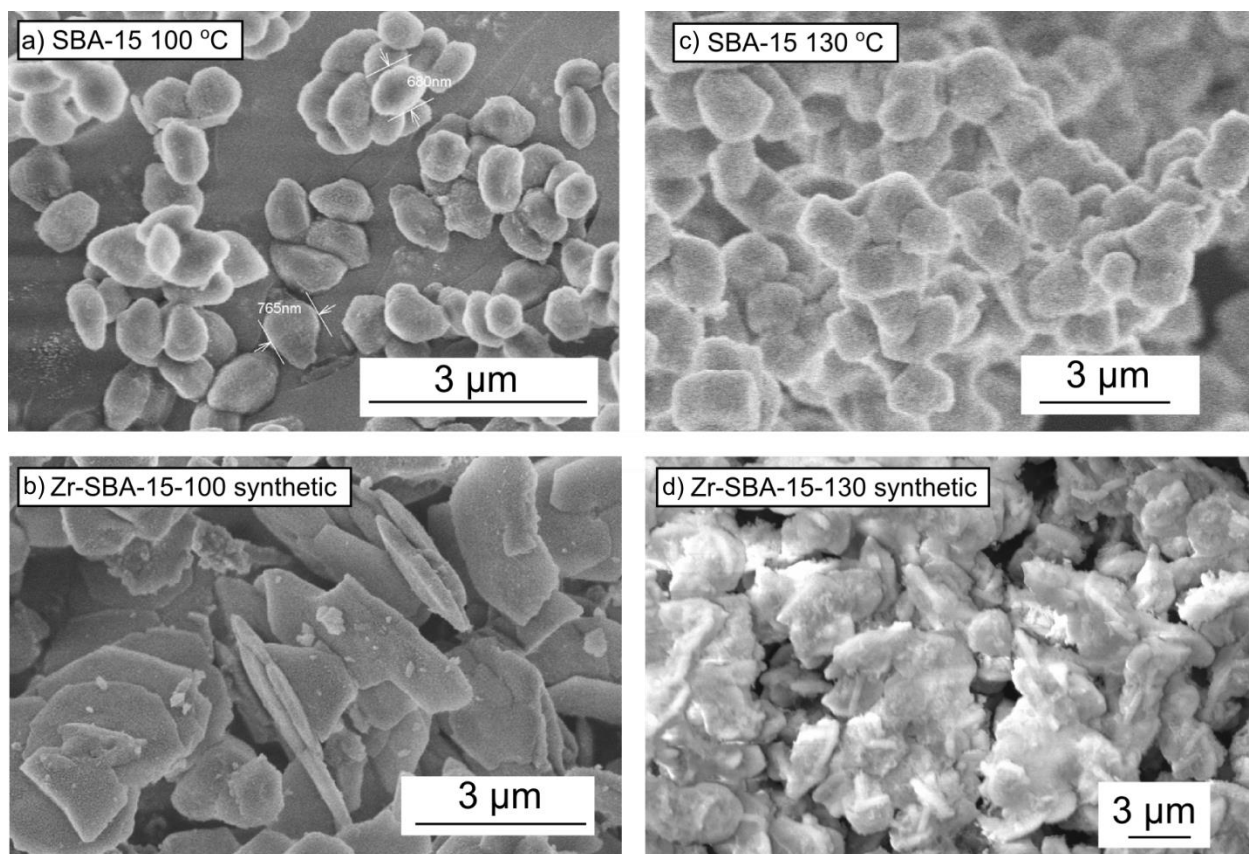
Figure 3.4 SEM images of parent SBA-15 (a,c) and Zr-SBA-15 (b,d) prepared at Zr/Si ~0.1 by the synthetic method.

Overall, the array of materials prepared here represents a set of supports for PEI incorporation having varying degrees of similarity in textural, morphological and surface properties. Synthetic Zr-SBA-15 allowed for the incorporation of Zr into the silica while keeping constant surface area and pore volume, at the expense of altered particle morphology and pore size. The post-synthetic Zr-SBA15 method allowed for the incorporation of Zr into the silica while keeping constant particle morphology and pore size, at the expense of altered surface area and pore volume. Additionally, the Zr in the synthetic technique was rigorously characterized in prior work to be solely isolated metal

species in the $SiO_2$ framework.[46,47] In contrast, the post-synthetic Zr incorporation was not subjected to such characterization, and the presence of agglomerates (noted in the TEM images), indicates that, at minimum, a significant portion the Zr in the post-synthetic materials was not atomically dispersed.

### 3.3.2   PEI Impregnation and $CO_2$ Adsorption

PEI was incorporated into each of the support materials at a common weight loading of 30%. This loading of PEI represents a moderate filling of the pores (~40%), and was the same weight content used in our prior work to investigate the effect of surface properties on $CO_2$ adsorption.[46,47] Figure 3.5 shows the $CO_2$ capacity, measured under 400 ppm $CO_2$ (simulated air concentration), of adsorbents prepared with SBA15-100 (5a) and SBA15-130 (5b) as supports. The capacities are shown as a function of Zr content and method of Zr incorporation. Additionally, the post-synthetic Al-SBA15-100 adsorbents are shown in figure 3.5a for comparison.
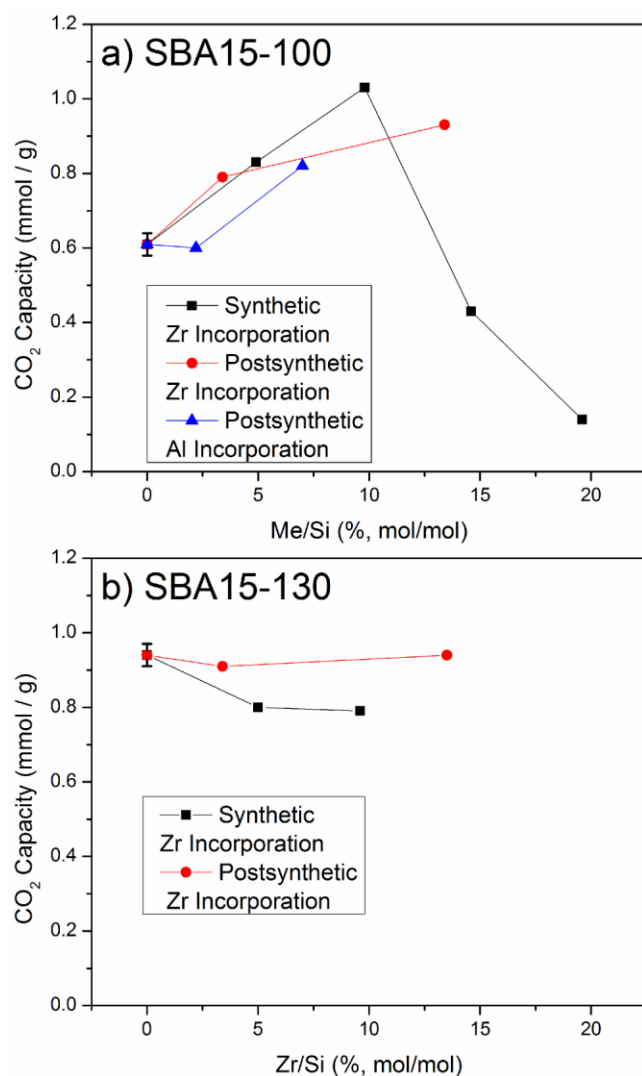
Figure 3.5. $CO_2$ capacities of SBA-15 materials impregnated with PEI at 30 weight % as a function of Zr loading. $CO_2$ capacities were measured at 400 ppm $CO_2$ at 30 $^{\circ}$C for 12h. Error bars estimated using multiple runs on Zr-free sample.

For the synthetic Zr-SBA15-100 supported set of materials, the $CO_2$ capacity increased from ~0.6 mmol/g (corresponding to an amine efficiency of 0.09 mol $CO_2$/mol N) and reached a maximum of 1.0 mmol / g (0.14 mol $CO_2$/mol N) at ~0.1 mol Zr/ mol Si before falling at higher Zr loadings, due to severely compromised textural properties of the support material, as shown in table 3.1. This trend was qualitatively similar to that

observed in our previous studies,[46,47] though to a lesser magnitude. The change in capacity for the post-synthetic Zr-SBA15-100 followed a similar trend, increasing as a function of loading to a similar maximum capacity value. Higher Zr content materials were not examined. In our previous study the addition of Zr on the SBA-15 via the synthetic method increased both the acidity and basicity of the SBA-15. The increase in capacity was hypothesized to have resulted from this surface modification, whereby the amphoteric surface may have helped to redistribute the PEI in a more efficient manner for $CO_2$ interaction in the pore.

Unlike the zirconated SBA15-100 materials, the adsorbents prepared with the SBA15-130 family of materials showed different adsorption characteristics upon addition of Zr. There was no increase in capacity of the post-synthetic Zr-SBA15-130 set, and an apparent decrease in the capacity of the synthetic Zr-SBA15-130. The parent SBA15-130 supported adsorbent had a higher capacity (0.94 mmol / g) than the parent SBA15-100, and importantly, the capacity of the parent SBA15-130 / PEI adsorbent was similar to the maximum observed in the Zr-SBA15-100 materials. As described above, compared to the SBA15-100, the SBA15-130 had a higher pore volume, larger pore size, a lower intrawall pore volume, and a larger particle size. It is well established that increases in pore size and pore volume result in increased amine efficiency of impregnated PEI, while it is less well understood what effect the smaller, intra-wall pores or particle morphology have. We thus ascribe the higher $CO_2$ capacity of the SBA15-130 to the improved properties of the mesopore structure relative to the SBA15-100. Upon addition of Zr by either the synthetic or post-synthetic methods, the capacity of the SBA15-130 material did not

increase. These data clearly indicate that doping of Zr on SBA-15 to increase the $CO_2$ adsorption characteristics of impregnated PEI is not a universally applicable methodology at the given PEI content. This result led us to reexamine our initial hypothesis that Zr has an inherent effect on improving PEI efficiency independent of the alterations in the textural and morphological properties induced by the doping.

We posit that two of the physical alterations to the SBA-15 resulting from the Zr doping may have contributed to the increased efficiency of the PEI in adsorbing $CO_2$. For the synthetic Zr-SBA15-100, it is hypothesized that the drastic change to the particle morphology from oval shaped particles to platelet shaped particles, was a contributing factor to the observed increase in $CO_2$ capacity. Such has been shown previously to increase the amine efficiency of impregnated PEI due to the shortening of the SBA-15 pores.[42] For the post-synthetic Zr-SBA15-100, it is hypothesized that the deposition and subsequent filling of the smaller intrawall pores by the Zr contributed to the improved performance. These smaller pores, which are not expected to be prevalent in the SBA15-130 materials as argued above, contribute to an effective roughness of the silica surface, increasing the local surface area. Partial filling of these pores by Zr and the subsequent reduction in surface area, as observed upon post-synthetic Zr incorporation, would reduce the amount of PEI interacting with rough pore walls and in mouths of the smaller pores. Since the effect that these pores have on the efficiency of impregnated amines in $CO_2$ adsorption experiments has been explicitly studied only to a limited degree, a full elucidation of their effect remains an open question. It is thus reasonable to hypothesize that some amount of impregnated PEI may adsorb in the mouths of these micropores and

thus become inaccessible to $CO_2$. Filling of the pores or smoothing of the wall with Zr or another material would reduce the amount of PEI 'lost' in these smaller pores, resulting in improved capacity. This hypothesis is supported by adsorption data for post-synthetically doped Al-SBA15-100 based adsorbents, shown in figure 3.5a. These samples showed an increase in capacity only at the higher Al content, where the capacity increase was similar to that of the post-synthetic Zr-SBA15 at a similar heteroatom loading (~5%). Importantly, as shown in table B.1 of the appendix B, the loss in pore volume of the post-synthetic Al-SBA15 was similar to that of the Zr-SBA15 sample at the metal loading of ~5% (shown in table 3.1), suggesting that the Al filled a similar amount of the intra-wall pores, correlating qualitatively with the trend in $CO_2$ capacities.

### 3.3.3 Zirconated SBA-15 with Controlled Morphology

To assess the hypothesis that particle morphology contributed to the observed increase in $CO_2$ capacity of the supported PEI in Zr-SBA15-100, an attempt was made to prepare synthetic Zr-SBA15-100 without significantly altering the morphology of the material relative to the parent SBA15-100. SBA-15 is formed kinetically from the condensation of silicon containing precursors around polymeric micelles in acidic solution. The synthesis conditions in the time just after the addition of the silicon precursor can be very important in the formation and final properties of the material.[53] While we did not extensively explore or rigorously elucidate the effects of various conditions early in the Zr-SBA15 synthesis on the particle morphology, synthetic Zr-SBA15 at Zr/Si contents of 0.05 and 0.1 with ellipsoidal particle morphology (similar to native SBA15 samples) were successfully prepared. The primary difference in the

88

synthesis between these materials and the set described above was the temperature at which the Zr and TEOS were added to the mixture. For the synthetic Zr-SBA15-100 materials described above, the $ZrOCl_2$ $8H_2O$ and TEOS were sequentially added while the $P123/H_2O/NaCl$ solution was at room temperature. After addition, the mixture was placed in an oil bath and the temperature was increased to 40 $^o$C. For the synthetic Zr-SBA15-100 materials described in this section, the P123/H2O/NaCl solution was pre-equilibrated at 40 $^o$C, and the $ZrOCl_2$ $8H_2O$ and TEOS were subsequently added. An SEM image of the resultant material at a Zr/Si of 0.1 is presented in figure B.4 of appendix B, showing that the particles were ellipsoidal in shape, similar to the parent SBA15-100. $N_2$ physisorption isotherms of the ellipsoidal Zr-SBA-15 materials are presented in figure B.5 of appendix B. Figure 3.6 shows the $CO_2$ capacity of the ellipsoidal Zr-SBA15-100 materials when impregnated with PEI at 30 wt%, along with the synthetic Zr-SBA15-100 materials described above as having platelet-like morphology, for comparison. Here, the materials are denoted by their morphology as either 'platelet' or 'ellipsoidal' Zr-SBA-15.
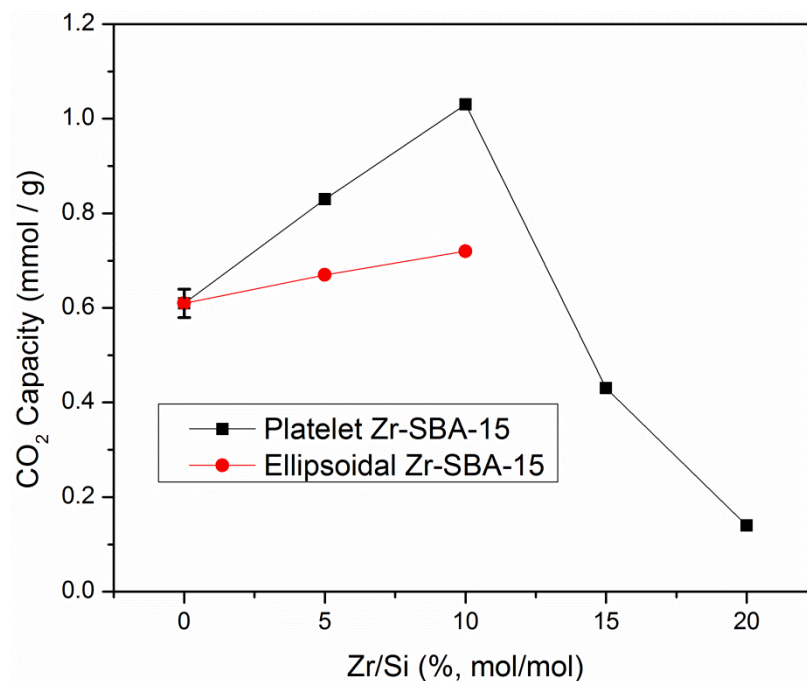
Figure 3.6. $CO_2$ capacities of synthetically doped Zr-SBA-15 / PEI adsorbents at 30 weight % PEI with differing morphology of SBA-15. $CO_2$ capacities were measured at 400 ppm $CO_2$ at 30 $^{\circ}$C for 12h. Error bars estimated using multiple runs on Zr-free sample.

The capacity of the ellipsoidal Zr-SBA15-100 adsorbents increased as a function of Zr content in the support, but to a much more moderate degree compared to the original set. While the textural properties of these ellipsoidal Zr-SBA15-100 set of materials differed from the parent SBA15-100 to a larger degree than the platelet Zr-SBA15-100 set of materials, the capacities here are interpreted as representing the underlying effect of zirconia on PEI in the SBA-15, which is much less than originally postulated.[46,47] All together, the results presented here underlie the dominant importance of support textural properties compared to surface acid/base character in the creation of supported PEI $CO_2$ adsorbents.

### 3.4 Conclusions

SBA-15 was prepared according to two synthesis procedures, with the resulting materials differing in textural and morphological properties. Zirconium was doped onto the materials via two methods, either during or after the SBA-15 synthesis, and the textural and morphological properties of the resultant Zr-SBA15 materials were altered in ways that depended on the method of Zr incorporation. When these materials were used as supports for PEI in $CO_2$ adsorption experiments at a common PEI loading of 30 wt%, the changes in $CO_2$ capacity were dependent on the method of SBA-15 synthesis, but not on the method of Zr incorporation. The SBA-15 prepared with higher pore volume, larger mesopores and less intra-wall pores had a higher $CO_2$ capacity (0.95 mmol / g) when impregnated with PEI compared to the SBA-15 support prepared via the 'standard' method (0.61 mmol / g). Incorporation of Zr into the larger-pore SBA-15 support did not result in increased $CO_2$ capacities when PEI was impregnated. Conversely, the incorporation of Zr into the standard SBA-15 support resulted in increased capacities by a maximum of ~60%, regardless of the Zr incorporation method. However, comparison of the Zr-doped materials derived from both parent SBA15's revealed that alterations to the particle morphology and intrawall pore volume were major contributing factors to increased capacity on the less optimal material family. These results highlight the complexity and importance of the interconnection between surface properties, pore properties, and particle morphology on the efficiency of impregnated PEI in $CO_2$ adsorption performance.

## 3.5 References

(1)     Choi, S.; Drese, J. H.; Jones, C. W. Adsorbent Materials for Carbon Dioxide Capture from Large Anthropogenic Point Sources. *ChemSusChem* **2009**, *2* (9), 796–854.

(2)     Bollini, P.; Didas, S. A.; Jones, C. W. Amine-Oxide Hybrid Materials for Acid Gas Separations. *J. Mater. Chem.* **2011**, *21* (39), 15100–15120.

(3)     Didas, S. A.; Sakwa-Novak, M. A.; Foo, G. S.; Sievers, C.; Jones, C. W. Effect of Amine Surface Coverage on the Co-Adsorption of $CO_2$ and Water: Spectral Deconvolution of Adsorbed Species. *J. Phys. Chem. Lett.* **2014**, *5*, 4194–4200.

(4)     Serna-Guerrero, R.; Da'na, E.; Sayari, A. New Insights into the Interactions of $CO_2$ with Amine-Functionalized Silica. *Ind. Eng. Chem. Res.* **2008**, *47* (23), 9406–9412.

(5)     Alkhabbaz, M. A.; Bollini, P.; Foo, G. S.; Sievers, C.; Jones, C. W. Important Roles of Enthalpic and Entropic Contributions to $CO_2$ Capture from Simulated Flue Gas and Ambient Air Using Mesoporous Silica Grafted Amines. *J. Am. Chem. Soc.* **2014**, *136*, 8–11.

(6)     Bollini, P.; Brunelli, N. A.; Didas, S. A.; Jones, C. W. Dynamics of $CO_2$ Adsorption on Amine Adsorbents. 2. Insights Into Adsorbent Design. *Ind. Eng. Chem. Res.* **2012**, *51*, 15153–15162.

(7)     Zeleňák, V.; Badaničová, M.; Halamová, D.; Čejka, J.; Zukal, a.; Murafa, N.; Goerigk, G. Amine-Modified Ordered Mesoporous Silica: Effect of Pore Size on Carbon Dioxide Capture. *Chem. Eng. J.* **2008**, *144* (2), 336–342.

(8)     Sanz, R.; Calleja, G.; Arencibia, A.; Sanz-Pérez, E. S. Amino Functionalized Mesostructured SBA-15 Silica for $CO_2$ Capture: Exploring the Relation between the Adsorption Capacity and the Distribution of Amino Groups by TEM. *Microporous Mesoporous Mater.* **2012**, *158*, 309–317.

(9)     Sayari, A.; Belmabkhout, Y. Stabilization of Amine-Containing $CO_2$ Adsorbents: Dramatic Effect of Water Vapor. *J. Am. Chem. Soc.* **2010**, *132* (18), 6312–6314.

(10)    Ren, Y.; Ma, Z.; Bruce, P. G. Ordered Mesoporous Metal Oxides: Synthesis and Applications. *Chem. Soc. Rev.* **2012**, *41* (14), 4909–4927.

(11)    Davis, M. E. Ordered Porous Materials for Emerging Applications. *Nature* **2002**, *417*, 813–821.

(12)    Kresge, C. T.; Leonowicz, M. E.; Roth, W. J.; Vartuli, J. C.; Beck, J. S. Ordered Mesoporous Molecular Sieves Synthesized by a Liquid-Crystal Template Mechanism. *Nature* **1992**, *359*, 710–712.

(13)    Zhao, D.; Feng, J.; Huo, Q.; Melosh, N.; Fredrickson, G.; Chmelka, B.; Stucky, G. Triblock Copolymer Syntheses of Mesoporous Silica with Periodic 50 to 300 Angstrom Pores. *Science (80-. ).* **1998**, *279*, 548–552.

(14)     Lee, H. I.; Kim, J. H.; Stucky, G. D.; Shi, Y.; Pak, C.; Kim, J. M. Morphology-Selective Synthesis of Mesoporous SBA-15 Particles over Micrometer, Submicrometer and Nanometer Scales. *J. Mater. Chem.* **2010**, *20* (39), 8483–8487.

(15)     Ford, D. M.; Simanek, E. E.; Shantz, D. F. Engineering Nanospaces: Ordered Mesoporous Silicas as Model Substrates for Building Complex Hybrid Materials. *Nanotechnology* **2005**, *16* (7), S458–S475.

(16)     Van Der Voort, P.; Esquivel, D.; De Canck, E.; Goethals, F.; Van Driessche, I.; Romero-Salguero, F. J. Periodic Mesoporous Organosilicas: From Simple to Complex Bridges; a Comprehensive Overview of Functions, Morphologies and Applications. *Chem. Soc. Rev.* **2013**, *42*, 3913–3955.

(17)     Kumar, P.; Guliants, V. V. Periodic Mesoporous Organic-Inorganic Hybrid Materials: Applications in Membrane Separations and Adsorption. *Microporous Mesoporous Mater.* **2010**, *132*, 1–14.

(18)     Kruk, M.; Jaroniec, M.; Ko, C. H.; Ryoo, R. Characterization of the Porous Structure of SBA-15. *Chem. Mater.* **2000**, *12* (7), 1961–1968.

(19)     Kärger, J.; Valiullin, R. Mass Transfer in Mesoporous Materials: The Benefit of Microscopic Diffusion Measurement. *Chem. Soc. Rev.* **2013**, *42* (9), 4172–4197.

(20)    Son, W.-J.; Choi, J.-S.; Ahn, W.-S. Adsorptive Removal of Carbon Dioxide Using Polyethyleneimine-Loaded Mesoporous Silica Materials. *Microporous Mesoporous Mater.* **2008**, *113*, 31–40.

(21)    Wang, L.; Yao, M.; Hu, X.; Hu, G.; Lu, J.; Luo, M.; Fan, M. Amine-Modified Ordered Mesoporous Silica: The Effect of Pore Size on $CO_2$ Capture Performance. *Appl. Surf. Sci.* **2015**, *324*, 286–292.

(22)    Yan, X.; Zhang, L.; Zhang, Y.; Yang, G.; Yan, Z. Amine-Modified SBA-15 : Effect of Pore Structure on the Performance for $CO_2$ Capture. *Ind. Eng. Chem. Res.* **2011**, *50*, 3220–3226.

(23)    Zhang, H.; Goeppert, A.; Czaun, M.; Prakash, G. K. S.; Olah, G. A. $CO_2$ Capture on Easily Regenerable Hybrid Adsorbents Based on Polyamines and Mesocellular Silica Foam. Effect of Pore Volume of the Support and Polyamine Molecular Weight. *RSC Adv.* **2014**, *4* (37), 19403–19417.

(24)    Vilarrasa-Garcia, E.; Moya, E. M. O.; Cecilia, J. A.; Cavalcante, C. L.; Jiménez-Jiménez, J.; Azevedo, D. C. S.; Rodríguez-Castellón, E. $CO_2$ Adsorption on Amine Modified Mesoporous Silicas: Effect of the Progressive Disorder of the Honeycomb Arrangement. *Microporous Mesoporous Mater.* **2014**, *209*, 172–183.

(25)    Wang, D.; Wang, X.; Ma, X.; Fillerup, E.; Song, C. Three-Dimensional Molecular Basket Sorbents for $CO_2$ Capture: Effects of Pore Structure of Supports and Loading Level of Polyethylenimine. *Catal. Today* **2014**, *233*, 100–107.

(26)    Galarneau, A.; Cambon, H.; Di Renzo, F.; Fajula, F. True Microporosity and Surface Area of Mesoporous SBA-15 Silicas as a Function of Synthesis Temperature. *Langmuir* **2001**, *17* (26), 8328–8335.

(27)    Ryoo, R.; Ko, C. H.; Kruk, M.; Antochshuk, V.; Jaroniec, M. Block-Copolymer-Templated Ordered Mesoporous Silica : Array of Uniform Mesopores or Mesopore - Micropore Network ? *J. Phys. Chem. B* **2000**, *104*, 11465–11471.

(28)    Yan, X.; Komarneni, S.; Yan, Z. $CO_2$ Adsorption on Santa Barbara Amorphous-15 (SBA-15) and Amine-Modified Santa Barbara Amorphous-15 (SBA-15) with and without Controlled Microporosity. *J. Colloid Interface Sci.* **2013**, *390* (1), 217–224.

(29)    Heydari-Gorji, A.; Yang, Y.; Sayari, A. Effect of the Pore Length on $CO_2$ Adsorption over Amine-Modified Mesoporous Silicas. *Energy and Fuels* **2011**, *25* (9), 4206–4210.

(30)    Heydari-Gorji, A.; Belmabkhout, Y.; Sayari, A. Polyethylenimine-Impregnated Mesoporous Silica : Effect of Amine Loading and Surface Alkyl Chains on $CO_2$ Adsorption. *Langmuir* **2011**, *27*, 12411–12416.

(31)    Heydari-Gorji, A.; Sayari, A. $CO_2$ Capture on Polyethylenimine-Impregnated Hydrophobic Mesoporous Silica: Experimental and Kinetic Modeling. *Chem. Eng. J.* **2011**, *173* (1), 72–79.

(32)    Yue, M. B.; Chun, Y.; Cao, Y.; Dong, X.; Zhu, J. H. $CO_2$ Capture by As-Prepared SBA-15 with an Occluded Organic Template. *Adv. Funct. Mater.* **2006**, *16* (13), 1717–1722.

(33)    Kuwahara, Y.; Kang, D.-Y.; Copeland, J. R.; Brunelli, N. A.; Didas, S. A.; Bollini, P.; Sievers, C.; Kamegawa, T.; Yamashita, H.; Jones, C. W. Dramatic Enhancement of $CO_2$ Uptake by Poly(ethyleneimine) Using Zirconosilicate Supports. *J. Am. Chem. Soc.* **2012**, *134* (26), 10757–10760.

(34)    Kuwahara, Y.; Kang, D.-Y.; Copeland, J. R.; Bollini, P.; Sievers, C.; Kamegawa, T.; Yamashita, H.; Jones, C. W. Enhanced $CO_2$ Adsorption over Polymeric Amines Supported on Heteroatom-Incorporated SBA-15 Silica: Impact of Heteroatom Type and Loading on Sorbent Structure and Adsorption Performance. *Chem. Eur. J.* **2012**, *18* (52), 16649–16664.

(35)    Gunathilake, C.; Jaroniec, M. Mesoporous Alumina–zirconia–organosilica Composites for $CO_2$ Capture at Ambient and Elevated Temperatures. *J. Mater. Chem. A* **2015**, *3* (6), 2707–2716.

(36)    Chen, S. Y.; Jang, L. Y.; Cheng, S. Synthesis of Zr-Incorporated SBA-15 Mesoporous Materials in a Self-Generated Acidic Environment. *Chem. Mater.* **2004**, *16* (21), 4174–4180.

(37)    Dragoi, B.; Dumitriu, E.; Guimon, C.; Auroux, a. Acidic and Adsorptive Properties of SBA-15 Modified by Aluminum Incorporation. *Microporous Mesoporous Mater.* **2009**, *121* (1-3), 7–17.

(38)    Liu, Z.; Terasaki, O.; Ohsuna, T.; Hiraga, K.; Shin, H. J.; Ryoo, R. An HREM Study of Channel Structures in Mesoporous Silica SBA-15 and Platinum Wires Produced in the Channels. *Chemphyschem* **2001**, *2* (4), 229–231.

(39)    Chen, S. Y.; Tang, C. Y.; Chuang, W. T.; Lee, J. J.; Tsai, Y. L.; Chan, J. C.; Lin, C. Y.; Liu, Y. C.; Cheng, S. A Facile Route to Synthesizing Functionalized Mesoporous SBA-15 Materials with Platelet Morphology and Short Mesochannels. *Chem. Mater.* **2008**, *20* (12), 3906–3916.

(40)    Kjellman, T.; Alfredsson, V. The Use of in Situ and Ex Situ Techniques for the Study of the Formation Mechanism of Mesoporous Silica Formed with Non-Ionic Triblock Copolymers. *Chem. Soc. Rev.* **2013**, *42* (9), 3777–3791.

# CHAPTER 4

# INFLUENCE OF ADDITIVES ON THE AMINE EFFICIENCY OF

# SUPPORTED PEI

Parts of this chapter are adapted from 'Sakwa-Novak, M. A.; Tan, S.; Jones, C. W. Role of Additives in Composite PEI/Oxide CO2 Adsorbents: Enhancement in the Amine Efficiency of Supported PEI by PEG in CO2 Capture from Simulated Ambient Air. *ACS Appl. Mater. Interfaces.* **2015**, **DOI:** 10.1021/acsami.5b07545' with permission of The American Chemical Society.

## 4.1    Introduction & Motivation

Amine efficiencies of supported amine materials are typically reported to be lower than the theoretical maximum of one half set by the $CO_2$-amine reaction chemistry. This has been hypothesized to be associated with amines that are not in close proximity to one another in low loaded materials[1–3] or amines that are buried and subjected to $CO_2$ diffusional limitations in highly loaded materials.[4] Hence, an important research focus has been to develop synthetic strategies to engineer supported amine materials to have increased amine efficiencies. One route that is effective in this regard is to incorporate non-amine containing molecules or polymers into poly(ethylenimine) (PEI) impregnated porous materials. PEI is the most frequently reported aminopolymer used for $CO_2$ adsorption in solids, due to its amine rich structure and commercial availability. Poly(ethylene glycol) (PEG), has been incorporated into amine containing solids and has led to improved capacities, and in some cases, kinetics.[5–10] Additionally, PEG has been

shown to reduce the oxidation of supported amines, suggested to be the result of hydrogen bonding between the PEG and PEI.[11–13] Similarly, improvements have been shown to result from the incorporation of a wide range of co-impregnated surfactant molecules,[14–16] including those left from the micelle template used during silica syntheses[17–19] as well as grafted and ungrafted silanes[20–25] and inorganics such as potassium carbonate.[26] A more detailed summary of these studies is provided in section C.1 of appendix C.

Several hypotheses have been proposed to explain the additive promoting effect, including improved dispersion of impregnated PEI,[14,17] a reduction in the organic viscosity,[10] and an increase in the theoretical amine efficiency through the formation of bicarbonates.[7] Compelling evidence that the nature of the enhancement is kinetic (rather than thermodynamic) has been reported in several papers, where the optimal adsorption temperature of decreased for additive incorporated samples relative to their counterparts with no additive, reflecting an effective decrease in the aforementioned diffusional resistances. However, a more fundamental description of what gives rise to this phenomena has not been compellingly elucidated. Recently, Baker et al. addressed this question directly with the hypothesis that the promoting effect of PEG was due to the Lewis basicity of the polymer, however their study did not fully validate the hypothesis.[27] While additive molecules have generally enhanced the performance of supported polyamines, the degree of improvement has been a strong function of the experimental conditions such as material composition and adsorption temperature. In this regard, the goal of this work was to explicitly assess the effect of additive incorporation on the

adsorption performance of PEI impregnated mesoporous oxides upon exposure to ultra-dilute, 400 ppm $CO_2$. This was done to directly assess the efficacy of the strategy for improving materials for air capture processes, and also to ensure that $CO_2$ physisorption, which can begin to convolute adsorption data at $CO_2$ partial pressures above ~0.1 bar,[28] was negligible and thus provides for a suitable experimental platform to study the underlying adsorption phenomena. Additionally, practical considerations such as pore filling, adsorption dynamics and support characteristics were carefully studied. The effect of three additives, CTAB, PEG200, and PEG1000 were systematically co-impregnated with PEI into a model SBA-15 silica support. The best performing additive, PEG200, was subsequently studied at varying PEI loadings and on two varieties of mesoporous alumina. A kinetic threshold was reached, whereby at PEG/PEI ratios that correspond to nearly equimolar OH/ reactive ($1^o$, $2^o$) amine ratios, the adsorption became completely thermodynamically controlled.

## 4.2   Experimental

### 4.2.1   Preparation of Materials

Chemicals: All chemicals were used as purchased from the supplier. Pluronics P123, tetraethylorthosilicate (TEOS) (98%, Reagent Grade), nitric acid, poly(ethylenimine) (PEI) ($M_w$ 800, $M_n$ 600), and poly(ethylene glycol) (avg mol wt. 200) were purchased from Sigma Aldrich. Methanol (ACS Grade) and hydrochloric acid (fuming, ACS grade) were purchased from BDH Chemicals. Psuedoboehmite (74.3 % $Al_2O_3$, Capitol B) and the 'commercial' γ-alumina (Sasol SBa-200) were purchased from Sasol North America.

Cetyl trimethylammonium bromide (CTAB) (99+%. TLC grade) was purchased from Acros Organics. Poly(ethylene glycol) (avg mol wt. 1000) was purchased from J.T. Baker. Ethanol (200 proof) was purchased from Koptec.

SBA-15 Silica was synthesized according to the following procedure: 24 g of Pluronic P123 was dissolved in an acidic solution of 120 mL fuming (~37%) HCl and 636 g $H_2O$ under stirring at room temperature in a 2L Erlenmeyer flask. Once the polymer template was fully dissolved, 46.26 g of TEOS was drop wise added to the mixture by pipette. This solution was vigorously stirred at 40 $^o$C for 20 hours, before the stir bar was removed and the synthesis mixture was hydrothermally aged at 100 $^o$C under ambient pressure for 24 hours. After aging, the material was immediately filtered and washed with copious amounts of DI $H_2O$, before drying at 70 $^o$C overnight. Finally, the template was removed by calcination at 550 $^o$C for 10 hours, with a ramp rate of 2 $^o$C per minute and an intermediate $H_2O$ removal step of 200 $^o$C for 2 hours.

Mesoporous Templated γ-Alumina was prepared by a method used previously for the synthesis and preparation of γ-alumina supported amine materials,[29,30] but developed elsewhere.[31–33] P123 was used as a soft template in the self-assembly of pseudoboehmite nanoparticles into a mesoporous structure. To prepare the alumina, 13.75 g of psuedoboehmite was first peptized by dispersing and sonicating for 90 minutes in an acidic mixture consisting of 1.27 g nitric acid (~70%) and 200 mL DI $H_2O$ followed by aging at 60 $^o$C for 17 hours. Separately, 15.3 g P123 was dissolved in 200 mL of ethanol, and the peptized psuedoboehmite containing dispersion was slowly added to this and the resultant mixture was stirred at room temperature for 24 hours. Solvent evaporation was

then performed by aging at 60 $^oC$ for 48 hours in an open beaker. The resulting yellowish solid was further dried at 75 $^oC$ before being calcined in static air at 700 $^oC$ for 4 hours with an intermediate drying step at 150 $^oC$ to remove water. A temperature ramp rate of 1 $^oC$ / min was used for both temperature steps.

Preparation of Adsorbents: Adsorbents were prepared by impregnation of a given amount of PEI and additive into a support material in one step using methanol as a solvent. Prior to adsorbent preparation, the silica or alumina support materials were dried under vacuum (~20 mtorr) overnight at ~100 $^oC$ to remove adsorbed species. To prepare the adsorbent, 0.25 g of dried support material was weighed and dispersed in 20 mL of methanol in a 100 mL round bottom flask. Separately, given amounts of PEI and additive were weighed and added to a 25 mL round bottom flask, before 10 mL of methanol was added. The two mixtures, one containing the support and the other containing the organic contents, were stirred separately for 1 hour to equilibrate. Then, the solution containing PEI and additive was added by pipette to the solution containing support. This mixture was then stirred for 3 hours to equilibrate. Finally, the methanol was removed by rotary evaporation at ~60 $^oC$ and the resulting powder was further dried under high vacuum (~20 mtorr) at ~60 $^oC$ for 12-18 hours before collection. Samples were stored in vials under ambient conditions prior to evaluation.

### 4.2.2   Characterization Methods

Thermogravimetric Analysis was used to estimate total organic compositions of adsorbents using a Netzsch STA409PG. 10-14 mg of sample was heated from ambient condition to 900 $^oC$ in the presence of air and the weight loss was recorded. Total organic

loadings were taken as the sample weight loss between 120 $^o$C and 900 $^o$C, and were normalized by the residual mass of the sample recorded at 900 $^o$C. Strongly bound water and water produced via silanol or aluminol condensation was subtracted from this value by estimation from TGA analysis of the appropriate bare support.

Elemental Analysis for carbon, nitrogen and hydrogen was performed by Atlantic Microlabs (Norcross, GA). Samples were dried at 100 $^o$C under vacuum at the facility prior to analysis to ensure a dry material basis. Estimates of the ratio of additive to PEI in a given sample were derived from the obtained C/N ratio according to equation 1 (g Additive / g PEI was derived explicitly as a function of the other, known or measured, quantities).

$$\frac{g\ C}{g\ N} = \frac{\frac{g\ C}{g\ PEI}\ g\ PEI + \frac{g\ C}{g\ Additive}\ g\ Additive}{\frac{g\ N}{g\ PEI}\ g\ PEI} \tag{1}$$

Nitrogen Physisorption experiments were performed on a Micromeritics Tristar II 3020 instrument at 77 K. Surface areas were estimated using the BET method, using data obtained below a partial pressure of 0.3. Pore volumes were estimated by the total $N_2$ sorption at a partial pressure of 0.99. Surface areas and pore volumes of composite materials (organic + inorganic) were normalized to per gram $SiO_2$ or $Al_2O_3$ using the inorganic weight percent derived from TGA experiments. Pore size distribution of the SBA-15 was estimated using the NLDFT equilibrium model with Quantachrome VersaWin software. Pore size distributions of the alumina samples were estimated using the BdB-FHH method employing the adsorption branch of the $N_2$ isotherms and

assuming cylindrical pores. NLDFT was not used for the alumina PSD calculations due to the nature of the calculation, requiring a silica surface.

X-ray Diffraction patterns were collected using a PANalytical X'Pert diffractometer using Cu-K-alpha radiation.

FTIR Spectroscopy: A Bruker Vertex 80v optical bench was used to collect FTIR spectra. For powder samples, ~ 1 mg of sample was mixed with ~ 100 mg KBr and pressed to pellets. For polymer samples, a small amount of (liquid) polymer was brushed onto a preformed KBr pellet.

X-ray Photoelectron Spectroscopy spectra were collected on a Thermo K-Alpha spectrometer and a monochromatic Al kα X-ray source. Scans were taken from 0 to 1350 eV with a scanning step of 0.1 eV. The spectrum was calibrated using the C1s peak at 284.6 eV. Vacuum pressure of $4 \times 10^{-7}$ torr was employed in the analytical chamber during analysis.

CO2 Adsorption experiments were performed by thermogravimetric analysis (TGA) using a TA Instruments Q500 apparatus using 14 mg (+/- 1 mg) of material. Estimates of $CO_2$ capacities were obtained by pretreating the given sample under a flow of helium at 110 $^{\circ}$C for 3 hours, followed by thermal equilibration at 30 $^{\circ}$C and subsequent exposure to a gas mixture of 400 ppm $CO_2$ balanced by helium at the same temperature for 12 hours.

### 4.3    Results and Discussion

An SBA-15 silica was synthesized and used as a model support to study the effect of additive mixtures on impregnated PEI during $CO_2$ adsorption. The $N_2$ physisorption

profile, NLDFT pore size distribution and small angle XRD pattern of the SBA-15 are shown in figures 4.1 a-c. The textural properties derived from the $N_2$ physisorption data are tabulated in table 4.1. The NLDFT pore size distribution suggested a primary mesopore size of 8.6 nm, which corresponded well with the $d_{100}$ spacing of ~9.2 nm derived from XRD. The surface area and pore volume of the SBA-15 were consistent with those found in the literature.
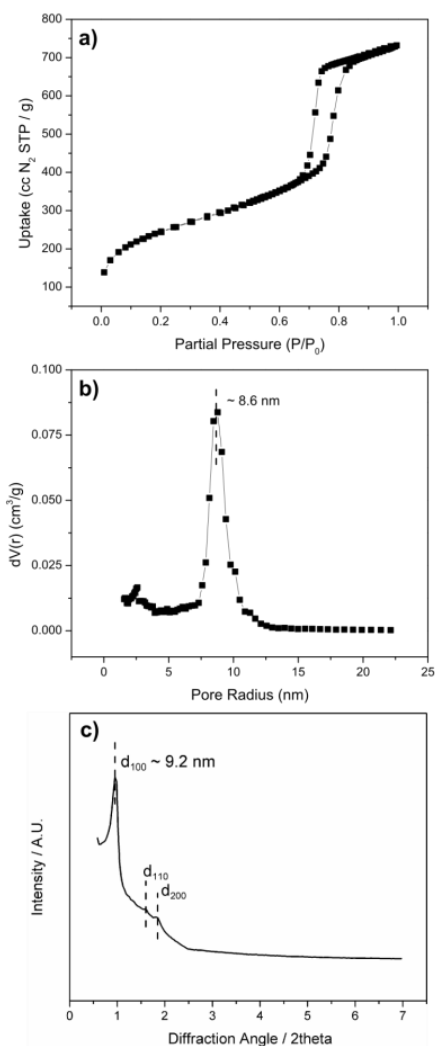
Figure 4.1 N$_2$ physisorption (a), NLDFT pore size distribution (b), XRD pattern (c), of bare SBA-15.

## 4.3.1 Effect of Additive Type on Amine Efficiency in SBA-15

Three additives, cetyl trimethylammonium bromide (CTAB), Mw 200 poly(ethylene glycol) (PEG200) and Mw 1000 poly(ethylene glycol) (PEG1000), were co-incorporated with poly(ethylenimine) (PEI) into the SBA-15 to assess how the nature and quantity of additive changed the amine efficiency of the adsorbent at 400 ppm CO$_2$. To prepare an adsorbent, specific amounts of additive and PEI were dissolved in methanol and subsequently equilibrated with an SBA-15/methanol dispersion before the methanol was removed by rotary evaporation. FTIR spectra, reported in figure C.1 of appendix C, confirmed that the additives were incorporated into the resultant materials. Additional spectra of PEI and PEG physically mixed as liquids, impregnated alone, and co-impregnated into SBA-15 are provided in figure C.3 of appendix C as well.

Table 4.1 shows the physical and textural properties of the resultant materials, as well as the CO$_2$ capacities measured by TGA. Each of the materials shown in table 4.1 was prepared with a constant PEI to SiO$_2$ ratio of ~0.45 in the preparation mixture. The slight discrepancy between this PEI to SiO$_2$ ratio in the preparation mixture and that reported in table 4.1 for the non-additive containing control material reported is attributed to adsorbed water on the silica and small losses of silica during sample handling, which would decrease the effective silica weight in the mixture slightly.

Table 4.1 Physical, textural and $CO_2$ adsorption properties of SBA-15/PEI/Additive mixtures

| Additive | Organic / Silica[a] (g Org/g $SiO_2$) | Carbon / Nitrogen[b] (mol C/ mol N) | Additive / PEI[c] g / g | Surface Area[d] $m^2$ / g $SiO_2$ | Pore Volume[e] $cm^3$ / g $SiO_2$ | Amine Content[b] mmol N / g | $CO_2$ Capacity mmol $CO_2$ / g |
|---|---|---|---|---|---|---|---|
| *Reference Materials* | | | | | | | |
| Bare SBA-15 | - | - | - | 880 | 1.13 | - | - |
| PEI (no PEG) | 0.51 | 2.2 | - | 317 | 0.67 | 6.36 | 0.63 |
| PEG200 (no PEI) | 0.33 | - | - | 35 | 0.11 | - | 0.00 |
| *Low Molecular Weight PEG (PEG200)* | | | | | | | |
| PEG200 | 0.54 | 2.6 | 0.31 | 236 | 0.50 | 5.75 | 0.79 |
| PEG200- low | 0.66 | 3.2 | 0.61 | 263 | 0.54 | 4.97 | 0.73 |
| PEG200- med | 1.32 | 5.6 | 1.82 | 147 | 0.33 | 3.88 | 0.64 |
| PEG200- high | 2.13 | 8.8 | 3.42 | 1 | 0.00 | 3.42 | 0.49 |
| *High Molecular Weight PEG (PEG1000)* | | | | | | | |
| PEG1000-low | 0.65 | 2.9 | 0.47 | 262 | 0.53 | 5.37 | 0.71 |
| PEG1000- med | 1.39 | 5.8 | 1.92 | 4 | 0.01 | 4.17 | 0.49 |
| PEG1000- high | 2.29 | 10.2 | 4.08 | 1 | 0.00 | 2.84 | 0.30 |
| *CTAB* | | | | | | | |
| CTAB- low | 0.60 | 2.8 | 0.32 | 277 | 0.56 | 5.70 | 0.55 |
| CTAB- med | 1.30 | 5.7 | 1.77 | 74 | 0.17 | 4.63 | 0.31 |
| CTAB- high | 1.99 | 8.1 | 3.60 | 47 | 0.12 | 4.03 | 0.21 |

[a]Estimated by TGA; [b]Estimated from elemental analysis; [c]Estimated from elemental analysis using equation 1; [d]Estimated by the BET method from $N_2$ physisorption; [e]Estimated from total $N_2$ adsorbed at $P/P_0 = 0.99$

For each of the additives co-incorporated with PEI, as the organic content increased the C/N ratio and correspondingly the additive/PEI mass ratio also increased while the surface areas and pore volumes decreased. Since the additives were non-amine containing (with the exception of the quaternary amine in CTAB, which has a much higher C/N ratio than PEI) the amine content per gram of adsorbent decreased as the additive content increased.

The $CO_2$ capacities for the PEI/PEG200 and PEI/PEG1000 were higher than the reference material at low PEG/PEI content; however the $CO_2$ capacities of the samples decreased as the additive content increased for each additive molecule. For the PEI/PEG200 samples, as the content of PEG increased, the relative decrease in the $CO_2$ capacity was less than the relative decrease in the amine loading, indicating that the amine efficiency increased in these materials even as the $CO_2$ capacity decreased. Most related studies in the literature have focused solely on changes to the $CO_2$ capacity, while the amine efficiency is arguably a more practically important metric. It is important to note that that the reference sample with (only) PEG200 had a negligible $CO_2$ uptake at the 400 ppm adsorption condition, indicating that the increased capacities of PEI/PEG200 samples were not simply a result of PEG adsorbing $CO_2$ independently of PEI. The amine efficiencies of each sample plotted against the estimated additive/PEI mass ratio are shown in figure 4.2. The horizontal line drawn through the figure represents the amine efficiency of the reference PEI/SBA-15 material with no additive. Samples at common additive/PEI content were grouped into low, medium and high loading groups for ease in observation of later data analysis.
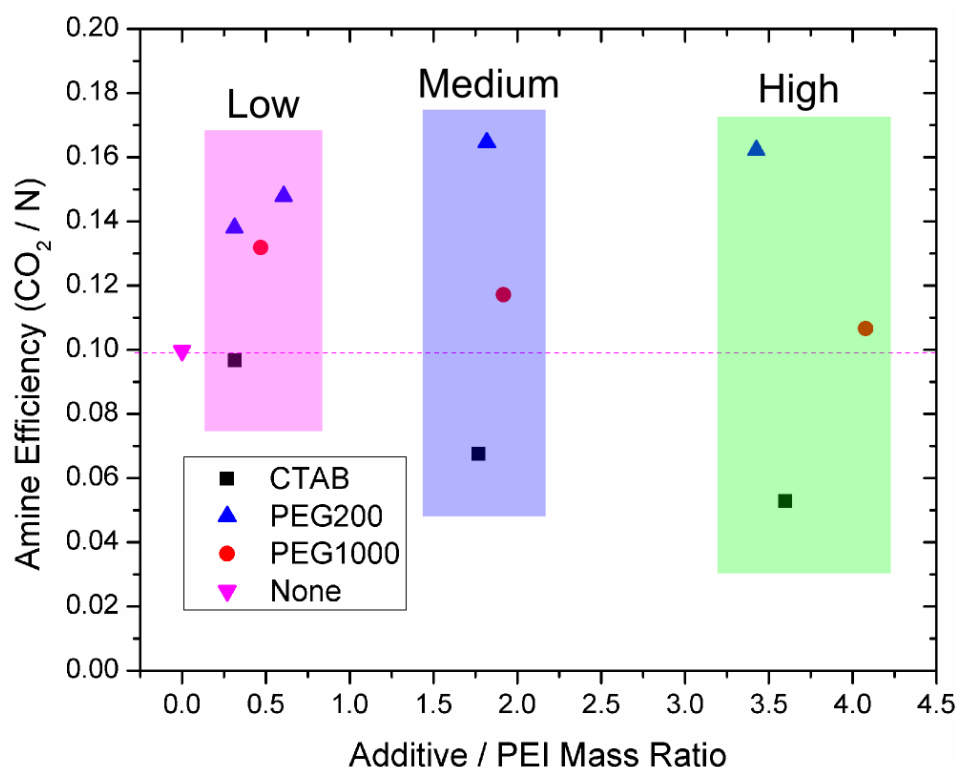
Figure 4.2 Amine efficiency as a function of additive/PEI mass ratio for CTAB, PEG200, and PEG1000 co-incorporated with PEI into SBA-15. Horizontal line represents amine efficiency for PEI/SBA-15 without additive. The PEI/$SiO_2$ mass ratio was held constant at ~0.45 for all samples.

The incorporation of both low and high molecular weight PEG increased the amine efficiency over all of the loadings tested, while the incorporation of CTAB decreased the amine efficiency. The incorporation of both low and high molecular weight PEG increased the amine efficiency over all of the loadings tested, while the incorporation of CTAB decreased the amine efficiency. This is contrary to the findings of Wang et al.,[14,34] who reported an increase of ~10% in the $CO_2$ capacity of a porous silicas and carbons impregnated with PEI and 5 wt% of CTAB, and Sayari et al.[17] who reported a near doubling of the $CO_2$ capacity during adsorption at room temperature when PEI was impregnated in a pore expanded MCM-41 with CTAB left behind from the silica

110

synthesis. However, the materials here contained much higher amounts of CTAB than in Wang's study and were measured under ultra-dilute $CO_2$ pressures, whereas in Sayari's study the adsorption gas was pure $CO_2$. Notably, the adsorbents were prepared with supports of differing properties in each case as well. The trends in figure 4.2 also show that the amine efficiency decreased as the additive levels increased in the PEG1000 and CTAB incorporated samples, while the opposite was true in the PEG200 incorporated samples.

### 4.3.2 Pore Filling Characteristics

Physical differences between the materials were probed with $N_2$ physisorption and XPS analysis. BET surface areas and pore volumes derived from $N_2$ physisorption and normalized per gram $SiO_2$ are reported in table 4.1. The percentage reduction in pore volume caused by pores being filled or blocked by organic was estimated by normalizing the $N_2$ physisorption isotherms per gram $SiO_2$, and comparing the final pore volumes of the materials with those of the unmodified SBA-15 support. Figure 4.3 shows this percentage reduction in pore volume plotted against the additive/PEI mass ratio for materials with all three additives at varying loading. Samples are grouped by common additive/PEI content, as with figure 4.2.
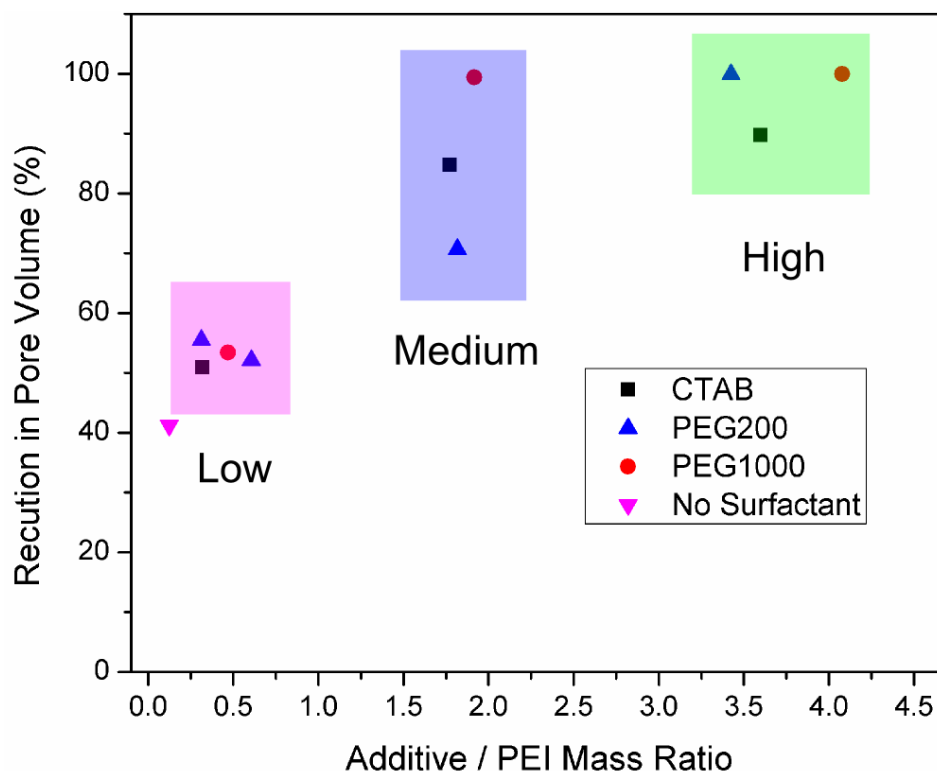
Figure 4.3 Percentage of pore volume filled by organic as a function of estimated additive/PEI mass ratios for CTAB, PEG1000, and PEG200 incorporated samples.

The percentage of pore volume filled or blocked by organic increased with the addition of additive for each set of materials. At additive/PEI ratios of ~0.5 g/g, the pore volumes of the adsorbents were very similar, with just over 50% of the pore volume filled. Similarly, at the highest additive/PEI content the pores of the SBA-15 were nearly full or blocked for each sample set, though the reduction in pore volume of the CTAB sample was slightly less than the others. At the intermediate ~2 g/g additive/PEI content there were stark differences in the reduction in pore volume. The physisorption profiles of the samples at this composition, normalized per gram $SiO_2$, are shown in figure 4.4.
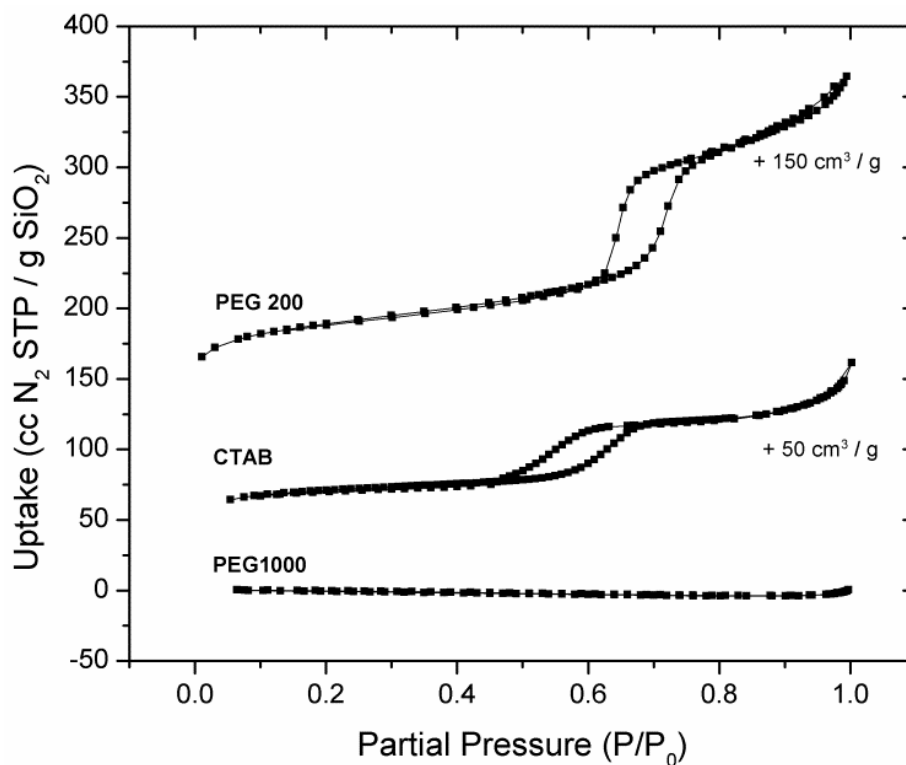
Figure 4.4 $N_2$ Physisorption profiles for PEI and PEG200 (top), CTAB (middle), and PEG1000 (bottom) co-incorporated SBA-15 samples prepared at additive/PEI mass ratios of ~2 (medium additive loading).

The PEI/PEG200 and PEI/CTAB samples retained the characteristic SBA-15 isotherm shape with shifted hysteresis regions, indicating effective reductions in pore size relative to the bare SBA-15 in both cases. The PEI/PEG1000 sample adsorbed negligible amounts of $N_2$ and was effectively nonporous. Importantly, the mass content of organic in the materials in figure 4.4 were all within 10% of each other, as indicated in table 4.1, and differences in the bulk density of the different organic mixtures were too small to account for the observed differences in pore volume (see figure C.3 of appendix C). Due to the large quantity of organic contained in the sample, the expected occupied volume of organic exceeded the pore volume of the bare SBA-15 for each of the samples shown in

figure 4.4, suggesting that there may have been some appreciable organic deposition on the external surface of the particle.

To further investigate this possibility, XPS spectra of the samples at the medium additive loading were measured, as well as for the reference PEI/SBA-15 with no additive. For SBA-15 particles, which are expected to be ~500-1000 nm in diameter,[35] XPS provides a good representation of the surface, probing only a few nanometers deep. Table 4.2 shows various molar ratios derived from the XPS measurements, along with the bulk C/N molar ratio obtained from elemental analysis for comparison. The raw XPS spectra are provided in figure C. 4 of appendix C.

Table 4.2 Molar ratios derived from XPS spectra and elemental analysis for samples with medium additive loading

|  | *SBA/PEI* *mol / mol* | *SBA/PEI/CTAB* | *SBA/PEI/PEG200* | *SBA/PEI/PEG1000* |
|---|---|---|---|---|
| **C/Si** | 1.1 | 2.3 | 1.5 | 3.0 |
| **O/Si** | 1.7 | 1.7 | 2.0 | 2.5 |
| **N/Si** | 0.5 | 0.4 | 0.4 | 0.5 |
| **C/N** | 2.3 | 6.6 | 3.8 | 6.0 |
| **C/N (EA)** | 2.3 | 5.7 | 5.6 | 5.8 |

The C/Si ratios of the samples containing additive were each higher than that of the reference PEI/SBA-15, indicating an enhanced degree of organic deposition on the outer surface of the particles. The C/Si ratios followed a similar trend as the reduction in pore volume shown in figure 4.3, with the PEI/PEG1000 sample having the greatest amount of organic on the surface, followed by PEI/CTAB and finally PEI/PEG200. O/Si ratios were higher in both PEI/PEG samples than the SBA/PEI control, providing a signature of PEG on the particle exterior of these samples. The surface N/Si ratios were

similar for all the samples, suggesting that the amount of PEI deposited on the exterior of the particle did not significantly change during the preparation with or without additive. However, N and Si had the weakest signal in the spectra, and thus may have the highest intrinsic error associated with integration of the peaks.

The bulk C/N was very similar for each sample while the surface C/N varied between samples. For the control PEI/SBA-15 sample, the C/N ratio measured by both techniques was identical, providing merit for the use of this comparison in distinguishing physical differences within a single material. The most striking difference between surface and bulk C/N was that of the PEI/PEG200, where the surface C/N was significantly lower than the bulk but still higher than that of the PEI/SBA-15 control. This indicates that there was some PEG on the exterior of the particle, consistent with the C/Si and O/Si data, but to a lesser degree than in the bulk. Thus much of the PEG200 likely went inside the pores of the SBA-15 along with the PEI. Taken together with the TGA, $N_2$ physisorption and bulk density data, which suggest that this sample contained enough organic to completely fill the pores but retained significant porosity, we hypothesize that the PEI and PEG may have packed in the pores in such a way that the confinement induced a difference in the density of the mixture relative to the bulk (unconfined).

The PEI/PEG1000 had comparable surface and bulk C/N content, indicating that either all of the organic was deposited on the surface, or there was a distribution of homogeneously mixed organic in the interior and exterior of the particles. The significant C and O content on the exterior of the particle coupled with the physisorption data

showing no porosity suggests a disproportionate deposition of organic on the exterior of the particle. The PEI/CTAB had a higher surface C/N than bulk, indicating a higher content of CTAB on the particle exterior, consistent with the increased C/Si surface ratio. The efficient filling of pores is expected to be an important practical consideration in the scale up of adsorbents to structured contactors of hierarchical pore structure such as hollow fibers.[16,36] As such, these findings of heterogeneities in the deposition of polyamine/additive mixtures onto porous particles is an important development, and to our knowledge such have not been previously identified in the literature.

At a more fundamental level, the observed differences in organic deposition and pore filling are hypothesized to derive from additive/PEI molecular interactions. Specifically, through clusters formed between PEG and PEI, but not CTAB and PEI, due to hydrogen bonding interactions. PEG and PEI likely hydrogen bond primarily through interactions between the alcohol end groups on the PEG and primary and secondary amines on the PEI. CTAB likely does not interact as well with the PEI due to the lack of H bonding sites. PEG/PEI clusters would contain multiple PEG chains per PEI chain as a single PEI chain contains ~22 N groups, 75% of which are primary or secondary [37,38], while PEG contains two alcohol groups. Thus, clusters of PEI/PEG1000 would likely be larger in radius than PEI/PEG200 and would be more susceptible to blocking SBA-15 mesopores during the solvent removal step of the synthesis, where capillary forces likely play a role in forcefully drawing solution into the pores of the solid. We hypothesize that this is what causes the pore blockage observed in $N_2$ physisorption of the PEI/PEG1000 sample. Smaller clusters of PEG200 and PEI could have the opposite effect, promoting

116

pore filling, by reducing the interaction between amine groups on the PEI and hydroxyls on the pore surface of the silica, thus allowing PEI to settle in a dispersed configuration.

### 4.3.3    Effect of PEI loading on Amine Efficiency in SBA-15

To further explore the promoting effect of PEG200 on supported PEI, SBA-15 was co-impregnated with PEG200 at two additional $PEI/SiO_2$ ratios. Figure 4.5 shows the amine efficiencies as a function of the $PEG/SiO_2$ quantity for each PEI loading. Table C. 1 in appendix C presents the relevant data in tabulated form for these samples.
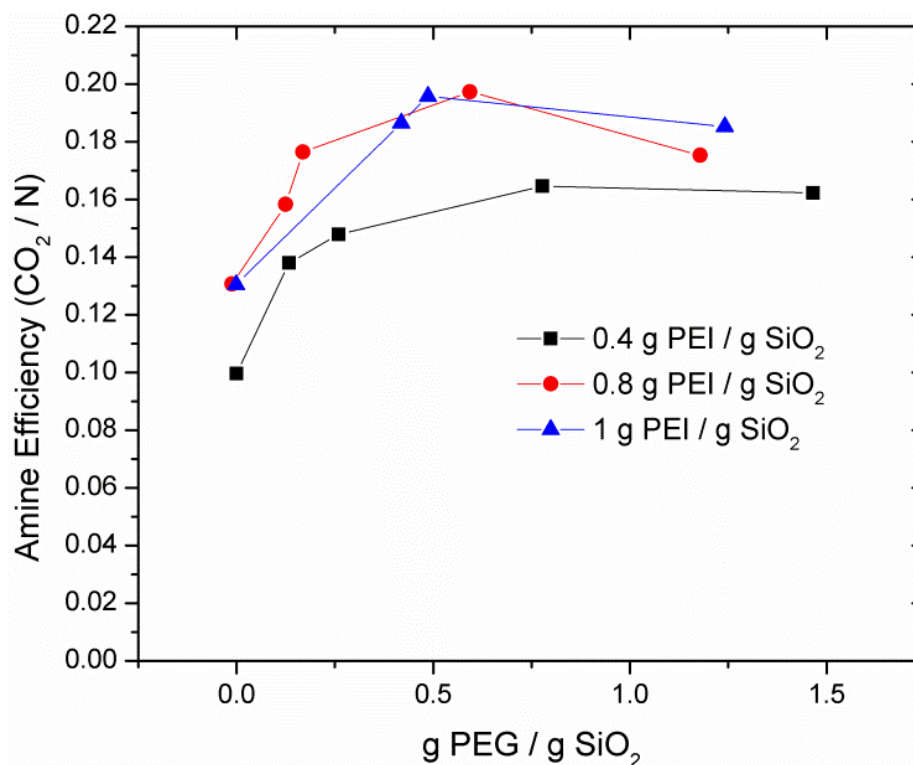


Figure 4.5 Amine efficiency of PEI co-impregnated with PEG200 at varying PEG200 loadings at three $PEI/SiO_2$ loadings plotted against estimated $PEG/SiO_2$ mass ratios estimated from equation 1 and TGA estimations of total organic loading.

The promoting effect of PEG on the amine efficiency was not strongly influenced by the quantity of PEI in the sample, as the shapes of the curves are very similar for each of the PEI loadings tested. The curves of the sample sets at the two higher PEI loadings were essentially overlapping and shifted a constant value above that for the lowest amine loading. For each of the three PEI loadings, the relative increase from minimum to maximum was similar at ~60% of the initial efficiency.

### 4.3.4 CO$_2$ Adsorption Dynamics

Fractional uptake (normalized adsorbed amount vs. time) plots of CO$_2$ adsorption onto samples discussed in the preceding sections are shown in figure 4.6. These provide a qualitative comparison of the adsorption dynamics independent of the total amount of CO$_2$ adsorbed.In figure 4.6 a-c samples of varying additive type and amount are shown, and the data are grouped by similarity in additive/PEI content. In figure 4.6 d-f samples of varying PEI and PEG200 content are shown, and the data are grouped by similarity in PEI loading.
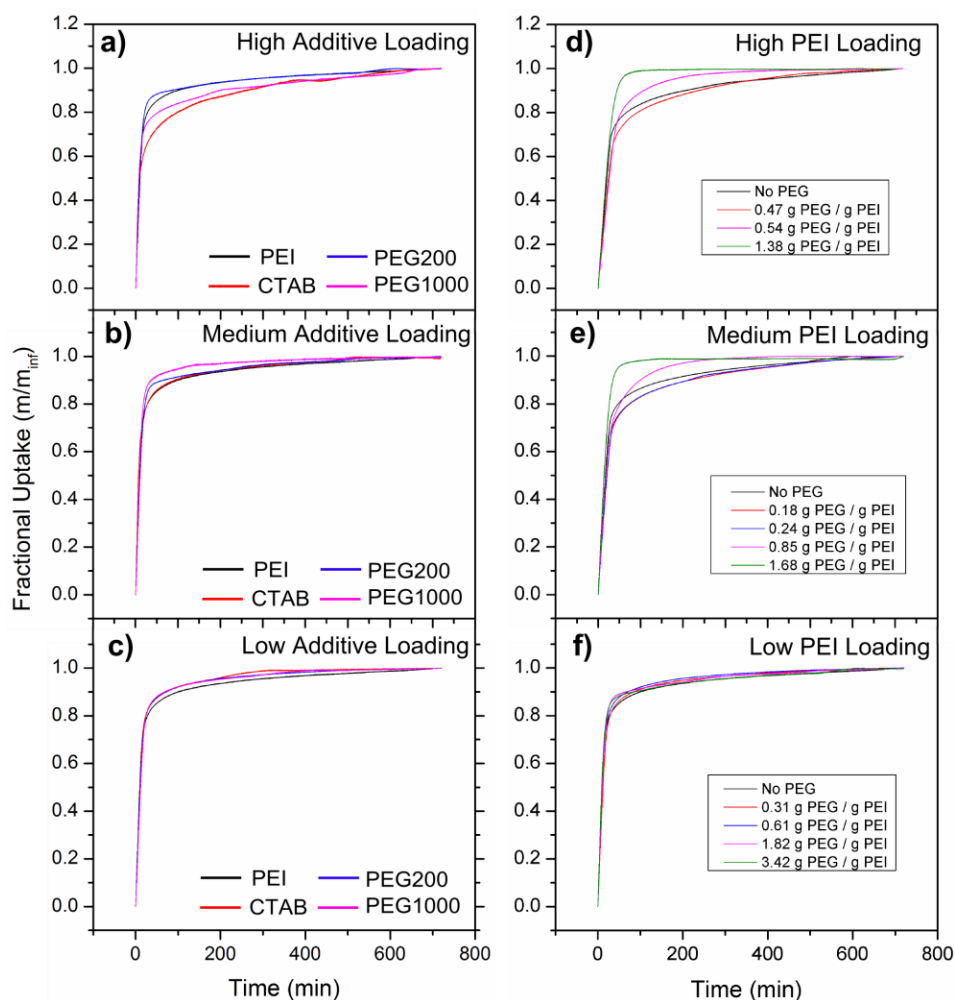
Figure 4.6 Fractional uptakes of adsorbents prepared with varying additive at a single PEI loading (a-c) and with PEI and PEG200 at varying PEI loading (d-f).

The uptakes are characterized by a region of rapid mass uptake at early times of $CO_2$ exposure, followed by a transition to a slow approach to equilibrium in the long time region. Such is commonly reported in the literature for supported amines. While a simple model of gas diffusion into a sphere yields a curve with a qualitatively similar shape,[39] the literature suggests that the two regions are the result of two regimes of differing mass transfer resistance.[4] The early-time rapid uptake region is likely controlled by gas phase

119

mass transfer of $CO_2$ to highly accessible amines, perhaps those that are exposed to void space in the pores of the particle. In the long-time region, the slow approach to equilibrium is likely controlled by $CO_2$ diffusion through an amine barrier layer. This may be due to $CO_2$ diffusion through amines that are buried under other amines,[4] or a result of inter-amine cross-linking through bound $CO_2$,[40,41] which would rigidify the PEI and create a physical barrier for $CO_2$ to diffuse through.

The fractional uptake curves were similar at the low and medium additive loadings as shown in figure 4.6b and 4.6c, even though the amine efficiencies were improved (shown in figure 4.2). Thus, the changes in amine efficiency were manifested at very early times of $CO_2$ adsorption, suggesting that the additives served to increase the fraction of readily accessible amines. At the higher additive loading, the samples containing CTAB and PEG1000 showed a deviation from the initial region of rapid mass uptake at a lower fractional uptake (y-axis value), than the PEG200 and PEI counterparts, reflecting a diminished kinetic performance. In figure 4.6 d-f, the effect of PEG200 on the uptake dynamics at varying PEI loading is shown. At the low PEI loading the uptake curves were nearly identical, while the dynamics showed a marked improvement at the two higher PEI loading at high PEG content. In both cases, at the highest PEG/PEI content the slow approach to equilibrium in the long-time region was not observed. At these two highest PEG/PEI ratios, the content of alcohol end groups of impregnated PEG approached the content of reactive ($1^{o}$ and $2^{o}$) amines of PEI (75% of total N),[37,38] taking values of 0.61 and 0.75 mol OH/ mol N for medium and high PEI loadings.

Using this observation as an indication that the physical origin of the promoting nature of PEG may be related to OH/N interactions, the observed kinetic improvement is rationalized in the context of the PEI/PEG cluster formation discussed in the preceding section. Specifically, it is hypothesized that as PEI and PEG cluster together, PEG physically shields PEI chains from one another and from the silica wall. At equimolar OH/N, each reactive amine interacts with an end of a PEG chain and hence PEI/PEI interactions are substantially reduced. This physical shielding of neighboring PEI chains from one another is likely to promote intrachain $CO_2$ adsorption events (rather than interchain). This would reduce the extent of $CO_2$ induced PEI cross linking and the resulting barrier formation and diffusional limitations. Both molecular weights of PEG may interact with PEI to improve performance in this fashion, but the observed effect is subject to the clusters being able to efficiently enter the pores of the material. Our data is consistent with this, where at low loadings of PEG1000, where the hypothesized PEG/PEI clusters would have a lower PEG/PEI chain ratio and therefore be smaller, the clusters are more likely to efficiently enter the SBA-15 pores and an improved $CO_2$ capacity and amine efficiency are observed. However, as the PEG content is increased and the clusters grow in size, clogging at pore mouths occurs and more amines become buried and thus are not available for $CO_2$ adsorption, even at long adsorption times. Since CTAB likely would not have such interactions with PEI, and deposits on the particle exterior disproportionally, it simply may completely block pores at their entrance and bury the impregnated amines at moderate loadings, hence reducing the amine efficiency

121

without significantly altering the dynamics. The relative size of the clusters and pore diameter of the support thus becomes an important metric for future studies.

To further investigate the kinetic threshold identified above, amine efficiencies of the samples at the medium and high PEI loadings with and without PEG at the highest PEG content were measured at 40 and 50 $^{o}$C, with the results of these experiments shown in figure 4.7.
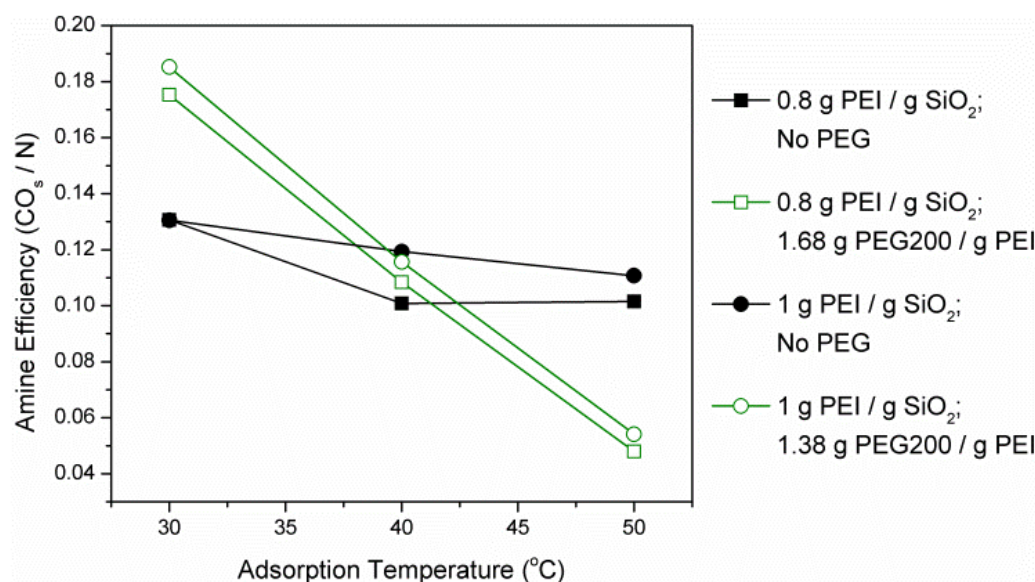


Figure 4.7 Amine efficiency as a function of adsorption temperature for materials prepared at 0.7 (squares) and 0.9 (circles) g PEI / g SiO$_2$ with PEG200 at the highest PEG/SiO$_2$ loading (green, hollow) and without PEG (black, solid)

The amine efficiencies decreased at increased adsorption temperature for each sample; however the samples with PEG showed much sharper reductions in amine efficiency at increased temperature than those without PEG. Typically, amine efficiencies of PEI impregnated aminosilica adsorbents show a maximum value at temperatures above 30 $^{o}$C at higher partial pressures of CO$_2$, reflecting kinetically controlled systems during the lower temperature experiments.[42] The results in figure 4.7 suggest that these

kinetic effects may be less important under ultra-dilute adsorption conditions, where only the most reactive amines will be active, compared to more typical experiments done under higher partial pressures of $CO_2$ (0.1-1 bar). The steep decrease in capacity of the PEG/PEI samples relative to the samples without PEG indicate a system that is strongly controlled by thermodynamics, thus corroborating the above finding that the adsorption is completely thermodynamically controlled at PEG/PEI ratios approaching equimolar $OH/(1^o, 2^o)$ N ratios.

### 4.3.5  Incorporation of PEI and PEG200 in Mesoporous γ-Alumina Supports

Finally, while SBA-15 silica was a useful model for probing adsorption phenomena due to its well-structured nature, such a silica support may not be practical for use in a commercial process. We have previously demonstrated that steam stripping is a potentially practical method for the regeneration of supported amine materials, and that mesoporous alumina is more robust than silica to the conditions imposed by such a process.[29,43–45] While others have suggested that certain silica compositions may also be hydrothermally stable,[46] it is important to explicitly extrapolate the findings of the PEG/PEI/SBA-15 system to other oxides that could be employed as adsorbent supports. As such, the use of PEG as an additive in two γ-alumina supported materials was also explored. One alumina was prepared in house using a soft template (P123), referred to here as 'templated' alumina, while the other was a commercially available Sasol Sba-200 alumina referred to here as 'commercial alumina'. The physisorption profiles, pore size distributions and XRD patterns of the alumina supports are provided in figures C.5 and C.6 of appendix C, while the physical and textural properties of the samples derived from

such experiments are tabulated in table C.2 in appendix C. Figure 8 shows the amine efficiency of the adsorbents plotted as a function of the PEG/PEI ratio for adsorbents prepared at ~0.45 g PEG200 / g PEI (analogous to figure 2) as well as that of the SBA-15 materials prepared at the same PEI/SiO$_2$ loading, for comparison.
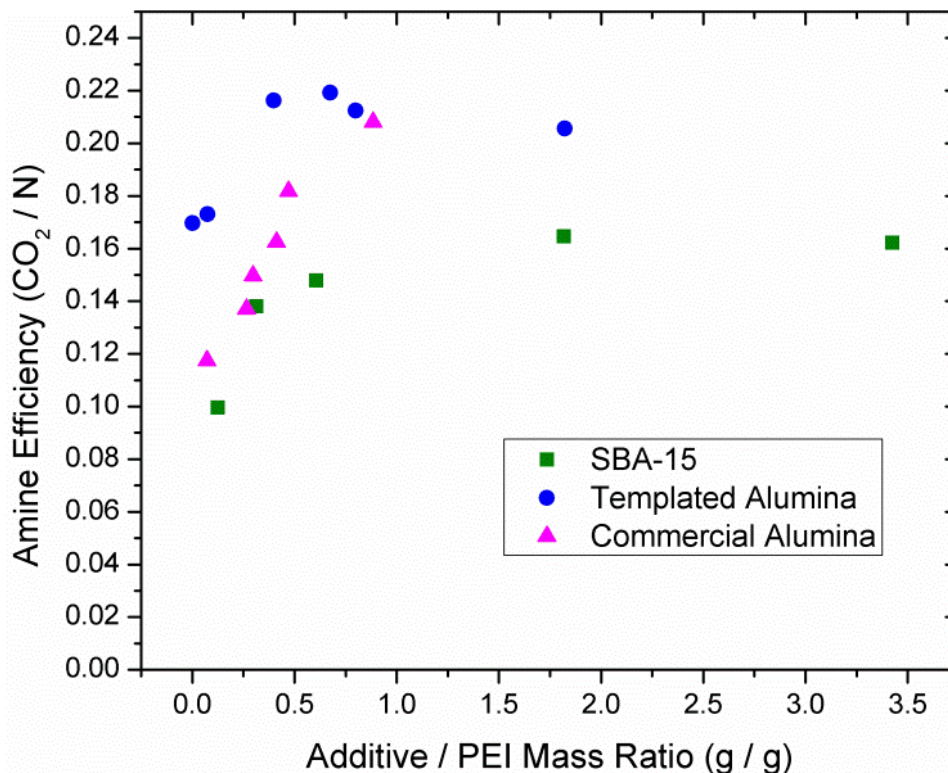


Figure 4.8 Amine efficiency plotted as a function of PEG200/PEI mass ratio as estimated from equation 1 for SBA-15 (green), templated alumina (blue) and commercial alumina (magenta).

The amine efficiencies of the samples without additive differed between supports used, perhaps due to differences in the textural or acid/base properties of the parent support material. The PEI/SBA-15 had an efficiency of ~0.10, the PEI/commercial alumina was slightly higher at ~0.12 and the PEI/templated alumina was significantly higher at ~0.17 mol CO$_2$ / mol N. The pore size of the supports followed the same trend

from small to large, suggesting that for these materials, pore size is an important textural property. The acid/base properties likely differed between the supports as well, with the SBA-15 having mild acidity derived from the surface hydroxyls, while the commercial alumina has been shown to have mild acidity,[47,48] and the templated alumina has been shown to have a basic surface.[31] Each material showed the expected increase in amine efficiency with increased PEG200 quantity. The templated alumina reached a maximum before decreasing, while the commercial alumina did not show a maximum. It was attempted to incorporate a higher quantity of PEG into this alumina at the given PEI/alumina content but the attempts were unsuccessful, likely due to the much lower pore volume of that support compared to the others used (~0.45 vs 1 $cm^3/$ g). Interestingly, the shapes of the curves for each of these samples were qualitatively different, while those for differing PEI content on the same support (figure 4.6) were very similar. This may be due to differences in the textural properties of the supports, or to a differing nature of the PEI-surface interaction that is altered upon the addition of the PEG, however these hypotheses were not explored. Nonetheless, these data explicitly demonstrate that the addition of PEG200 to PEI is effective in improving the amine efficiency of PEI supported in alumina, which is important for the further development and engineering of practical materials for $CO_2$ capture.

## 4.4   Conclusions

Additive molecules, particularly low molecular weight PEG, PEG200, substantially increased the amine efficiency of PEI supported on mesoporous silica and alumina adsorbing $CO_2$ from dry simulated air. Amine efficiencies were increased by a

maximum of ~60% for each of the PEI loadings tested on SBA-15 silica. A threshold PEG/PEI ratio was identified, at which the adsorption is completely thermodynamically controlled, and which corresponds to equimolar OH / reactive ($1^o$, $2^o$) amine ratios, providing the means to hypothesize a physical origin of the behavior. It is suggested that PEG and PEI cluster together to reduce PEI/PEI and PEI/SiO$_2$ interactions, the former of which is dominant at high PEI loadings and the latter of which is dominant at low PEI loading, and that a reduction in PEI/PEI interactions would lead to a higher probability of intrachain $CO_2$ adsorption events, thus reducing the extent of $CO_2$-induced PEI crosslinking. A non-homogenous deposition of organic on the interior/exterior of the SBA-15 particles is observed, with the larger molecules (PEG1000, CTAB) preferentially depositing on the particle exterior; thus the PEG/PEI promoting effect is subject to efficient organic incorporation into the support pores. Finally, the use of PEG200 was explicitly demonstrated to be effective in improving the amine efficiency of PEI when supported on mesoporous alumina, a more robust support for practical applications.

## 4.5    References

(1)     Aziz, B.; Hedin, N.; Bacsik, Z. Quantification of Chemisorption and Physisorption of Carbon Dioxide on Porous Silica Modified by Propylamines: Effect of Amine Density. *Microporous Mesoporous Mater.* **2012**, *159*, 42–49.

(2)     Harlick, P. J. E.; Sayari, A. Applications of Pore-Expanded Mesoporous Silica 5. Triamine Grafted Material with Exceptional $CO_2$ Dynamic and Equilibrium Adsorption Performance. *Ind. Eng. Chem. Res.* **2007**, *46*, 446–458.

(3)     Brunelli, N. A.; Didas, S. A.; Venkatasubbaiah, K.; Jones, C. W. Tuning Cooperativity by Controlling the Linker Length of Silica- Supported Amines in Catalysis and $CO_2$ Capture. *J. Am. Chem. Soc.* **2012**, *134*, 13950–13953.

(4)     Bollini, P.; Brunelli, N. A.; Didas, S. A.; Jones, C. W. Dynamics of $CO_2$ Adsorption on Amine Adsorbents. 2. Insights Into Adsorbent Design. *Ind. Eng. Chem. Res.* **2012**, *51*, 15153–15162.

(5)     Wang, J.; Wang, M.; Li, W.; Qiao, W.; Long, D.; Ling, L. Application of Polyethyleneimine-Impregnated Solid Adsorbents for Direct Capture of Low-Concentration $CO_2$. *AIChE J.* **2015**, *61* (3), 972–980.

(6)     Satyapal, S.; Filburn, T.; Trela, J.; Strange, J. Performance and Properties of a Solid Amine Sorbent for Carbon Dioxide Removal in Space Life Support Applications. *Energy & Fuels* **2001**, *15* (2), 250–255.

(7)     Xu, X.; Song, C.; Andrésen, J. M.; Miller, B. G.; Scaroni, A. W. Preparation and Characterization of Novel $CO_2$ "molecular Basket" Adsorbents Based on Polymer-Modified Mesoporous Molecular Sieve MCM-41. *Microporous Mesoporous Mater.* **2003**, *62* (1-2), 29–45.

(8)     Arenillas, a.; Smith, K. M.; Drage, T. C.; Snape, C. E. $CO_2$ Capture Using Some Fly Ash-Derived Carbon Materials. *Fuel* **2005**, *84* (17), 2204–2210.

127

(9)     Goeppert, A.; Meth, S.; Prakash, G. K. S.; Olah, G. A. Nanostructured Silica as a Support for Regenerable High-Capacity Organoamine-Based $CO_2$ Sorbents. *Energy Environ. Sci.* **2010**, *3* (12), 1949–1960.

(10)    Meth, S.; Goeppert, A.; Prakash, G. K. S.; Olah, G. A. Silica Nanoparticles as Supports for Regenerable $CO_2$ Sorbents. *Energy & Fuels* **2012**, *26*, 3082–1090.

(11)    Tanthana, J.; Chuang, S. S. C. In Situ Infrared Study of the Role of PEG in Stabilizing Silica-Supported Amines for $CO_2$ Capture. *ChemSusChem* **2010**, *3* (8), 957–964.

(12)    Srikanth, C. S.; Chuang, S. S. C. Spectroscopic Investigation into Oxidative Degradation of Silica-Supported Amine Sorbents for $CO_2$ Capture. *ChemSusChem* **2012**, *5*, 1435–1442.

(13)    Srikanth, C. S.; Chuang, S. S. C. Infrared Study of Strongly and Weakly Adsorbed $CO_2$ on Fresh and Oxidatively Degraded Amine Sorbents. *J. Phys. Chem. C* **2013**, *117*, 9196–9205.

(14)    Wang, J.; Long, D.; Zhou, H.; Chen, Q.; Liu, X.; Ling, L. Surfactant Promoted Solid Amine Sorbents for $CO_2$ Capture. *Energy Environ. Sci.* **2012**, *5* (2), 5742–5749.

(15)    Wang, J.; Wang, M.; Zhao, B.; Qiao, W.; Long, D.; Ling, L. Mesoporous Carbon-Supported Solid Amine Sorbents for Low- Temperature Carbon Dioxide Capture. *Ind. Eng. Chem. Res.* **2013**, *52*, 5437–5444.

(16)    Labreche, Y.; Fan, Y.; Rezaei, F.; Lively, R. P.; Jones, C. W.; Koros, W. J. Poly(amide-imide)/Silica Supported PEI Hollow Fiber Sorbents for Postcombustion $CO_2$ Capture by RTSA. *ACS Appl. Mater. Interfaces* **2014**, No. 6, 19336–19346.

(17)    Heydari-Gorji, A.; Belmabkhout, Y.; Sayari, A. Polyethylenimine-Impregnated Mesoporous Silica : Effect of Amine Loading and Surface Alkyl Chains on $CO_2$ Adsorption. *Langmuir* **2011**, *27*, 12411–12416.

(18)    Heydari-Gorji, A.; Sayari, A. $CO_2$ Capture on Polyethylenimine-Impregnated Hydrophobic Mesoporous Silica: Experimental and Kinetic Modeling. *Chem. Eng. J.* **2011**, *173* (1), 72–79.

(19)    Yue, M. B.; Chun, Y.; Cao, Y.; Dong, X.; Zhu, J. H. $CO_2$ Capture by As-Prepared SBA-15 with an Occluded Organic Template. *Adv. Funct. Mater.* **2006**, *16* (13), 1717–1722.

(20)    Fauth, D. J.; Gray, M. L.; Pennline, H. W.; Krutka, H. M.; Sjostrom, S.; Ault, A. M. Investigation of Porous Silica Supported Mixed-Amine Sorbents for Post-Combustion $CO_2$ Capture. *Energy* **2012**.

(21)    Sanz, R.; Calleja, G.; Arencibia, A.; Sanz-Pérez, E. S. $CO_2$ Uptake and Adsorption Kinetics of Pore-Expanded SBA-15 Double-Functionalized with Amino Groups Rau L. *Energy & Fuels* **2013**, *27*, 7637–7644.

(22)    Liu, J.; Cheng, D.; Liu, Y.; Wu, Z. Adsorptive Removal of Carbon Dioxide Using Polyethyleneimine Supported on Propanesulfonic-Acid-Functionalized Mesoporous. *Energy & Fuels* **2013**, *27*, 5416–5422.

(23)    Choi, S.; Drese, J. H.; Eisenberger, P. M.; Jones, C. W. Application of Amine-Tethered Solid Sorbents for Direct $CO_2$ Capture from the Ambient Air. *Environ. Sci. Technol.* **2011**, *45* (6), 2420–2427.

(24)    Sanz, R.; Calleja, G.; Arencibia, A.; Sanz-Pérez, E. S. Development of High Efficiency Adsorbents for $CO_2$ Capture Based on a Double-Functionalization Method of Grafting and Impregnation. *J. Mater. Chem. A* **2013**, *1* (6), 1956–1962.

(25)    Choi, S.; Gray, M. L.; Jones, C. W. Amine-Tethered Solid Adsorbents Coupling High Adsorption Capacity and Regenerability for $CO_2$ Capture from Ambient Air. *ChemSusChem* **2011**, *4* (5), 628–635.

(26)    Wang, X.; Song, C. New Strategy To Enhance $CO_2$ Capture over a Nanoporous Polyethylenimine Sorbent. *Energy & Fuels* **2014**, *28*, 7742–7745.

130

(27) Zhu, J.; Baker, S. N. Lewis Base Polymers for Modifying Sorption and Regeneration Abilities of Amine-Based Carbon Dioxide Capture Materials. *ACS Sustain. Chem. Eng.* **2014**, *2*, 2666–2674.

(28) Serna-Guerrero, R.; Belmabkhout, Y.; Sayari, A. Modeling CO2 Adsorption on Amine-Functionalized Mesoporous Silica: 1. A Semi-Empirical Equilibrium Model. *Chem. Eng. J.* **2010**, *161* (1-2), 173–181.

(29) Chaikittisilp, W.; Kim, H.-J.; Jones, C. W. Mesoporous Alumina-Supported Amines as Potential Steam-Stable Adsorbents for Capturing $CO_2$ from Simulated Flue Gas and Ambient Air. *Energy & Fuels* **2011**, *25*, 5528–5537.

(30) Bali, S.; Chen, T. T.; Chaikittisilp, W.; Jones, C. W. Oxidative Stability of Amino Polymer–Alumina Hybrid Adsorbents for Carbon Dioxide Capture. *Energy & Fuels* **2013**, *27* (3), 1547–1554.

(31) Fulvio, P. F.; Brosey, R. I.; Jaroniec, M. Synthesis of Mesoporous Alumina from Boehmite in the Presence of Triblock Copolymer. *ACS Appl. Mater. Interfaces* **2010**, *2* (2), 588–593.

(32) Zhang, Z.; Pinnavaia, T. J. Mesoporous Gamma-Alumina Formed through the Surfactant-Mediated Scaffolding of Peptized Pseudoboehmite Nanoparticles. *Langmuir* **2010**, *26* (12), 10063–10067.

(33)   Liu, Q.; Wang, A.; Wang, X.; Gao, P.; Wang, X.; Zhang, T. Synthesis, Characterization and Catalytic Applications of Mesoporous Γ-Alumina from Boehmite Sol. *Microporous Mesoporous Mater.* **2008**, *111* (1-3), 323–333.

(34)   Wang, J.; Huang, H.; Wang, M.; Yao, L.; Qiao, W.; Long, D.; Ling, L. Direct Capture of Low-Concentration $CO_2$ on Mesoporous Carbon-Supported Solid Amine Adsorbents at Ambient Temperature. *Ind. Eng. Chem. Res.* **2015**, *54* (19), 5319–5327.

(35)   Lee, H. I.; Kim, J. H.; Stucky, G. D.; Shi, Y.; Pak, C.; Kim, J. M. Morphology-Selective Synthesis of Mesoporous SBA-15 Particles over Micrometer, Submicrometer and Nanometer Scales. *J. Mater. Chem.* **2010**, *20* (39), 8483–8487.

(36)   Labreche, Y.; Lively, R. P.; Rezaei, F.; Chen, G.; Jones, C. W.; Koros, W. J. Post-Spinning Infusion of Poly(ethyleneimine) into Polymer/silica Hollow Fiber Sorbents for Carbon Dioxide Capture. *Chem. Eng. J.* **2013**, *221*, 166–175.

(37)   Drese, J. H.; Choi, S.; Lively, R. P.; Koros, W. J.; Fauth, D. J.; Gray, M. L.; Jones, C. W. Synthesis-☐"Structure-☐"Property Relationships for Hyperbranched Aminosilica CO2 Adsorbents. *Adv. Funct. Mater.* **2009**, *19* (23), 3821–3832.

(38)   Von Harpe, A.; Petersen, H.; Li, Y.; Kissel, T. Characterization of Commercially Available and Synthesized Polyethylenimines for Gene Delivery. *J. Control. Release* **2000**, *69* (2), 309–322.

132

(39)    Ruthven, D. M. *Principles of Adsorption & Adsorption Processes*; John Wiley & Sons: New York, 1984.

(40)    Wilfong, W. C.; Chuang, S. S. C. Probing the Adsorption/Desorption of $CO_2$ on Amine Sorbents by Transient Infrared Studies of Adsorbed $CO_2$ and $C_6H_6$. *Ind. Eng. Chem. Res.* **2014**.

(41)    Wilfong, W. C.; Srikanth, C. S.; Chuang, S. S. C. In Situ ATR and DRIFTS Studies of the Nature of Adsorbed $CO_2$ on Tetraethylenepentamine Films. *ACS Appl. Mater. Interfaces* **2014**, *3* (2), 2–11.

(42)    Xu, X.; Song, C.; Andresen, J. M.; Miller, B. G.; Scaroni, A. W. Novel Polyethylenimine-Modified Mesoporous Molecular Sieve of MCM-41 Type as High-Capacity Adsorbent for CO 2 Capture. *Energy & Fuels* **2002**, *16* (6), 1463–1469.

(43)    Sakwa-Novak, M. A.; Jones, C. W. Steam Induced Structural Changes of a Poly(ethylenimine) Impregnated Γ - Alumina Sorbent for $CO_2$ Extraction from Ambient Air. *ACS Appl. Mater. Interfaces* **2014**, *6*, 9245–9255.

(44)    Li, W.; Choi, S.; Drese, J. H.; Hornbostel, M.; Krishnan, G.; Eisenberger, P. M.; Jones, C. W. Steam-Stripping for Regeneration of Supported Amine-Based $CO_2$ Adsorbents. *ChemSusChem* **2010**, *3* (8), 899–903.

(45)    Li, W.; Bollini, P.; Didas, S. A.; Choi, S.; Drese, J. H.; Jones, C. W. Structural Changes of Silica Mesocellular Foam Supported Amine-Functionalized $CO_2$ Adsorbents upon Exposure to Steam. *ACS Appl. Mater. Interfaces* **2010**, *2* (11), 3363–3372.

(46)    Hammache, S.; Hoffman, J. S.; Gray, M. L.; Fauth, D. J.; Howard, B. H.; Pennline, H. W. Comprehensive Study of the Impact of Steam on Polyethyleneimine on Silica for $CO_2$ Capture. *Energy & Fuels* **2013**, *27*, 6899–6905.

(47)    Baca, M.; de la Rochefoucauld, E.; Ambroise, E.; Krafft, J. M.; Hajjar, R.; Man, P. P.; Carrier, X.; Blanchard, J. Characterization of Mesoporous Alumina Prepared by Surface Alumination of SBA-15. *Microporous Mesoporous Mater.* **2008**, *110* (2-3), 232–241.

(48)    Baca, M.; Carrier, X.; Blanchard, J. Confinement in Nanopores at the Oxide/water Interface: Modification of Alumina Adsorption Properties. *Chem. - A Eur. J.* **2008**, *14* (20), 6142–6148.

# CHAPTER 5

# FUNCTIONALIZATION OF MONOLITHIC ALUMINA

# HONEYCOMBS WITH PEI

## 5.1    Introduction & Motivation

As noted in chapter 1, it is proposed to disperse polymeric amines in a honeycomb monolith structure, similar to that of a catalytic converter, as such a structure provides a high surface area substrate that imposes low pressure drop on fluids moving through its channels. There is very little understanding of how to engineer high performing monolithic adsorbents beyond structure/performance relationships derived in literature for powder sorbents. The functionalization of porous monolithic structures with polymeric amines for $CO_2$ capture has been explored in the literature only to a limited degree. Meso-macroporous silica monoliths have been impregnated with PEI and tetra(ethylenepentamine) (TEPA) and investigated for gas adsorption in several papers.[1–6] Higher adsorption capacities have been observed with the monolithic supports than with powders, a phenomena that has largely been explained by the increased total pore volume and pore connectivity in the structured materials. However, these monoliths were not of the preferred honeycomb channel arrangement noted above. Other macrostructures with hierarchical pore systems have been impregnated with PEI as well, such as polymeric hollow fibers spun to contain silica particles within the polymeric matrix.[7–10] PEI incorporation into the silica monoliths has been carried out using wet impregnation

135

techniques that are popular for powder sorbents. Conversely, a step for PEI incorporation into the hollow fibers was integrated into the solvent exchange process of fiber preparation by immersing fibers in a solution of methanol and PEI to impregnate the embedded silica.[8]

Most of these studies have focused more on the performance of the materials, and less on developing scalable PEI impregnation procedures or thorough characterizations of the sorbent properties. Specifically, there has been no investigation or discussion as to the preferred occupancy regimes (micropores vs. mesopores vs. macropores) of the amines upon impregnation into hierarchically porous materials. Efficient incorporation of amines into the micro and mesopores of a hierarchical material is likely to play a critical role in defining important performance characteristics such as amine accessibility, propensity for amine leaching, and wasted heat (from heating of unused amine in a temperature swings). It is therefore critical to develop scalable and effective techniques of amine incorporation into practical structures for inexpensive wide scale production and deployment of $CO_2$ capture technologies. Additionally, the performance of such structured adsorbents has not been assessed in the context of literature precedents for adsorption capacities and uptake rates.

In this chapter, we report on the systematic scale up of powder sorbents to monolithic sorbents. Small pieces of monolithic alumina were functionalized with PEI and thoroughly compared to powders prepared with the same alumina support. Compared to analogous powders, the monolithic sorbents showed a larger discrepancy in the expected mesopore filling of PEI, suggesting that PEI deposited in macropores to a larger

136

extent in the monoliths than in the powders. A larger monolithic sorbent was stable to five cycles of $CO_2$ adsorption followed by steam stripping, and showed similar thermodynamic performance to powders and smaller monolithic samples. Despite the similar performance in the monoliths and powders, this physical difference suggests that there is room for improvement in the preparation of monolithic sorbents through novel and/or improved procedures.

## 5.2    Experimental

### 5.2.1    Materials

Poly(ethyleneimine) (PEI) (branched, Mw~ 800, Sigma-Aldrich), and methanol (ACS grade, BDH chemicals) were used as received from the supplier. Cylindrical monoliths of ~1 in diameter and ~4 in length were provided by Corning, Inc. The monoliths had a honeycomb channel arrangement with either 200 or 400 cells per square inch (cpsi) of frontal cell density. For both cell densities, the wall thickness was 7 mil (0.007 in.).The materials used in this study were either small pieces cut from a full cylindrical monolith, or powders created from crushing the smaller pieces with pestle and mortar. A single, full monolith cylinder (1 in. x 4 in.) with a cell density of 200 cpsi was used as well.

### 5.2.2    Monolith PEI Impregnation

All samples were dried under high vacuum (~20 mtorr) for 12-16 h under elevated temperature prior (~100 $^{\circ}$C) to PEI impregnation. Small monolith pieces, with weights ranging from ~ 0.1 – 0.25 g, were dipped in solutions containing PEI and

137

methanol (MeOH) through one of two methods described below. All impregnations were performed with a 20 mL total liquid (PEI/MeOH) volume in a capped 50 mL round bottom flask. Monolith pieces were suspended in solution by way of Nylon wire that was looped through several monolith channels and passed through the interior of a syringe. The syringe protruded through a rubber septa that capped the round bottom flask. Suspended monolith pieces were lowered into, or raised out of, solution by adjusting the syringe up or down in the septa. During monolith immersion, the PEI/MeOH solutions were stirred with a stir bar and magnetic stirrer. A picture of a typical setup is provided in appendix D, figure D.1.

In the *Capillary Method*, a given wt% PEI/MeOH solution was equilibrated under stirring for 30 min prior to monolith immersion. Monoliths were then dipped into the solution by lowering completely into the liquid, and subsequently immersing for either 5 min, 1 h or 6 h. Following immersion, the monolith pieces were lifted out of solution, and suspended above the dipping solution for 30 min to allow excess liquid to drip from the channels and exterior of the structure. Finally, the samples were dried under ~20 mtorr of vacuum at ~60 $^{\mathrm{o}}$C to fully remove the MeOH.

In the *Diffusion Method*, a PEI/MeOH solution at double the target PEI wt% was equilibrated under stirring for 30 min (e.g. a 60 wt% PEI solution would be prepared for a target final 30 PEI wt% solution). Separately, a monolith piece was immersed for 30 minutes in a quantity of methanol that, when combined with the concentrated PEI/MeOH solution, would result in the target solution concentration. The PEI/MeOH solution was then rapidly added to the monolith/MeOH system without lifting the monolith out of the

MeOH. The resultant mixture was stirred for a given amount of time and then treated in the same manner as in the *Capillary Method*.

### 5.2.3  Powder Preparation

Powders were prepared directly from monolith pieces by gentle grinding with a pestle and mortar. The monolith pieces were ground until a flowing powder was formed. Powder sorbents were prepared though a traditional impregnation method. Powder alumina was dried under vacuum at ~100 $^{o}$C prior to PEI impregnation. Each powder sample was prepared using 0.25 g of dry alumina. The alumina was dispersed in 20 mL of MeOH under stirring. Separately, a given amount of PEI was dissolved in 10 mL of MeOH. The two mixtures were allowed to stir separately for 1 h, before the solution containing PEI was added dropwise via pipette to the dispersion containing alumina. The resultant mixture was stirred for 3 h at room temperature. The solvent was then removed by rotary evaporation at ~50 $^{o}$C, before residually adsorbed solvent was further removed by drying under vacuum (~20 mtorr) at ~60 $^{o}$C overnight.

### 5.2.4  Characterization

Thermogravimetric Analysis – The organic and inorganic content of samples were estimated via TGA analysis by use of a NETSCH STA 449 F3 Jupiter. ~10-14 mg of sample were placed in a platinum pan and exposed to diluted (in $N_2$) air with a temperature ramp. The organic fraction of the sample was taken as the ratio of weight loss in the region of 120-900 $^{o}$C relative to the residual mass at 900 $^{o}$C. Organic loadings

derived in this manner were corrected by the weight loss of the bare alumina in the appropriate temperature region.

Nitrogen Physisorption – $N_2$ physisorption experiments were carried out on a Micromeritics Tristar II 3020. Samples were dried at 110 $^o$C under vacuum for 12h on a Schlenk line prior to the adsorption analysis. Approximately 200 mg of sample was used in each analysis. Surface areas were estimated with the BET method, pore volumes estimated using the total $N_2$ adsorbed at $P/P_0 \sim 0.99$, and pore size distributions derived using either the BdB-FHH, BJH (using the adsorption branch of the isotherm) or NLDFT models. BJH and NLDFT PSDs were derived using the VersaWin software package from Quantachrome.

Mercury Porosimetry – Mercury intrusion porosimetry was performed at Micromeritics (Norcross, GA). Samples were degassed at 100 $^o$C under vacuum prior to analysis. Mercury pressures of $0.2 - 60000$ psi were applied to 0.2g of sample at 18 $^o$C. A mercury/alumina contact angle of $130^o$ was assumed in the conversion of mercury pressure to pore size using the Washburn equation.[11]

XPS – XPS spectra were recorded on a Thermo K-Alpha spectrometer and a monochromatic Al kα X-ray source. Prior to analysis, samples were dried overnight under vacuum to remove adsorbed species. Scans from 0 to 1350 eV were measured with a scanning step of 0.1 eV. The spectra were calibrated using the C1s peak at 284.6 eV. A chamber vacuum pressure of $4 \times 10^{-7}$ torr was employed during the analysis. All samples were measured in 'powder' form. Samples prepared as monoliths were crushed to form powders prior to experiment.

<u>SEM Imaging</u> – SEM images were recorded on a Hitachi SU8010 microscope. Samples were prepared by depositing on carbon tape and subsequently sputtering with gold for 60s.

<u>$CO_2$ Adsorption</u> – $CO_2$ adsorption was performed by TGA analysis and in fixed bed experiments. TGA experiments were carried out on a TA Instruments Q500for 12 h under a 90 mL/min flow of 400 ppm $CO_2$ / He. Prior to exposure to the $CO_2$ containing gas, the samples were pretreated under He flow at 110 $^o$C for 3 h. Fixed bed, steam stripping experiments were carried out on a home-made flow adsorption apparatus equipped with a Sussman MBA-3 boiler to provide steam. A schematic of the system is provided in the appendix A, figure A.1. A full monolith core (1 inch diameter, 3 inches length) was used in these experiments. The monolith was wrapped in Teflon tape and place inside of a cylindrical stainless steel monolith housing container. The top of the monolith was wrapped with a thicker layer of Teflon tape as to create an interface between the tape and the inside edge of the housing container to minimize gas bypass. The container was sealed on the top and bottom with O-rings, and connected to the system piping by way of ¼" Swagelok adapters. The monolith was subjected to cycles of (i) drying under hot $N_2$ (1 L/min, lines upstream of container heated externally with heat tape and monolith chamber heated with a fluid heating jacket), (ii) cooling under ambient $N_2$ (1 L/min), (iii) $CO_2$ adsorption (400 ppm $CO_2/N_2$, 12.5 SLM), and (iv) steam exposure (~5 g/min, 110-120 $^o$C saturated).

## 5.3 Results and Discussion

### 5.3.1 Preparation and Characterization of Sorbents

Extruded honeycomb monoliths prepared with Sasol Sba-200 mesoporous γ-alumina powder were provided by Corning and used in this study. The honeycombs were received as cylindrical structures of ~1 inch diameter and ~4 inches length, with a cell density of either 200 or 400 cells per square inch (cpsi) and a wall thickness of 7 mil (0.007 inch, ~180 μm). The SEM image in figure 5.1a reveals the square channel cross section and wall thickness of the structures. Figures 5.1b and 5.1c show the macroporous nature of the wall on length scales of 10-50 μm. These images illustrate that the walls of the monolith consisted of purely of γ-alumina particles sintered together to form a network of particles and voids with sizes on the length scale of micrometers. For convenient analysis using standard powder characterization instrumentation, smaller monolith pieces (~200 mg) that retained the honeycomb structure were cut from the larger cylinders. Additionally, a powder analogue was prepared to provide comparison with the monolith pieces. The powder was formed by grinding bare monolith pieces with mortar and pestle. SEM images shown in figure 5.1(d-f) reveal the large particle size distribution of the powder. The images suggest that the powder was comprised of large primary porous particles, much smaller binder particles, and clusters of binder and primary particles.
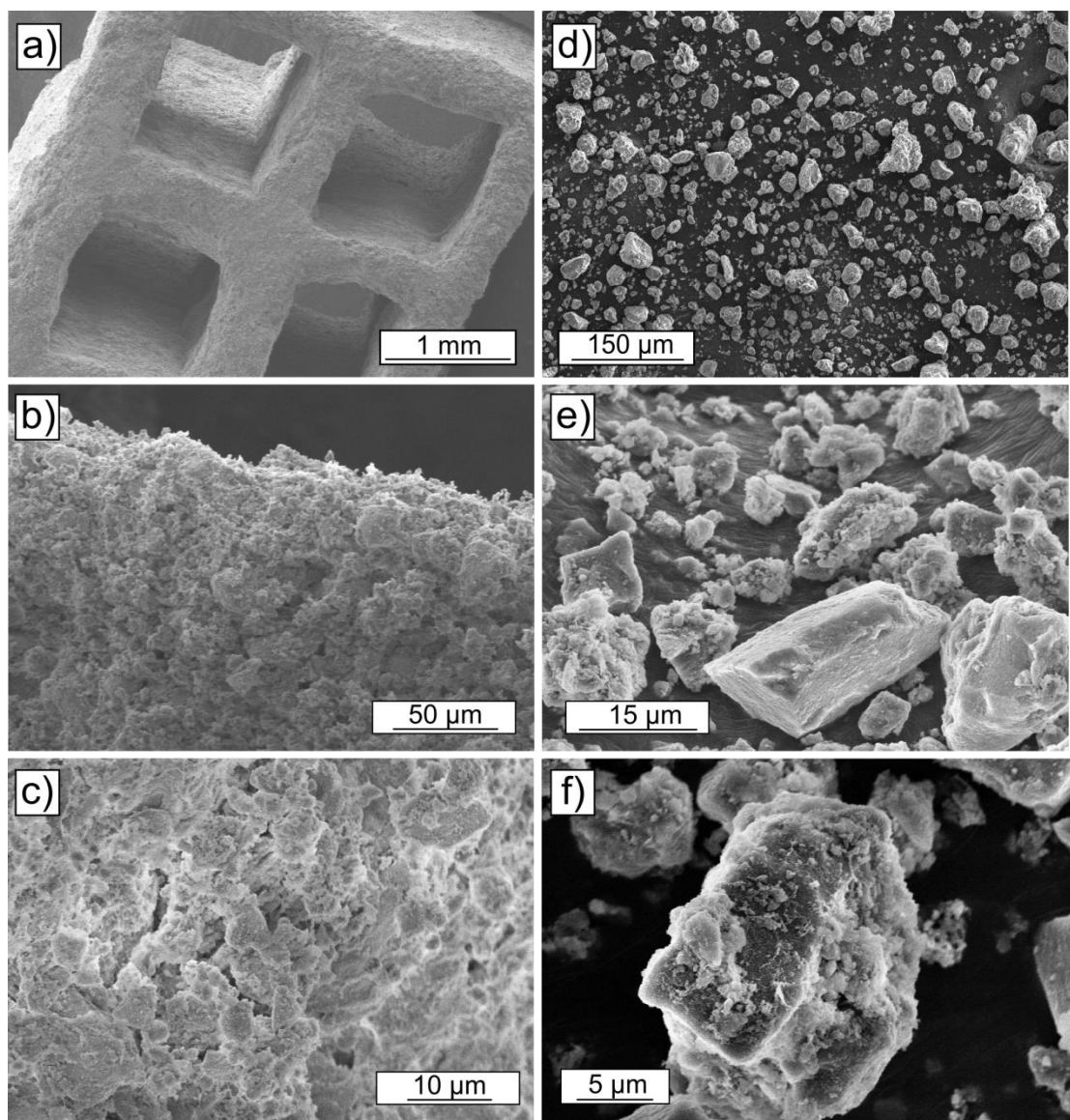
Figure 5.1 SEM images of small pieces of monolith (a-c) and powder (d-f) formed by grinding similar small pieces of monolith.

The monoliths and powders both contained measureable porosity in the meso and macropore size regimes. $N_2$ physisorption and mercury porosimetry were used to assess the porosity of the samples and their corresponding pore size distributions are shown in figure 5.2. The data show that the mesoporous characteristics of the monoliths and

powders were very similar, while there were differences in the macroporous nature of the samples. Consistent with the creation of new voids between alumina particles from the powder preparation, the macropore volume of the powder ($0.91$ cm$^3$/g) was significantly higher than that of the monolith ($0.54$ cm$^3$/g) while the mesopore volumes (obtained from the N$_2$ experiment) were very similar for both samples (~$0.42$ and $0.39$ cm$^3$/g for monolith and powder, respectively); the data are tabulated in table 5.1.



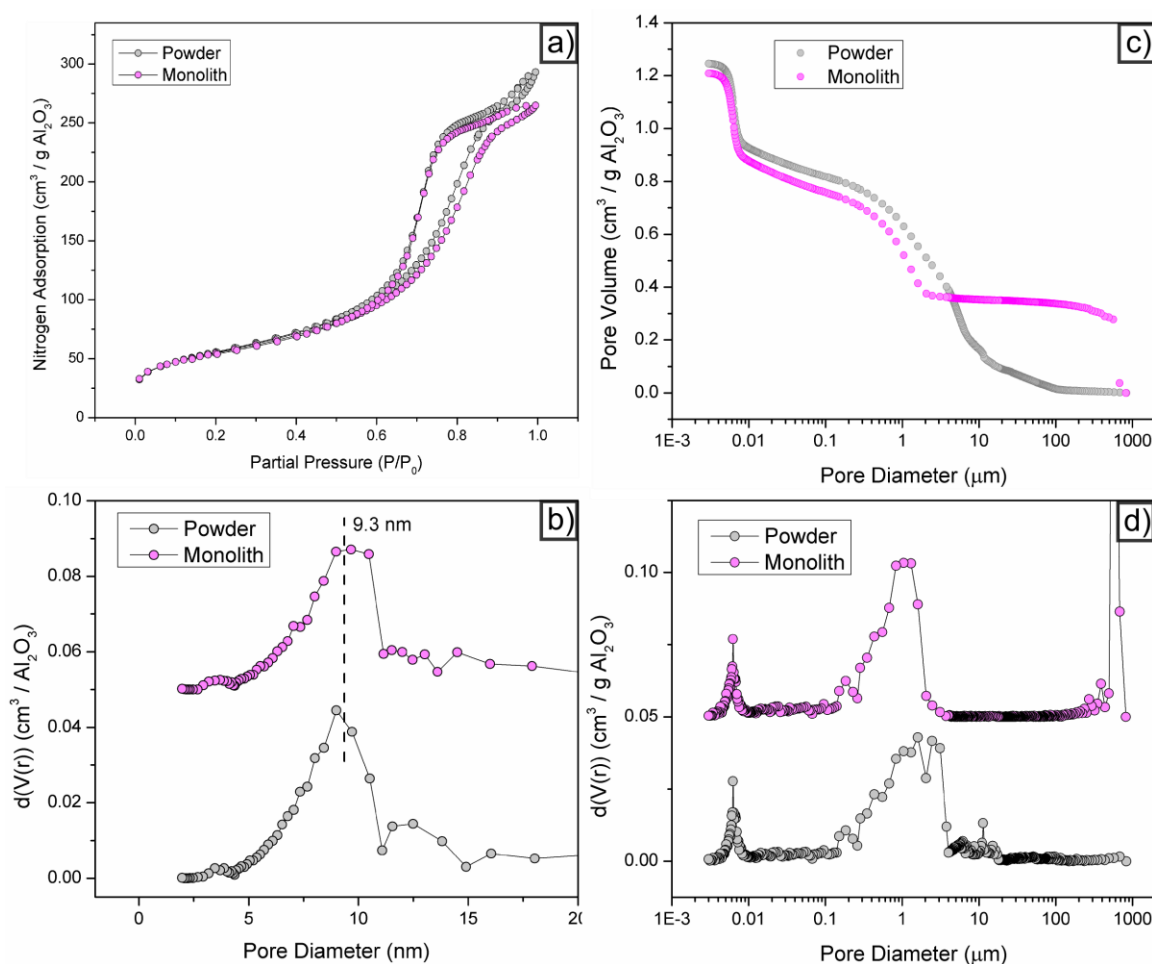Figure 5.2. N$_2$ physisorption isotherms (a), BdB-FHH pore size distributions (b), mercury porosimetry profiles (c), and the resulting pore size distributions (d) of a bare alumina monolith (magenta) and powder (grey). N$_2$ pore size distribution derived from the BdB-FHH method, using the adsorption branch of the N$_2$ isotherm. Pore size distributions of monoliths offset by $0.05$ cm$^3$/g in (b) and (d).

144

The N$_2$ isotherms of the monolith and powder nearly overlapped and show moderate N$_2$ uptake at low P/P$_0$ followed by a sharp N$_2$ uptake and hysteresis at high P/P$_0$, confirming the mesoporous nature of the alumina. Correspondingly, the pore size distributions of both sample types reflect a common mesopore structure, with a pore diameter centered at ~9 nm, and a low micropore volume. These data show that the mesoporosity of the alumina was not altered by crushing the monolith to form a powder. More stark differences are apparent in the mercury porosimetry profiles. The most striking of these is the large mercury uptake at large pore size (low mercury pressure) in the monolith sample, corresponding to filling of the extruded channels. Clearly, the channels were not present in the powders and such uptake is not observed in the powder profile. There is a gradual increase in the mercury uptake in pores of ~10-100 μm present in the powders but not in the monoliths, manifested as small peaks appearing only in the powder pore size distribution in this region. Finally, there is a sharp mercury uptake and gradual increase in sorption in pore sizes between ~100 nm to 10 μm in both the monolith and powder profiles. The bulk of the macroporosity of both samples fell in this regime, as is obvious in the pore size distributions. There was a wider range of macropore diameters in the powder, as evidenced by the smaller pore size at which the onset of the sharp mercury uptake occurred in the monolith sample.

PEI was impregnated into the monolith pieces by two methods, both of which involved the immersion of a monolith in a PEI/MeOH solution for a period of time followed by solvent removal via vacuum treatment. The two impregnation methods, denoted by the hypothesized means of PEI transport into the monolith pores, differed

most fundamentally by the nature of the fluid occupying the pores prior to introduction of PEI. In the 'capillary' based method, monolith pieces, previously in ambient air, were immersed into the PEI solution for a given amount of time before being removed and dried. It was hypothesized that capillary forces acting to displace the air in the pores with PEI/MeOH would play a significant role in drawing PEI into the structure. In the second, 'diffusion' based method, monolith pieces were immersed in methanol prior to introduction of PEI into the solution. Here, it was expected that the role of capillary forces in drawing PEI into the monolith pores would be substantially reduced as a result of the much smaller density difference between the fluid occupying the pores before and after introduction of PEI. As such, it was hypothesized that PEI would enter the pores of the structure primarily through diffusion and possibly convection (from the stirred solution), rather than convection induced by capillary forces. In both methods, the total volume of solution used in the impregnation of a single monolith piece was kept constant (20 mL), and in all cases the immersion of a monolith was followed by a short ambient drying treatment to remove excess liquid from the channels and exterior of the monolith and then subsequent vacuum treatment to fully remove the methanol.

The two impregnation methods yielded monolithic sorbents of similar composition and textural properties. Figure 5.3a shows the composition (g PEI / g $Al_2O_3$) of sorbents prepared by immersion in solutions of 30 wt% PEI for three times by both methods. The average sorbent composition varied between ~0.30 and 0.45 g PEI / g $Al_2O_3$ depending on the immersion time, for both methods. The horizontal line in figure 5.3a represents the particular sorbent composition at which the volume of PEI in the

sample matches the mesopore volume of the (bare) alumina. The average PEI loadings achieved for sorbents immersed for 1 h and 6 h by the capillary method were very close to this mesopore filling threshold. The sorbent loading prepared by the diffusion method and a 6h immersion time also was very close to this value.
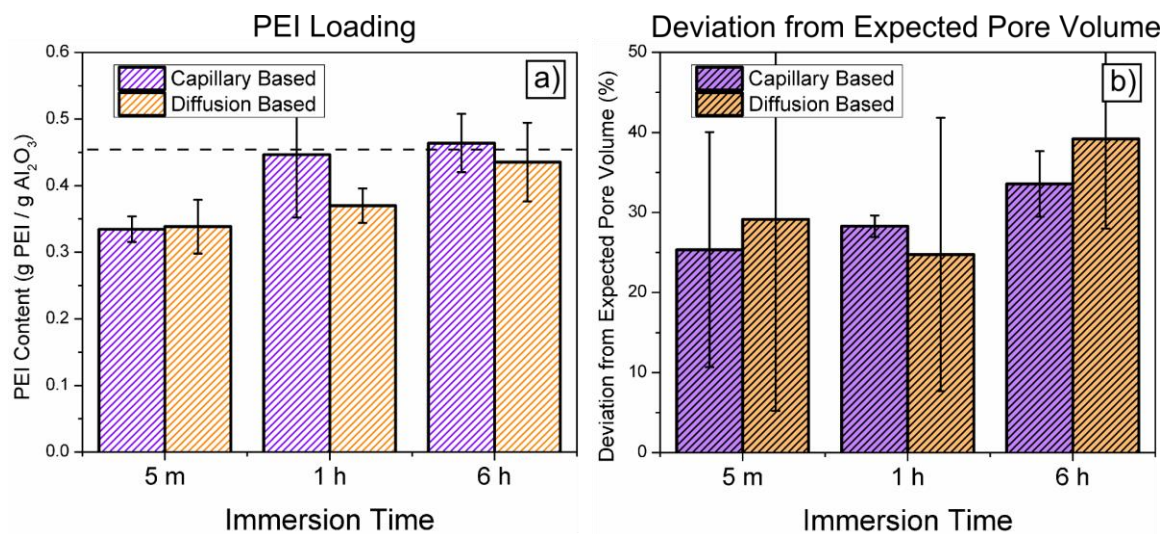


Figure 5.3 PEI content (left, a) and percentage difference in measured vs expected pore volume (right, b) for monolithic sorbents prepared by the capillary based method (purple) or diffusion based method (orange). Horizontal line in (a) represents PEI content equal to mesopore volume of bare alumina. Error bars determined from preparation of replicate monolith sorbents under similar conditions.

The textural properties of the sorbents prepared via both impregnation methods were also similar, though there was some degree of variability as indicated by the error bars in figure 5.3b. Importantly, the pore volume measured by $N_2$ physisorption deviated significantly from expected characteristics. Figure 5.3b shows the difference in measured vs. expected mesopore volume (expressed as percent of expected) of the monolithic sorbents. The expected mesopore volume was calculated by means of the loading and density of PEI, assuming exclusive occupation of mesopores by PEI, while the measured

pore volume was calculated from $N_2$ physisorption isotherms normalized to the total amount of $Al_2O_3$ in the sample. The discrepancy in pore volume ranged from 25-35% of the expected value, but had standard deviations that approached 50-75% of the average value. This variance was larger for the 'diffusion' based impregnation method for each of the immersion times, perhaps due to unequal penetration of the PEI into the smaller pores of the monolith without capillary induced convection.

The measured pore volumes of the monolithic sorbents were always *higher* than the expected value, and deviated to a greater extent than powders prepared at similar loadings. These findings are more clearly demonstrated in figure 5.4, where the pore volumes of monolithic and powder sorbents are shown as a function of PEI loading. All samples reported in figure 5.4 were prepared by the 'capillary' method, for consistency. Here, results of individual samples are presented rather than averages, as are shown in figures 5.3a and 5.3b. Solid lines representing the expected pore volume for given PEI loadings are drawn in the figure for comparison. The expected pore filling lines for powders and monoliths are slightly offset due to the small difference in measured pore volume of the bare powder and bare monolith. The figure establishes that monolithic sorbents had higher pore volumes than powder sorbents across the entire range of measured PEI content, and correspondingly deviated further from the expected pore filling.
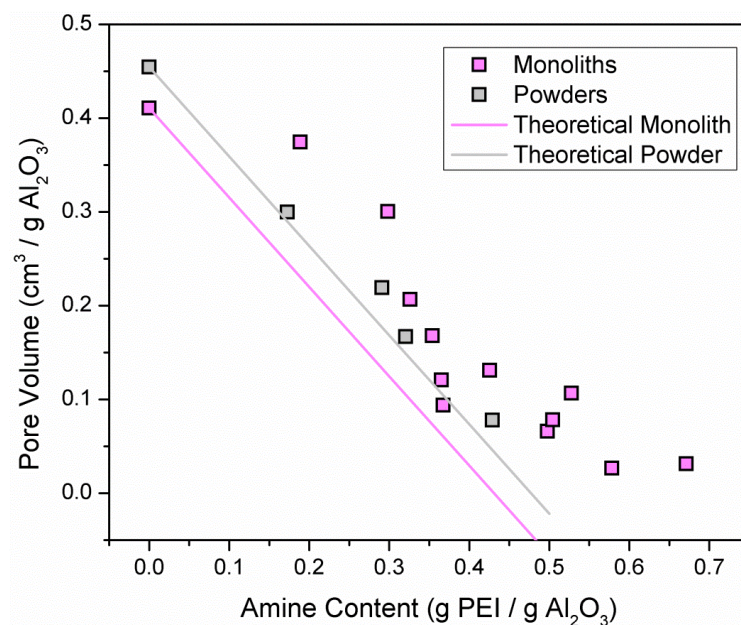
Figure 5.4 Normalized pore volume for monoliths (magenta) and powders (grey) at varying PEI content compared to expected pore volumes (solid lines). All monolith samples prepared via *capillary method*.

To explore the differences between the powder and monolith sorbents in greater detail, samples with common PEI content (+/- 0.02 g PEI / g $Al_2O_3$) were selected and further characterized. Tabulated in table 5.1 are the physical and textural properties of the selected sorbents. Each of the monolith samples was prepared using the 'capillary' method and an immersion time of 1 h. Powder and monolith pairs at similar amine content are labeled as having 'low', 'medium', or 'high' amine content, for simplicity in the subsequent discussion.

Table 5.1 Textural properties of selected monolithic and powder samples. Monoliths prepared using 'capillary method', an immersion time of 1h, and PEI contents of 5, 10 and 30 wt% for low, medium, and high PEI samples.

| Sample | Form | Amine Loading[a] | Surface Area[b] | Macropore Volume[c] | Mesopore Volume[b] | Expected Volume PEI[d] | Pore Volume Loss[b] |
|--------|------|------------------|-----------------|---------------------|--------------------|------------------------|---------------------|
|  |  | $g\ PEI\ /\ g$ $Al_2O_3$ | $m^2\ /\ g$ $Al_2O_3$ | $cm^3\ /\ g$ $Al_2O_3$ |  |  |  |
| Bare | Powder | n/a | 194 | 0.91 | 0.45 | n/a | n/a |
| *Bare* | *Monolith* | n/a | 195 | 0.54 | 0.41 | n/a | n/a |
| Low | Powder | 0.19 | 119 | - | 0.26 | 0.16 | 0.16 |
| *Low* | *Monolith* | 0.17 | 167 | - | 0.34 | 0.18 | 0.06 |
| Medium | Powder | 0.29 | 77 | - | 0.19 | 0.28 | 0.23 |
| *Medium* | *Monolith* | 0.30 | 127 | - | 0.27 | 0.28 | 0.12 |
| High | Powder | 0.43 | 16 | - | 0.08 | 0.41 | 0.34 |
| *High* | *Monolith* | 0.44 | 31 | - | 0.10 | 0.42 | 0.31 |

[a]Estimated from TGA. [b]Estimated from $N_2$ physisorption at P/P0 = 0.95. [c] Estimated from Hg porosimetry data between 100 nm and 100 um. [d]Estimated from TGA assuming a PEI density of 1.05 g/mL. Dashes represent measurements that were not made.

As described above, the mesoporous characteristics of the monolith and powder supports were nearly identical while the macropore characteristics differed. The mesoporosity was likely contained in the large, primary alumina particles shown in figure 5.1. These are unlikely to have been interrupted by the powder preparation, in which mainly the interconnections between such particles were broken. The BET surface areas of the monoliths and powders were identical, despite the necessarily larger external surface area of powders. Assuming a solid volume occupancy of 64% (typical of hard packing of spheres) and a nonporous alumina density of 4 g/cm$^3$, the total external surface area of particles ranging from 0.5-20 micron diameter ranges from 0.3-12 m$^2$/g based on geometric considerations and thus comprise only a small fraction of the total surface area (~200 m$^2$/g). Surface areas of pores in the micrometer range derived from

mercury analysis are consistent with these calculations, as shown in appendix D, figure D.2. Upon breaking the continuous network of the monolith, only a fraction of this external surface area would become exposed. The particular fraction would depend on the degree of interconnectivity between particles, where highly interconnected particles would have a higher fraction of newly exposed external surface area than less interconnected particles.

Full $N_2$ physisorption isotherms of the sorbents, shown in figure 5.5, show that both the powder and monolithic sorbents retained isotherm shapes similar to their bare counterparts, despite differences in total $N_2$ adsorbed. The monolithic sorbents adsorbed more $N_2$ over the entire partial pressure range of the experiment than the powder analogues. This suggests that less mesopore volume was filled or blocked by PEI in the monolithic sorbents compared to the powder sorbents. Additionally, each powder sample showed a slight uptick at partial pressures greater than 0.95, while the monolithic samples did not. This is due to $N_2$ condensation in small macropores, consistent with the larger macropore volume and pore size range described above. Pore size distributions were derived from the isotherms using three models (BdB-FHH, BJH, and NLDFT), and are shown in appendix D, figure D.3. Each of the sorbents showed a decrease in the average pore size from ~9 nm (bare support) to ~7 nm (sorbents), though there were not significant differences in the pore sizes of the monolithic sorbents compared to powders.
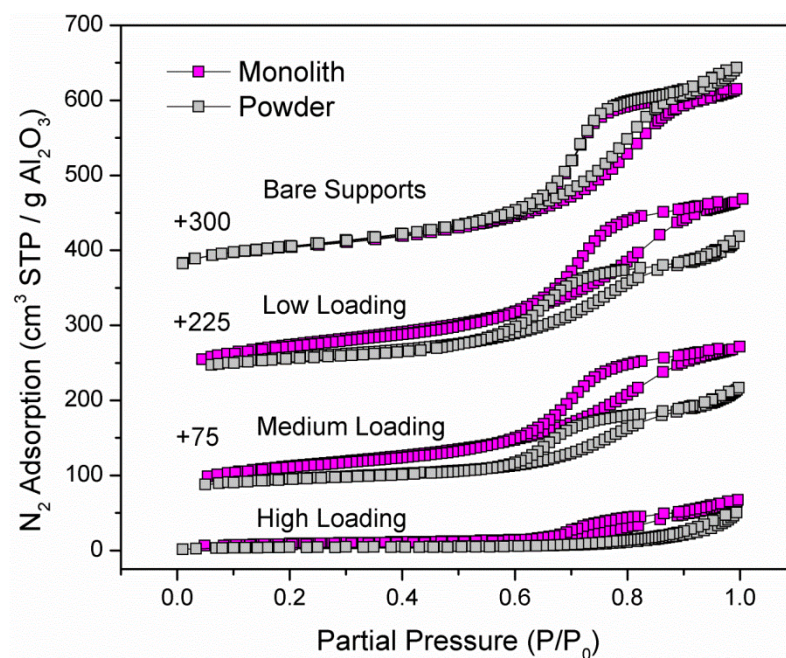
Figure 5.5. $N_2$ physisorption of alumina monolith (magenta) and powder (grey) sorbents. Powder and monolithic sorbents grouped by commonality in amine loading and offset from one another by the values indicated in the figure.

The differences in pore filling between monoliths and powders suggests that a fraction of the PEI was deposited in pore size regimes outside of that accessible to $N_2$ physisorption ($> \sim 100$ nm) in the monolithic sorbents. Conversely, it is suggested in literature that powder impregnation results in PEI depositing predominantly inside the mesopores of host mesoporous oxides.[12–15] The close but not extract agreement between measured and expected pore filling of the powders presented here are consistent with the literature precedent of efficient impregnation. The slight discrepancy may derive from a 'wetting layer' of polymer on the alumina surface, including the external surface area of particles. Such is established in literature of the creation of polymer nanostructures from

filling of anodic alumina,[16,17] and was recently proposed by our group as occurring on PEI/silica adsorbents.[15]

XPS analysis confirmed the presence of PEI on the exterior of particles in both powder and the monolithic samples. Figure 5.6 shows the surface composition derived from these experiments (mol N / mol Al) of powders and monoliths plotted against the bulk composition (estimated by TGA, assuming stoichiometric Al/O and C/N ratios for $Al_2O_3$ and PEI, respectively) of the corresponding material. The figure is bisected such that data falling above the bisecting line contain a higher surface PEI composition than bulk. It is important to note here that to obtain a 'wall averaged' particle surface composition of the monolithic sorbents, all samples were crushed to form powders prior to XPS measurements (i.e. 'powder' and 'monolith' here refer to the form of alumina that was used in *preparation of the sorbent*, but for XPS measurements all samples were in the form of powders).
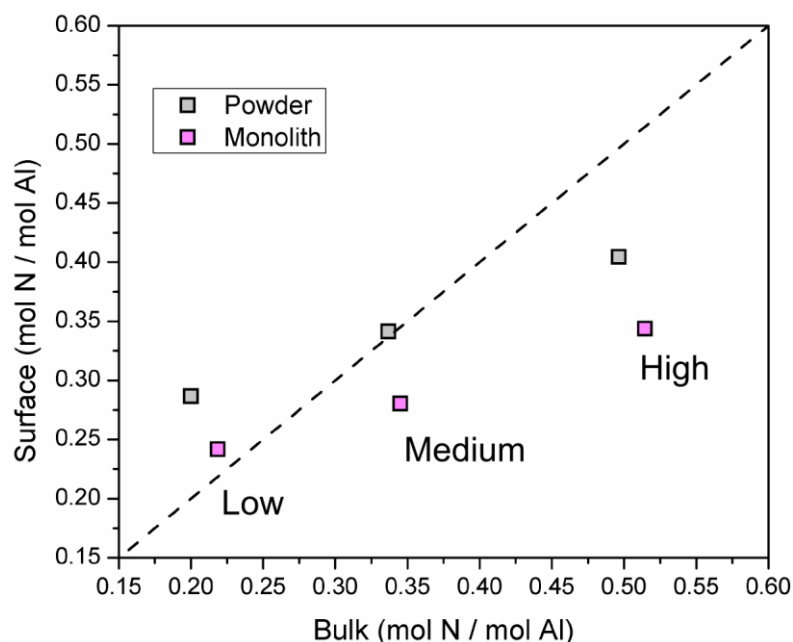
Figure 5.6. XPS surface compositions as a function of bulk compositions for monoliths (magenta) and powders (grey). Dotted line represents a surface/bulk ratio of 1. Bulk compositions estimated from TGA PEI content. PEI loading labels provided below each pair of data.

The surface PEI content of the powders was higher than that of the monoliths for each of the samples by a constant value of ~ 0.05 mol N / mol Al. This is hypothesized to have arisen from the exposure of additional external surface area from breaking the interconnections of the alumina while forming the powder for analysis. As discussed above, this was not expected to alter the measurable surface area appreciably, but would increase the Al content measured by XPS if the particles had a high degree of interconnection, and thus depress the N/Al ratios observed. The surface/bulk relationship was nearly proportional for both monoliths and powders with both sets having similar proportionality constants that were clearly < 1. The measured surface/bulk PEI values did not differ dramatically from 1:1, suggesting efficient incremental deposition of PEI in

areas not accessible to XPS (likely to be mesopores or small macropores). The data are consistent with the 'wetting' phenomena proposed above, as there was a greater proportion of PEI on the exterior of particles at low PEI loadings compared to high PEI loadings.

### 5.3.2 CO$_2$ Adsorption Performance

Sorbents were evaluated for CO$_2$ adsorption performance using TGA analysis for monolith pieces and powders, as well as fixed bed experiments on a larger monolith cylinder. Both experiments were run at 400 ppm CO$_2$ and 30 $^o$C to simulate ambient air. The performance of powders and monoliths in TGA experiments was very similar, despite the physical differences of the materials described above. Figure 5.7a shows the CO$_2$ capacities, while figure 5.7b shows the normalized adsorption dynamics for each sample. Corresponding amine efficiencies are reported in the appendix D, figure D.4. The similarity in adsorption performance between sorbents of similar bulk composition but differing textural and surface properties imply that similar fractions of PEI remained accessible to CO$_2$ during adsorption. We note that there was variability in the measured CO$_2$ capacities of samples at similar composition (g PEI/ gAl$_2$O$_3$) beyond the error inherent to the TGA apparatus (+/- ~0.03 mmol / g). This is shown in the appendix D, table D.1. This may have derived from differences in the efficiency of PEI deposition from sample to sample, although there were no obvious trends in CO$_2$ capacity and deviation in expected mesopore filling to support this hypothesis.
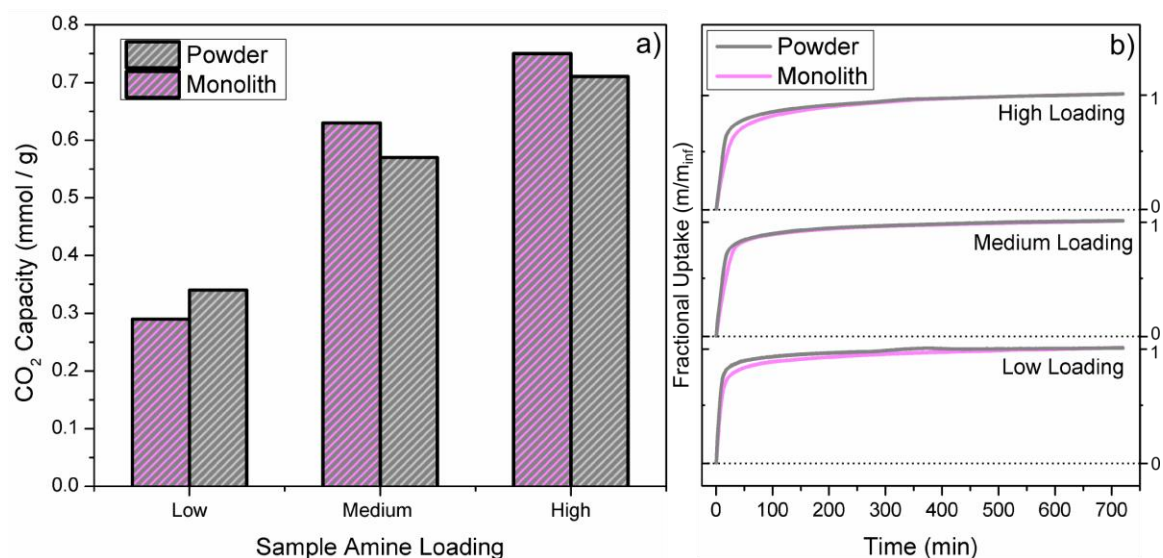
155

Figure 5.7. $CO_2$ capacities (a) and fractional uptakes (b) for monolithic (magenta) and powder (gray) samples grouped by amine loading. Data collected *via* TGA at 30 °C and 400 ppm for 12 h of adsorption.

A larger monolithic sorbent (1 in. x 4 in. cylinder, ~24 g) maintained a capacity of ~0.7 mmol $CO_2$ / g during cycles of adsorption and steam stripping desorption, as shown in figure 5.8c, comparing well the performance of the small monolith pieces and powders. This larger monolith had a common wall thickness (7 mil) but lower cell density (200 cpsi) than the smaller monolith pieces detailed above, and was prepared by immersion in 30 wt% PEI/MeOH for 1 h. Five cycles of $CO_2$ adsorption followed by steam desorption and a drying step (to ensure experimental consistency between cycles) were imposed on the sample for analysis. The adsorption capacities in cycles 2-5 were stable but slightly lower than that of cycle 1 (~0.9 mmol / g). This may have been derived from minor PEI leaching or rearrangement in the monolith, as has been observed for powder sorbents exposed to steam,[18,19] that could change the adsorption properties of the sorbent. While these capacities are similar to the powders and small monoliths tested at

156

similar PEI loading, there have been capacities reported as high as ~1.7 mmol / g for alumina/PEI sorbents in simulated air capture experiments reported in this thesis (chapter 2) and elsewhere.[12,19] A common difference between the sorbents showing these high capacities and the ones prepared here is a higher mesopore volume of the alumina support (~0.4 $cm^3$ / g here vs. 1-1.2 $cm^3$ / g in refs 12, 19). This asserts the importance of a large mesopore volume in setting material performance, even in the presence of significant macroporosity.

Figure 5.8 also shows a representative breakthrough curve during $CO_2$ adsorption (8a) and $CO_2$ and temperature profiles during steam desorption (8b). Compared to figure 7, the equilibration time of the large monolith was notably longer than the smaller pieces and powders. Thermocouples placed at the top and bottom of the monolith did not show large changes in temperature during adsorption (see appendix D, figure D.5), suggesting that mass transfer restrictions limited the equilibration time. The rapid and largely similar uptake dynamics in TGA experiments for both powders and small monolith pieces suggests that mass transfer in the meso and macropores of the alumina was inherently fast. Thus, the compromised dynamics of the larger sample may then have derived from external mass transfer limitations, in the 'gas-side' diffusion of $CO_2$ in the monolith channel to the wall. This effect would be exacerbated in the presence of an axial concentration gradient. Such would result in reduced the flux of $CO_2$ from the bulk gas into the walls down the length of a monolith channel at a given point in time. In these experiments, air passed through the channels at a linear velocity of ~0.4 m/s (12.5 liters / minute). Much higher linear velocities, up to ~12 m/s, have been suggested for air

157

capture to be effective on a large scale.[20] Higher linear velocities would increase the gas side mass transfer coefficient, which scales positively with the Reynolds number, and decrease the boundary layer thickness, which scales inversely with the Reynolds number. This combination would lead to an improvement in the mass transfer characteristics in the monolith channel. This may come at the expense of a lower capture fraction of processed $CO_2$, as higher gas velocities could lead to more $CO_2$ bypass through a channel without interaction with the wall. However, capture fraction is less important for air capture processes than capture from flue gas, as the product is extracted $CO_2$ rather than clean exhaust gas.
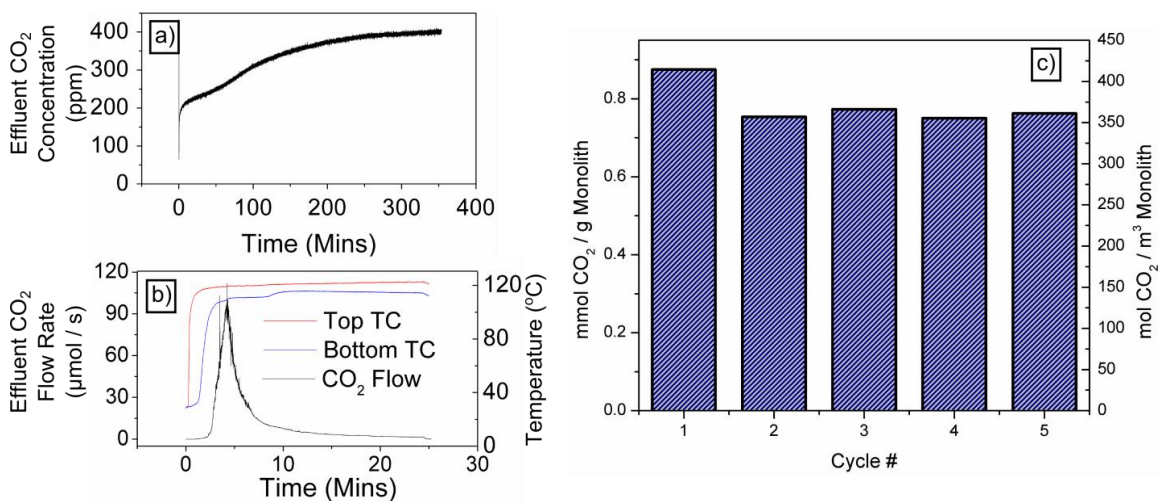


Figure 5.8. $CO_2$ breakthrough curve (a), steam desorption $CO_2$ and temperature profiles (b) and cyclic adsorption capacities (c) measured for larger monolithic sorbent in flow adsorption/steam stripping experiments.

The volumetric capacity of ~350 mol $CO_2$ / $m^3$ monolith achieved here was higher than the ~220 mol $CO_2$ / $m^3$ monolith modeled by Kulkarni,[21] though the cell densities were different between studies (200 cpsi here, 100 cpsi in Kulkarni's paper). Additionally, the adsorption equilibration time was estimated to be ~100 minutes in that

study with a ~1.8 m/s flowrate, whereas here full saturation took nearly three times as long albeit with disproportionately lower flowrate (0.4 m/s). The ~350 min saturation time and 350 mol $CO_2$ / $m^3$ capacity yields a time averaged adsorption rate of ~1 mol $CO_2$ / $m^3$ / min. This corresponds to a surface uptake rate of ~9 μmol / $m^2$ / s, assuming an internal geometric surface area of ~2000 $m^2/m^3$, which is appropriate for a 200 cpsi monolith.[22]

This is in line with estimates of benchmark uptake rates for air capture provided by Lackner.[20] However, the non-linear nature of the breakthrough curve implies that the instantaneous surface uptake rates during the early part of the adsorption were much higher than ~9 μmol / $m^2$ / s. Of course, the effective adsorption rate in a cyclic process would include the times of the other cycle steps as well; however, it is evident here that the cycle time for adsorption is likely to far exceed that for desorption and thus dominate the cycle dynamics for this type of process. The strong performance of this sorbent relative to these thermodynamic and kinetic benchmarks asserts promise for supported amines in monolithic contactors in direct air capture applications. Further engineering of the monolith structure, including tuning the wall properties and PEI impregnation efficiency, should lead to significant enhancement in the adsorption characteristics.

## 5.4    Conclusions

Monolithic $CO_2$ sorbents with a honeycomb channel arrangement were prepared through immersion of extruded alumina monoliths in solutions of PEI and methanol. Two immersion methods were investigated, differing by the fluid occupying the pores of the monolith prior to introduction of PEI. In both cases, there was a discrepancy between the

measured and expected filling of mesopores by PEI between ~25-35% (of the expected value). Monolithic sorbents consistently had higher mesopore volumes than expected based on the content of PEI, suggesting that some of the PEI deposited in the macropores of the structure. Conversely, powders prepared with the same alumina as the monoliths had good agreement in measured vs expected pore filling, despite having some quantity of PEI deposit on their exterior surface, as measured by XPS. The $CO_2$ adsorption performance of the powder and monoliths were comparable not only to one and other, despite their physical differences, but also to a large (1 inch diameter, 4 inch length) extruded monolith sorbent prepared in a similar manner. This larger structure was stable over the 5 cycles of $CO_2$ adsorption and steam desorption that were tested, and had a volumetric capacity of ~ 350 mol $CO_2$ / m$^3$, ~350 minute equilibration time under 400 ppm $CO_2$/N$_2$, 30 $^o$C and 0.4 m/s gas flow conditions, comparing well to literature precedents.

## 5.5    References

(1)    Chen, C.; Yang, S.-T.; Ahn, W.-S.; Ryoo, R. Amine-Impregnated Silica Monolith with a Hierarchical Pore Structure: Enhancement of $CO_2$ Capture Capacity. *Chem. Commun.* **2009**, No. 24, 3627–3629.

(2)    Wen, J. J.; Gu, F. N.; Wei, F.; Zhou, Y.; Lin, W. G.; Yang, J.; Yang, J. Y.; Wang, Y.; Zou, Z. G.; Zhu, J. H. One-Pot Synthesis of the Amine-Modified Meso-Structured Monolith $CO_2$ Adsorbent. *J. Mater. Chem.* **2010**, *20* (14), 2840.

(3)     Chen, Q.; Fan, F.; Long, D.; Liu, X.; Liang, X.; Qiao, W. Poly ( Ethyleneimine ) - Loaded Silica Monolith with a Hierarchical Pore Structure for $H_2S$ Adsorptive Removal. *Ind. Eng. Chem. Res.* **2010**, *49* (22), 11408–11414.

(4)     Witoon, T.; Chareonpanich, M. Synthesis of Hierarchical Meso- macroporous Silica Monolith Using Chitosan as Biotemplate and Its Application as Polyethyleneimine Support for $CO_2$ Capture. *Mater. Lett.* **2012**, *81*, 181–184.

(5)     Han, Y.; Hwang, G.; Kim, H.; Haznedaroglu, B. Z.; Lee, B. Amine-Impregnated Millimeter-Sized Spherical Silica Foams with Hierarchical Mesoporous– macroporous Structure for $CO_2$ Capture. *Chem. Eng. J.* **2015**, *259*, 653–662.

(6)     Gargiulo, N.; Verlotta, A.; Peluso, A.; Aprea, P.; Caputo, D. Modeling the Performances of a $CO_2$ Adsorbent Based on Polyethylenimine-Functionalized Macro-/mesoporous Silica Monoliths. *Microporous Mesoporous Mater.* **2015**, *215*, 1–7.

(7)     Li, F. S.; Qiu, W.; Lively, R. P.; Lee, J. S.; Rownaghi, A. a.; Koros, W. J. Polyethyleneimine-Functionalized Polyamide Imide (Torlon) Hollow-Fiber Sorbents for Post-Combustion $CO_2$ Capture. *ChemSusChem* **2013**, *6* (7), 1216–1223.

(8)     Labreche, Y.; Lively, R. P.; Rezaei, F.; Chen, G.; Jones, C. W.; Koros, W. J. Post-Spinning Infusion of Poly(ethyleneimine) into Polymer/silica Hollow Fiber Sorbents for Carbon Dioxide Capture. *Chem. Eng. J.* **2013**, *221*, 166–175.

(9)     Labreche, Y.; Fan, Y.; Rezaei, F.; Lively, R. P.; Jones, C. W.; Koros, W. J. Poly(amide-imide)/Silica Supported PEI Hollow Fiber Sorbents for Postcombustion $CO_2$ Capture by RTSA. *ACS Appl. Mater. Interfaces* **2014**, No. 6, 19336–19346.

(10)    Li, F. S.; Labreche, Y.; Lively, R. P.; Lee, J. S.; Jones, C. W.; Koros, W. J. Poly(ethyleneimine) Infused and Functionalized Torlon®-Silica Hollow Fiber Sorbents for Post-Combustion $CO_2$ Capture. *Polymer (Guildf).* **2014**, *55* (6), 1341–1346.

(11)    Giesche, H. Mercury Porosimetry: A General (practical) Overview. *Part. Part. Syst. Charact.* **2006**, *23* (1), 9–19.

(12)    Chaikittisilp, W.; Kim, H.-J.; Jones, C. W. Mesoporous Alumina-Supported Amines as Potential Steam-Stable Adsorbents for Capturing $CO_2$ from Simulated Flue Gas and Ambient Air. *Energy & Fuels* **2011**, *25*, 5528–5537.

(13)    Sanz, R.; Calleja, G.; Arencibia, A.; Sanz-Pérez, E. S. Amino Functionalized Mesostructured SBA-15 Silica for $CO_2$ Capture: Exploring the Relation between the Adsorption Capacity and the Distribution of Amino Groups by TEM. *Microporous Mesoporous Mater.* **2012**, *158*, 309–317.

(14)    Drese, J. H.; Choi, S.; Lively, R. P.; Koros, W. J.; Fauth, D. J.; Gray, M. L.; Jones, C. W. Synthesis-☐"Structure-☐"Property Relationships for Hyperbranched Aminosilica $CO_2$ Adsorbents. *Adv. Funct. Mater.* **2009**, *19* (23), 3821–3832.

(15)  Holewinski, A.; Sakwa-Novak, M. A.; Jones, C. W. Linking $CO_2$ Sorption Performance to Polymer Morphology in Aminopolymer/Silica Composites through Neutron Scattering. *J. Am. Chem. Soc.* **2015**, 150826161537006.

(16)  Steinhart, M.; Wendorff, J. H.; Greiner, A.; Wehrspohn, R. B.; Nielsch, K.; Schilling, J.; Choi, J.; Gösele, U. Polymer Nanotubes by Wetting of Ordered Porous Templates. *Science* **2002**, *296* (5575), 1997.

(17)  Zhang, M.; Dobriyal, P.; Chen, J. T.; Russell, T. P.; Olmo, J.; Merry, A. Wetting Transition in Cylindrical Alumina Nanopores with Polymer Melts. *Nano Lett.* **2006**, *6* (5), 1075–1079.

(18)  Hammache, S.; Hoffman, J. S.; Gray, M. L.; Fauth, D. J.; Howard, B. H.; Pennline, H. W. Comprehensive Study of the Impact of Steam on Polyethyleneimine on Silica for $CO_2$ Capture. *Energy & Fuels* **2013**, *27*, 6899–6905.

(19)  Sakwa-Novak, M. A.; Jones, C. W. Steam Induced Structural Changes of a Poly(ethylenimine) Impregnated Γ Alumina Sorbent for $CO_2$ Extraction from Ambient Air. *ACS Appl. Mater. Interfaces* **2014**, *6*, 9245–9255.

(20)  Lackner, K. S. Capture of Carbon Dioxide from Ambient Air. *Eur. Phys. J. Spec. Top.* **2009**, *176* (1), 93–106.

(21)  Kulkarni, A. R.; Sholl, D. S. Analysis of Equilibrium-Based TSA Processes for Direct Capture of $CO_2$ from Air. *Ind. Eng. Chem. Res.* **2012**, *51* (25), 8631–8645.

(22)    Williams, J. L. Monolith Structures, Materials, Properties and Uses. *Catal. Today*

       **2001**, *69*, 3–9.

# CHAPTER 6

# CONCLUSIONS AND PROPOSALS FOR FUTURE RESEARCH

## 6.1    Conclusions

A more comprehensive understanding of supported amine materials has come into view over the last 5 years. Many basic levers for tuning the performance of supported amines at the materials level have been demonstrated, and new reports of step change improvements in thermodynamic performance have become less frequent, particularly for amine/oxide adsorbents. Given this trend, the development of the technology has begun to move into the stages of scale up to practical systems and elucidation of fundamental underlying phenomena. The contributions discussed in the preceding chapters relate predominantly to the former of these areas. The efficacy of two performance levers, oxide surface properties and additive incorporation, were explicitly investigated for air capture, and additive incorporation was shown to be a more effective improvement strategy. Material degradation continues to be a major practical obstacle for supported amines, and here the hydrothermal stability of the target adsorbent composition under relevant operating conditions was probed to a more fundamental level than previously reported in the literature. Specific degradation mechanisms of the alumina were elucidated, and fortunately these did not substantially deteriorate the adsorption performance of the sorbent. Finally, powder and monolithic alumina sorbents were shown to have similar performance, though slightly differing physical characteristics. The

performance of a monolithic sorbent under semi-practical conditions was provided, in hopes of providing a baseline for future studies.

In the text that follows, ideas for potential new projects are provided. Suggestions are made for next steps that build directly from the work presented in this dissertation. Additionally, I have used the section as a repository for some other ideas that I spent some time thinking about but did not pursue, due either to constraints in my time or knowledge. I stress that this section has not been edited to nearly the same extent as the other chapters in this document, but I felt it was valuable to archive some of these ideas. It is intended primarily for future researchers, who are encouraged to build from these ideas as they see fit.

## 6.2    Future Project Ideas

### 6.2.1    Monolith Development

A baseline performance of PEI impregnated alumina honeycomb monoliths is presented in chapter 5, along with a comparison between these structures and analogous powders. While the performance of the monoliths and powders were similar, there was a greater degree of variability in the properties of the monoliths than with the powders with the preparation methods used. $CO_2$ profiles during adsorption and desorption were presented, but not analyzed in great detail. Finally, methods for improvement in the amine efficiency and adsorption dynamics of supported PEI were demonstrated in chapter 4 for powder sorbents, but remain unexplored in monoliths.  Two broad areas of future study thus emerge from these findings:

1. Development of monoliths of improved performance

2. Elucidation of relevant heat and mass transport phenomena, and their relation with materials properties

6.2.1.1 <u>Monolith Improvement Methods</u>

Improvement in the performance of monoliths could conceivably arise from three areas, listed in order of their hypothesized probability of leading to a step change in performance, based on experience and intuition. (i) Changing the oxide and amine materials utilized in creation of the monoliths, (ii) exploiting a material improvement lever (such as incorporation of PEG) demonstrated for powders, or (iii) Developing a new preparation method for monolith adsorbents resulting in improved properties.

### *6.2.1.1.1 Monolith Materials*

It is hypothesized that the important and tunable properties of the wall of a monolith are: (i) mesopore size and volume (ii) Macropore size and volume and (iii) Degree of connectivity of particles in monolith wall (related to wall tortuosity and packing density). The creation of monoliths with primary alumina particles that have smaller particle size that those reported in chapter 5 (1 micron instead of 20-30 micron), and larger pore volume (1 cm3/g instead of 0.45 cm3/g) would lead to immediate improvements in the volumetric capacity and adsorption kinetics of the monolith if the PEI were properly distributed in the mesopores of these materials. Of course, such a new monolith would be subject to appropriate mechanical stability. Additionally, the co-incorporation of PEG with PEI into a monolith should lead to an improvement in the

volumetric capacity equal to the relative improvement in amine efficiency, shown in chapter 4 to be ~60%. If this avenue is pursued, the efficacy of a simple dipping impregnation procedure should be explicitly explored. It was shown in chapters X and Y that organic deposition on the interior and exterior of particles is altered when additives exist in the preparation mixture and also is an issue when monoliths of hierarchical pore structure are utilized. Specifically, if the hypothesized clusters of PEG/PEI described in chapter 4 do exist, the mesopores of the primary oxide used in the monolith should be large enough to accommodate such clusters to efficiently penetrate their pores.

### 6.2.1.1.2 PEG/PEI Clusters

It was hypothesized that clusters formed from interactions between the end group alcohols on PEG and primary/secondary amines on PEI. This could be addressed in a number of ways. Modification of PEG to remove the H-bonding capability of the end groups or the incorporation of molecules of similar composition but differing architecture to linear PEG, such as a branched PEG oligomer, would provide insight to the hypothesis. It was also suggested that the relative size of clusters and oxide pore diameters may affect the efficient penetration of organic into the support. A systematic variation of this ratio, with assessment of the extent of pore filling and internal/external composition is a natural follow up to the work presented in chapter 4. This could be accomplished by varying the PEG chain size and oxide pore size, keeping constant PEG/PEI molar quantity and other oxide properties (pore volume, particle size, pore structure) and subsequent characterization by $N_2$ physisorption and compositional

analysis. Finally, more advanced characterization techniques could be used. Dynamic light scattering (DLS) or small angle neutron scattering (SANS) could provide a direct measurement of PEG/PEI clusters in solution. Quasi-elastic neutron scattering (QENS) or NMR could be used to probe the dynamics of the confined polymers in the system, which are likely to change in a co-impregnated system. In concert with MD simulations, these techniques could lead to a much more fundamental understanding of polymer behavior when confined in mesopores.

### 6.2.1.1.3 Solvent Removal in Monolith Preparation

An area left unstudied in chapter 5 regarding the preparation of monolith adsorbents was the effect of the drying step. Solvent removal is thought to be an important part of the powder synthesis impregnation method, drawing PEI into the mesopores of the support material through capillary forces. In chapter 5, the effect of capillary forces upon immersing a monolith in a PEI/methanol solution were shown to not be important in determining the final properties of the resultant composite. However, they still may be important in the solvent removal step if significant solvent remains in the macropores of the monolith after ambient drying.

### 6.2.1.1.4 PEI/Oxide Interactions

Further fundamental insight into the process of PEI impregnation into oxide structures could be gained from a study of the thermodynamics of PEI/metal oxide interactions. Gravimetric uptake experiments of oxides and solutions of PEI measured could be measured with a quartz crystal microbalance (QCM), and would provide

isotherms of PEI adsorption onto oxide surfaces. Combined with isothermal titration calorimetry (ITC), to measure the enthalpy of the interaction, and vibrational spectroscopy, to identify specific PEI/oxide bond formation or distortion, would lead to a comprehensive understanding of the thermodynamics of the system. Experiments could also be designed to measure relevant transport phenomena of PEI into oxides of hierarchical porous nature, such as the diffusivity of PEI in the macro and mesopores of a monolith under relevant preparation conditions. An understanding of the thermodynamic and kinetic phenomena relevant to the PEI impregnation method could then lead to a higher degree of control in the preparation of composite monolithic adsorbents.

### 6.2.1.1.5 Creation of "Model Monoliths"

The properties of a monolith wall such as the pore volume, pore size distribution, primary particle size, and tortuosity will likely have important roles in setting the kinetic performance of the monolith. Such properties also may play a role in the efficiency of PEI impregnation into the mesopores of the structure during adsorbent preparation. These properties are difficult to experimentally control, especially when dip coating an oxide onto a ceramic substrate such as alpha alumina or cordierite. The preparation of hierarchical porous silica monoliths is an active area of research in the literature. Established preparation methods exist for controlling the porous properties of the monolith.[1–4] Generally these are free standing bodies but do not contain the honeycomb array of channels that extruded monoliths can have that permits low pressure drop gas flow through the structure. It is proposed to utilize this body of knowledge to prepare

monoliths with a honeycomb channel array by use of a mold during the monolith synthesis. The mold could be easily fabricated to have inverse channels of a desired size, shape and density. This would be a method of creating monoliths with systematically varied wall properties, depending on the toolbox available in the literature. While this likely will not be a practical method for large scale production of monoliths, it could be a powerful tool for their study. Additionally, methods for preparing self-standing silica films have been developed that utilize PEI in their synthesis (but have not utilized the PEI in $CO_2$ adsorption applications).[5–7] Extrapolation of this concept to the 'monolith in a mold' could provide a way of pre-impregnating PEI into the pores of the silica during the silica synthesis. Such a 'one pot' preparation of a monolithic adsorbent has the potential to be advantageous in commercial manufacture of such sorbents, but would require extrapolation to alumina or another hydrothermally stable oxide in the presence of amines.

### 6.2.1.2  Heat and Mass Transfer Studies

The above strategies for improving the performance of monoliths are simple to gauge from a thermodynamic perspective; increases in total capacity reflect improvements in the thermodynamic performance. However, the dynamics of the adsorption process are also likely to be affected by alterations in the monolith properties and can be less straightforward to quantify at a fundamental level. An understanding of heat at mass transfer under relevant conditions at a single composition of a monolith is required before a comprehensive understanding of how the transport phenomena change with material properties can be derived.

### 6.2.1.2.1 Macroscopic Measurements on the System of Interest

Studies of heat and mass transfer of adsorption processes can be approached in several ways. One is to perform macroscopic experiments under relevant conditions, and subsequently fit mass, energy, and momentum balances to the data with adjustable parameters that reflect the unquantified dynamical processes in the system. With enough experiments under different conditions, the functionality of the fitting parameters with relevant environmental conditions (temperature, $CO_2$ concentration, gas flowrate, etc.) can be derived. At minimum, the information gained from such experiments provides some quantitative information about the particular system being studied. However, without careful care, that information may not be easily extrapolated to other systems, thus minimizing the impact to the broad scientific community.

For the PEI impregnated monolith system of interest, this approach would entail data collection and modeling of adsorption and desorption processes over many cycles, or under varied initial conditions. In practical operation, a cyclic steady state would be reached whereby the thermodynamic state of the system prior to a given step (the initial conditions in a model) would be similar between cycles. Initial temperature, adsorbed $CO_2$ content and adsorbed $H_2O$ content are the components of such a state that would be expected to play a role in the subsequent cycle step dynamics. However, it is difficult to predict or directly measure the H2O content with the current experimental infrastructure, especially given the additional complexity that $H_2O$ could conceivably exist as capillary condensed, adsorbed (on a solid), or dissolved (in PEI). These unknowns could be overcome by running enough cycles to achieve a cyclic steady state, and then comparing

experimental and simulated model data of 'steady state' cycle runs. To derive a more fundamental understanding of the system, dynamics could be quantified under systematically varied initial conditions. For instance, in a study of the adsorption cycle step, monoliths could be equilibrated at varied temperature and adsorbed water content prior to introduction of $CO_2$. One could additionally alter the relative humidity of and temperature of the feed gas, to adjust the rates and directions of thermal equilibration and $H_2O$ flux in or out of monolith walls. It is easy to imagine this becoming a substantial undertaking for a researcher, as there are many important experimental parameters to independently adjust.

Study of the dynamics of the desorption process is likely to be more challenging than the adsorption process. That does not mean the problem should be ignored, however, as the vast majority of the process energy requirement is consumed during desorption. As such, design of monoliths for rapid desorption is arguably more important than for rapid adsorption dynamics. The literature is far more abundant with studies probing adsorption, rather than desorption. An additional complexity is that heat transfer is likely to play a larger role in desorption than adsorption. The experimental apparatus used in data collection should be designed with the study of heat transfer in mind. This will require modification to the existing infrastructure. Specifically the monolith housing chamber should be re-designed to ensure predictable boundary conditions for process modeling. For study of steam desorption, this may mean designing the housing system in such a way as to approach no heat or mass flux from the outer edge of the monolith. This may look like housing that accommodates a monolith cylinder wrapped tightly with Teflon

tape and insulation. Additionally, a thermally insulating material could be used to prevent steam from heating the outer edge of the monolith chamber.

### 6.2.1.2.2 Controlled Transport Measurements

Another approach to studying transport phenomena in adsorbents is to perform more controlled experiments to probe transport in a specific regime. For single component mass transfer of $CO_2$ in an amine functionalized monolith during adsorption, there are at minimum four mass transfer regimes of interest: external (within the channel), macropore (in between the mesoporous particles), mesopore (in the void space of a mesopore, but not yet in contact with an amine), and within a bulk amine phase. Estimations of diffusivities and length scales to provide timescales of transport ($L^2/D$) for external, macropore and mesopore can be made. The appropriate transport mechanism (convection, bulk diffusion, Knudsen diffusion) can be identified *a priori* with a relatively high degree of confidence, and the length scales can be measured. The diffusivity of $CO_2$ within a bulk amine phase has not been directly measured in the literature, and the measurement or estimation of a diffusive length scale is not trivial. Macroscopic experiments under carefully chosen experimental conditions or microscopic experiments that directly probe the movement of molecules through spectroscopy are particularly useful for probing specific mass transfer regimes. This option could hold promise in a measurement of the diffusivity of $CO_2$ within PEI, a currently unquantified parameter.

### *6.2.1.2.3 Diffusivity of $CO_2$ in PEI*

The diffusivity of $CO_2$ within a bulk amine phase should, at maximum, be similar to that of $CO_2$ within a liquid or polymer of similar viscosity as PEI. At minimum, the diffusivity is exceedingly small and reflected in the very long tails of adsorption experiments commonly reported in literature. An additional level of complexity is incurred in that it is thought that the diffusivity may vary as a function of $CO_2$ loading from a high value to a low value. As discussed in chapter 4, this may be due to $CO_2$-induced cross linking and rigidification of PEI chains. An attempt was made to measure the 'slow' diffusivity of $CO_2$ in PEI by the ZLC method. Lack of confidence in the ZLC method (specifically its applicability for the $CO_2$/PEI/SBA-15 system), the small SBA-15 particles used (~1 micron diameter), and the experimental apparatus combined with data that was difficult to consistently reproduce (likely as a result of one of the above reason) prevented the results from being published. A mesoscopic technique such as IR (described here[8]) may be useful for the direct measurement of $CO_2$ diffusion within PEI. Additionally, an earnest effort could be given to using PFG-NMR to follow $^{13}CO_2$ within PEI. Dr. Hanno Leison (GT's solid state NMR technician) did not think the $^{13}CO_2$/PEI/SBA-15 system was a good fit for PFG-NMR due to long T1 relaxation times, even at temperatures of ~50 °C. These experiments were carried out under 1 bar $^{13}CO_2$ (24h exposure time) with a 40%wt PEI/SBA-15 sample. A partially saturated sample could show faster dynamics (and hence shorter T1 relaxation times) if $CO_2$ hopping is prevalent. Additionally, a class 2 sample would have more void space within a pore that could promote $CO_2$ hopping and improve the measurability of the dynamics.

### 6.2.1.2.4 Diffusivity of $CO_2$ in Meso/Macroporous Monoliths

A direct measurement of the gas phase diffusivity of CO2 in monolith walls may be possible with a Wicke-Kallenbach diffusion cell. Such an apparatus has been used by Hayes and Kolaczkowski[9] for the study of gas transport through monolith walls with a catalyst washcoat. These authors have published numerous papers on heat and mass transfer in catalytic honeycomb monoliths. The a diffusion cell would allow for the measurement of transport of $CO_2$ and $H_2O$ through monolith walls without external mass transfer limitations, given the nature of the measurement. As such, porous walled monoliths would need to be used in such a study. These experiments could be run with or without polymer in the pores of the monolith. The diffusion coefficients derived from the data could be compared with estimates based on the physical properties of the monolith (pore size, void volume) to derive tortuosity values. Additionally, non-interacting polymer (polyethylene, or all tertiary amine PEI) could be impregnated into the monolith walls, and differences in the diffusion of $CO_2$ and $H_2O$ noted with reference to those derived from the bare walls.

### 6.2.2    Operando-like FTIR as a New Experimental Tool

Vibrational spectroscopy, namely in-situ FTIR or in-situ DRIFTS, has been by far the most useful spectroscopic technique for probing $CO_2$/amine interactions on solid adsorbents. Operando-style FTIR, where a sample is exposed to an environment of flowing gas whose effluent is quantitatively monitored, and is transiently probed by FTIR, has not been used for the exploration of adsorbed species on supported amine

adsorbents. In the context of probing adsorbents (instead of catalysts), the primary difference between operando-IR and traditional FTIR is the flow of gas over a sample, as opposed to the dosing of gas into a sample chamber. In both cases, an equilibrium state of the adsorbate/adsorbent at a particular partial pressure of adsorbate can be probed. The advantage of using a flowing gas is the possibility to introduce a new species into the gas phase at constant (total) pressure after equilibration at a given partial and total pressure. Thus, the exchange rates and the relative affinity of different adsorbates to a surface can be probed as a function of initial condition. For example, a supported amine material could be saturated with a relevant partial pressure of $SO_2$, and subsequently (with minimal experimental interference) exposed to the same partial pressure of $SO_2$ in a gas mixture containing $CO_2$. Exchange between adsorbed $SO_2$ and $CO_2$ would be manifested in the resulting spectra, and could be probed transiently. It is easy to extrapolate this method to numerous different relevant gas mixtures at different initial conditions (i.e. $CO_2$ first, then expose to $SO_2$ / $CO_2$). Additionally, isotopic exchange experiments (saturate with a partial pressure of $^{13}CO_2$, subsequently introduce same partial pressure of $^{12}CO_2$) could provide a means of studying $CO_2$ diffusion within PEI, or the $CO_2$/amine equilibrium dynamics (exchange between free $CO_2$ and adsorbed carbamate).

### 6.2.3 Imines and Degraded PEI as $SO_2$ Sorbent

An important drawback to using supported PEI in air capture applications is the polymer degradation upon exposure to oxygen at regeneration temperatures ~100 $^o$C. A comprehensive understanding of the degradation mechanism and resulting product distribution of $O_2$ degraded PEI does not yet exist in the literature. The most detailed

177

picture of the resultant structures to date have been elucidated through HMBC, HMQC and $^{13}$C DEPT NMR studies. These studies have revealed that aldehydes and imines form upon oxidation of PEI. While not useful for $CO_2$ capture due to the lack of a proton, tertiary amines are effective $SO_2$ sorbents. It has been suggested that $SO_2$ interacts with the tertiary amines to form non-covalent adducts. The interaction of $SO_2$ with imines has not been explored in the context of adsorption and gas cleanup. While imines are likely to be less basic than tertiary amines, they still have a free electron pair that could interact with $SO_2$ in a similar way to tertiary amines. Practically, if degraded PEI formed imine species that were selective towards $SO_2$, the adsorbent could be recycled from a $CO_2$ capture application to an $SO_2$ capture application

## 6.3    References

(1)    El Kadib, A.; Chimenton, R.; Sachse, A.; Fajula, F.; Galarneau, A.; Coq, B. Functionalized Inorganic Monolithic Microreactors for High Productivity in Fine Chemicals Catalytic Synthesis. *Angew. Chemie - Int. Ed.* **2009**, *48* (27), 4969–4972.

(2)    Sachse, A.; Galarneau, A.; Fajula, F.; Di Renzo, F.; Creux, P.; Coq, B. Functional Silica Monoliths with Hierarchical Uniform Porosity as Continuous Flow Catalytic Reactors. *Microporous Mesoporous Mater.* **2011**, *140* (1-3), 58–68.

(3)    Petkovich, N. D.; Stein, A. Controlling Macro- and Mesostructures with Hierarchical Porosity through Combined Hard and Soft Templating. *Chem. Soc. Rev.* **2013**, 3721–3739.

(4)    Triantafillidis, C.; Elsaesser, M. S.; Hüsing, N. Chemical Phase Separation Strategies towards Silica Monoliths with Hierarchical Porosity. *Chem. Soc. Rev.* **2013**, *42* (9), 3833–3846.

(5)    Yang, B.; Edler, K. J. Free-Standing Ordered Mesoporous Silica Films Synthesized with Surfactant-Polyelectrolyte Complexes at the Air/Water Interface. **2009**, No. 15, 1221–1231.

(6)    Yang, B.; Jaber, R.; Edler, K. J. Silica-Surfactant-Polyelectrolyte Film Formation: Evolution in the Subphase. *Langmuir* **2012**, *28* (22), 8337–8347.

(7)     Yang, B.; Holdaway, J. a.; Edler, K. J. Robust Ordered Cubic Mesostructured Polymer/silica Composite Films Grown at the Air/water Interface. *Langmuir* **2013**, *29* (12), 4148–4158.

(8)     Kärger, J.; Binder, T.; Chmelik, C.; Hibbe, F.; Krautscheid, H.; Krishna, R.; Weitkamp, J. Microimaging of Transient Guest Profiles to Monitor Mass Transfer in Nanoporous Materials. *Nat. Mater.* **2014**, *13* (4), 333–343.

(9)     Zhang, F.; Hayes, R. E.; Kolaczkowski, S. T. A New Technique to Measure the Effective Diffusivity in a Catalytic Monolith Washcoat. *Chem. Eng. Res. Des.* **2004**, *82*, 481–489.

# APPENDIX A

# SUPPLEMENT TO CHAPTER 2

## A.1    Steam System Schematic
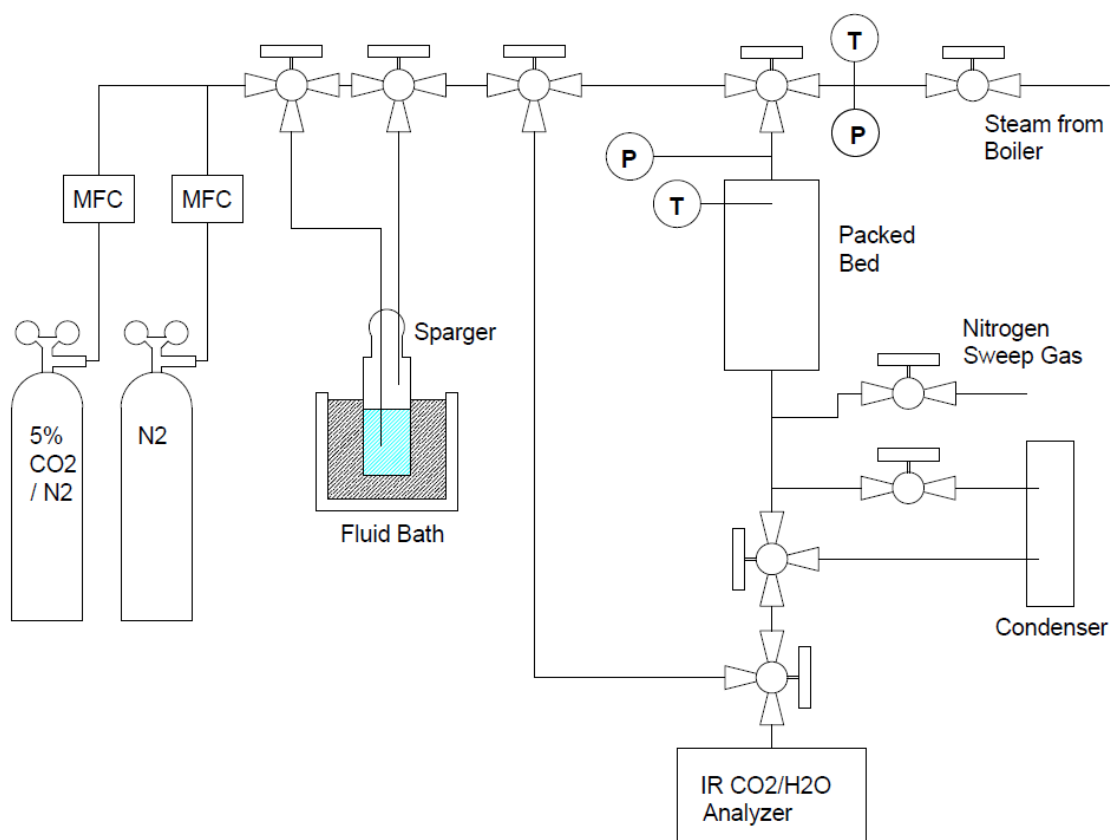


Figure A.1. Schematic of flow adsorption / steam stripping system used to perform humid adsorption capacity measurements and steam exposure experiments.

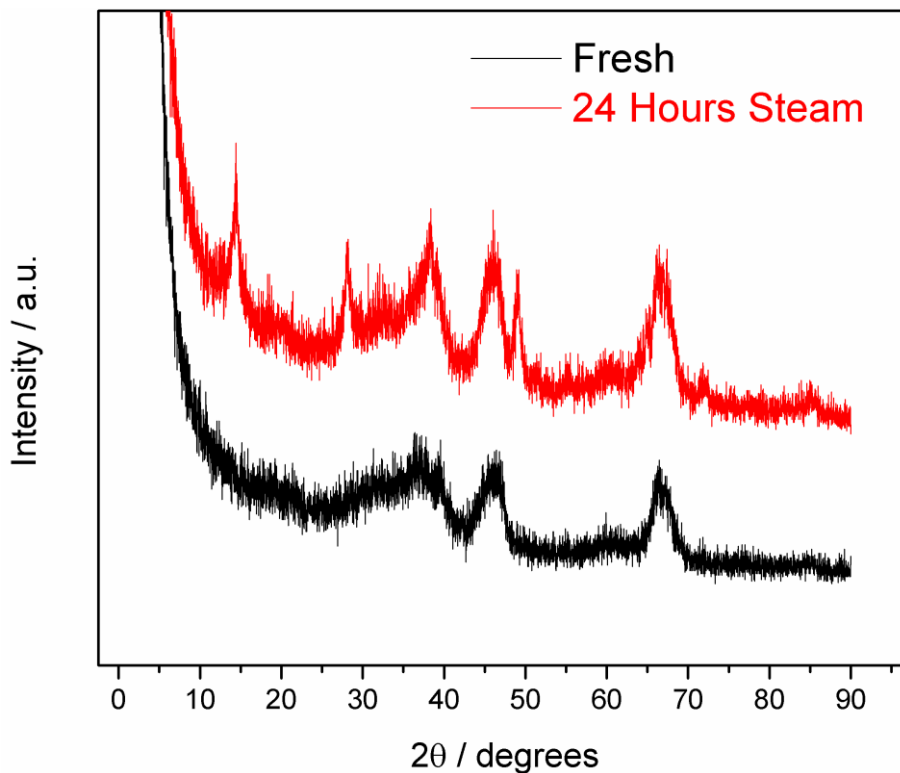**A.2    XRD Patterns of Bare Alumina Before and After Steam Treatment**



Figure A.2. XRD patterns of bare $\gamma$-alumina before and after exposure to steam for 24 hours.

**A.3    Oxidation of Cycled Sample**

Because the oxidation peak in the FTIR and FT-Raman spectrum of the cycled sample were not expected and the $CO_2$ capacity of the material remained relatively high after the cyclic steam treatment it was hypothesized that the sample was handled improperly after treatment and exposed to oxygen whilst at temperature at or above 70 $^o$C. To test whether the sample exposed to cyclic steam treatment was degraded via exposure to oxygen after steam treatment and the subsequent $CO_2$ capacity measurement,

the $CO_2$ capacity of the material was re-measured in two ways. The $CO_2$ capacity was measured at 50% relative humidity in the flow adsorption system in the exact same way as described in the experimental section, as well as under dry conditions on a TGA. For comparison of the dry $CO_2$ capacities measured by TGA, the $CO_2$ capacity of the sample exposed to 90 minutes of continuous steam exposure was measured as well. In the humid $CO_2$ capacity measurements just after steam treatment, these two materials had very similar $CO_2$ capacities. Figure S3 shows the results of these experiments. It is apparent that the $CO_2$ capacity of the cycled sample was much less when retested than it was just after steam treatment. The dry $CO_2$ capacity of the cycled sample was much less than that of the 90 minute continuously exposed sample. These results suggest that the cycled sample was exposed to oxygen at high temperature after the steam treatment and subsequent $CO_2$ capacity measurement. This is suspected to have occurred after the final desorption step of the post steaming $CO_2$ capacity measurement, when the $N_2$ flow would have been shut off and $O_2$ could have then leaked into the packed bed as it cooled. Because the bed is insulated, cooling can take several hours under static conditions and the sample was not immediately removed, so extended exposure to $O_2$ may have occurred at this point. Other samples were removed from the system before such extended exposure would have occurred.
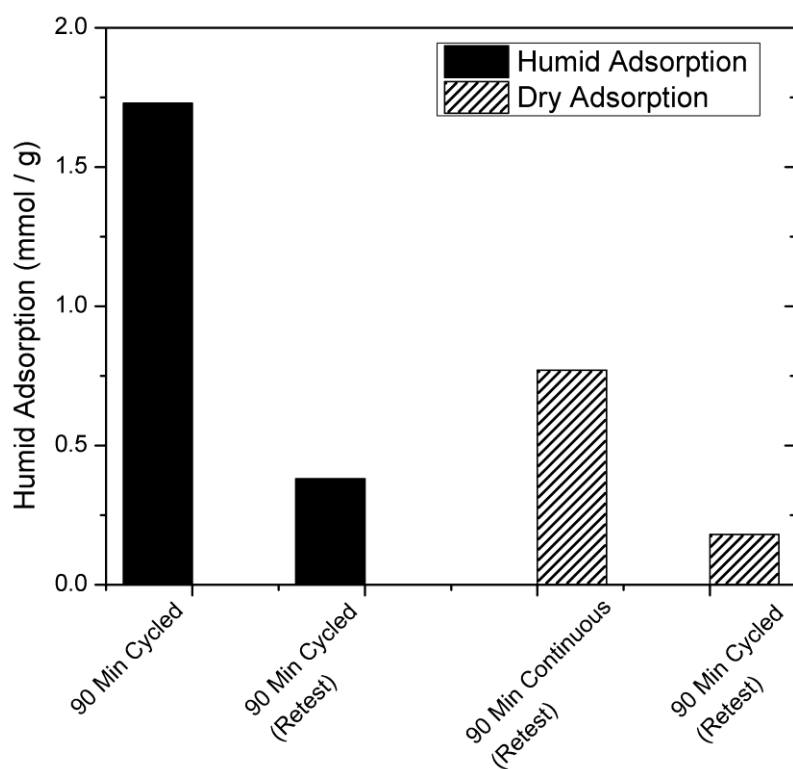
Figure A.3. $CO_2$ capacities of samples showing reduced capacity of the cycled sample due to amine oxidation after testing. Humid adsorption capacities measured from the flow adsorption system, while dry adsorption capacities measured with TGA, both at 400 ppm $CO_2$.

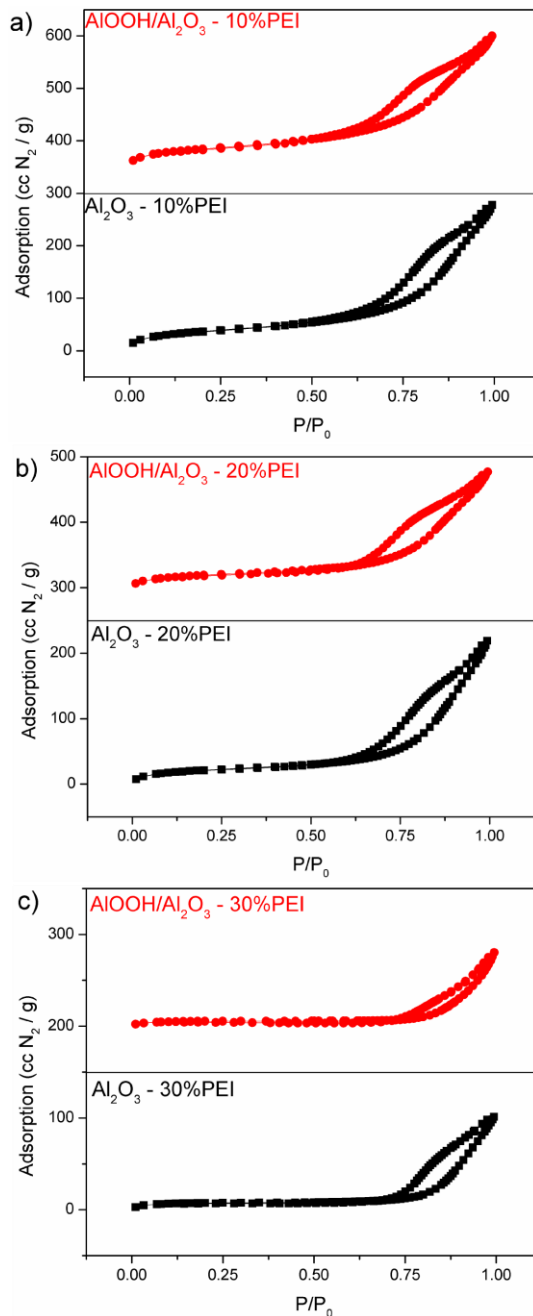## A.4 N$_2$ Physisorption Profiles of Sorbents with/without Boehmite at Various PEI

## Loadings



Figure A.4. . N$_2$ physisorption isotherms of sorbents comprised of 10 wt % (a), 20 wt % (b) and 30 wt % (c) PEI supported on a partial boehmite/$\gamma$-alumina support (red, top) and pure $\gamma$-alumina support (black, bottom).

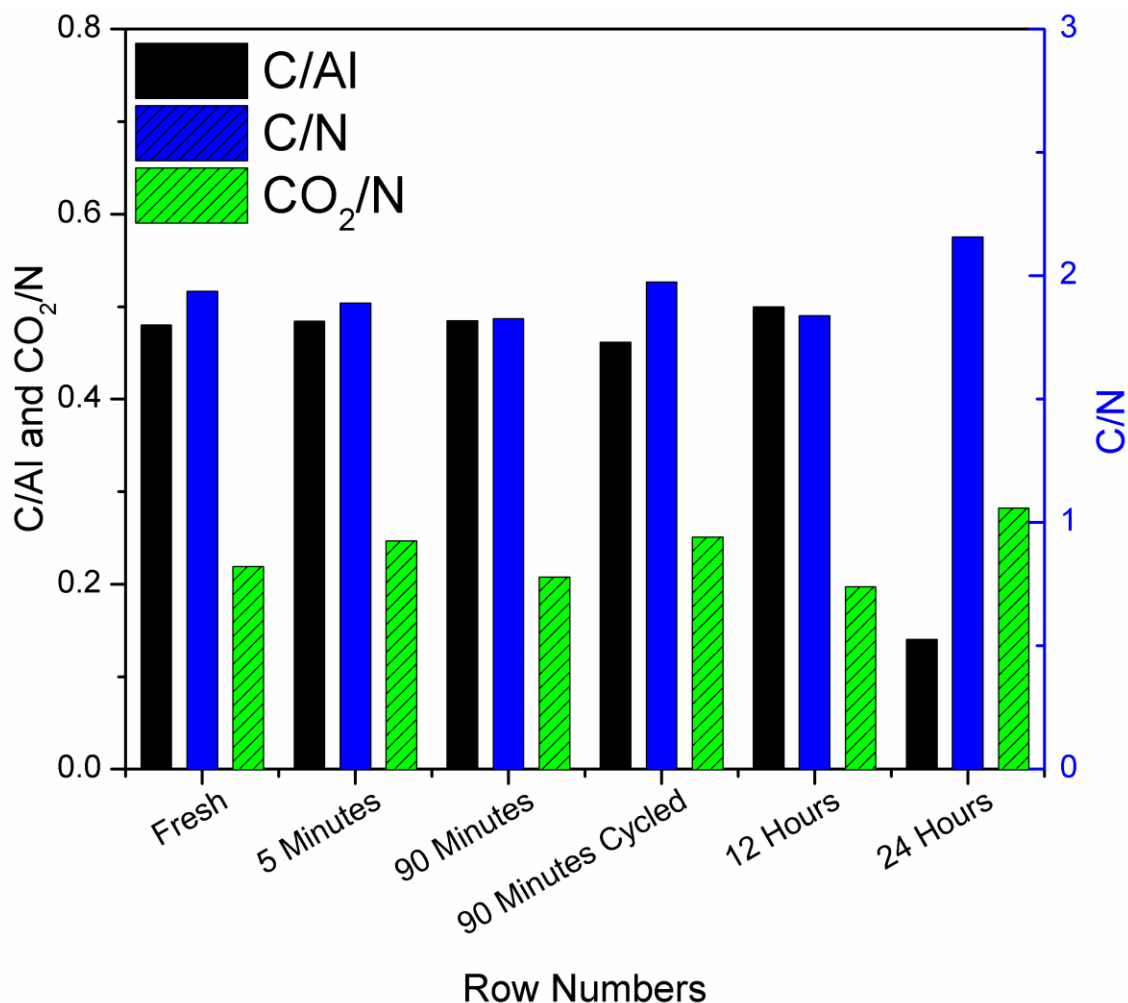**A.5   Comparison of Sorbent Composition After Steam Treatment for Various**

**Times**



Figure A.5. Sorbent composition after steam treatment experiments. C/Al ratios and C/N ratios determined from elemental analysis results

Figure S5 shows the C/Al, C/N and $CO_2$/N (amine efficiency) ratios of the samples after exposure to steam. C, N, and Al quantities are clearly associated with the sorbent composition and were determined by elemental analysis, while $CO_2$ refers to the amount of $CO_2$ adsorbed after steam treatment (figure 3). The C/Al ratio, representative of the

total organic loading in the sample, remained relatively constant for the samples exposed

to steam for less than 24 hours.

# APPENDIX B

# SUPPLEMENT TO CHAPTER 3
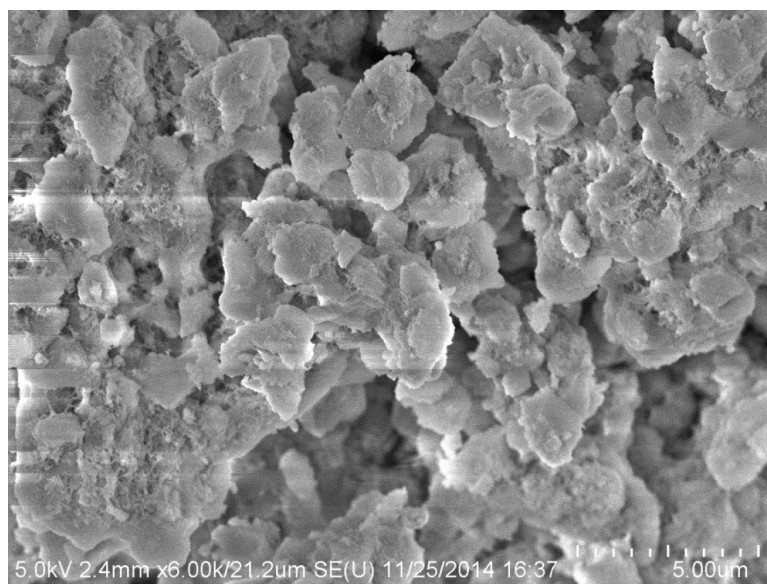
## B.1    Additional SEM Images



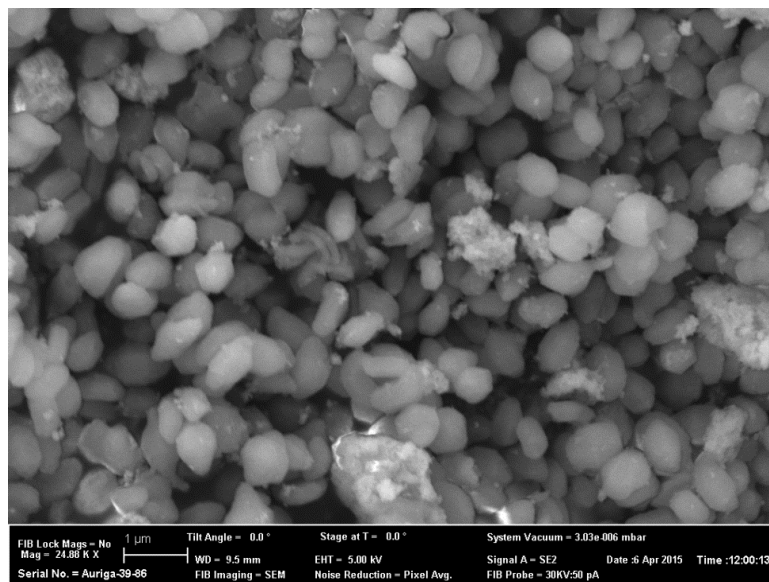Figure B.1 SEM image of synthetic Zr-SBA15-100 at Zr/Si ~0.05.



Figure B.2. SEM image of post-synthetic SBA15-100 at Zr/Si ~0.1.
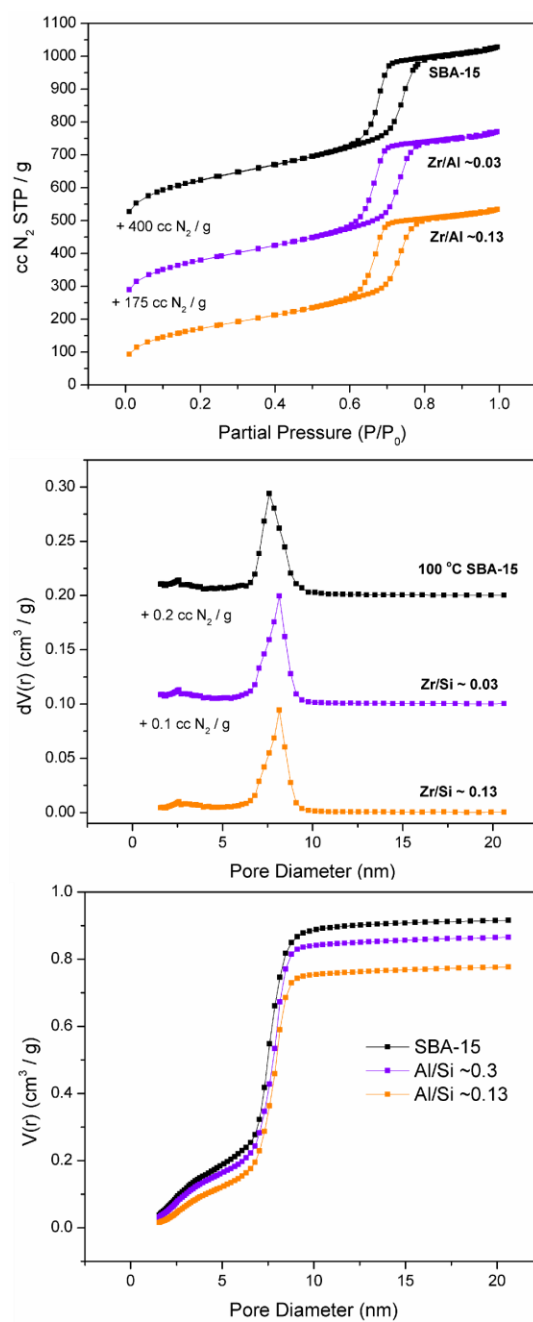
## B.2  Properties of Aluminum Doped SBA-15



Figure B.3. N$_2$ physisorption profiles (top), NLDFT PSDs (middle) and NLDFT cumulative PSDs (bottom) of the post-synthetically doped Al-SBA15-100 materials

Table B.1. Properties of Al-SBA15, synthetic Zr-SBA15 with modified synthesis, and large batch SBA15-130

| Sample Name | Al Incorporation Method | Synthesis Method | Me/Si Gel[a] | Me/Si[b] | Surface Area[c] | Pore Volume[d] | Pore Size[e] |
|---|---|---|---|---|---|---|---|
| | *Method* | *100/130* | *mol/mol* | *mol/mol* | *$m^2/g$* | *$cm^3/g$* | *nm* |
| *Aluminum doped SBA-15* | | | | | | | |
| Al03-SBA15-100-PS | Post Synthetic | 100 | 0.025 | 0.02 | 736 | 0.92 | 8.1 |
| Al13-SBA15-100-PS | Post Synthetic | 100 | 0.125 | 0.07 | 620 | 0.83 | 8.1 |
| *Synthetic Zr-SBA15 with controlled morphology* | | | | | | | |
| Zr05_2-SBA15-100-S | Synthetic | 100 | 0.05 | 0.05 | 784 | 0.99 | 10.1 |
| Zr10_2-SBA15-100-S | Synthetic | 100 | 0.10 | 0.10 | 656 | 1.10 | 10.9 |

[a]Based on content of $ZrOCl_2$ and TEOS (or expected Si content of SBA-15) added during synthesis; [b]Measured by elemental analysis; [c]Estimated using BET method from $N_2$ physisorption data; [d]Estimated using total $N_2$ adsorption at $p/p_0 = 0.99$; [e]Derived from NLDFT equilibrium model for $N_2$ adsorption onto cylindrical silica pores

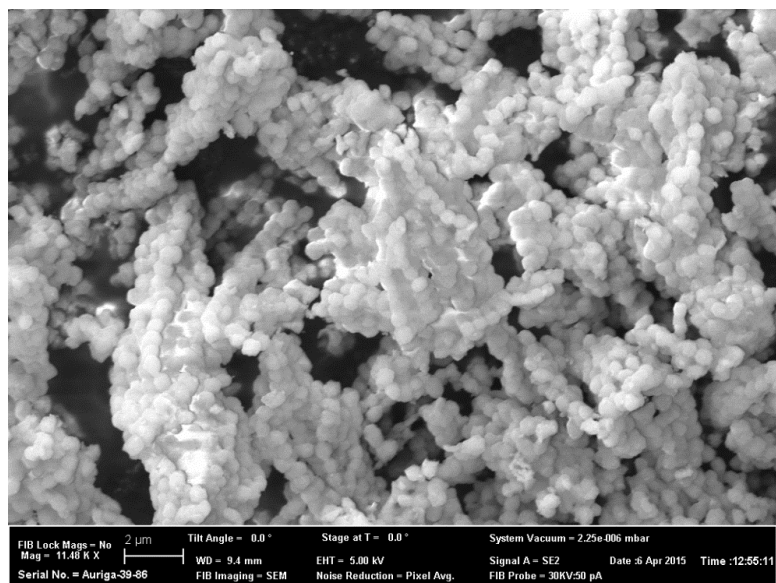## B.3 Characterization of Data of Morphologically Controlled Synthetic SBA15-100



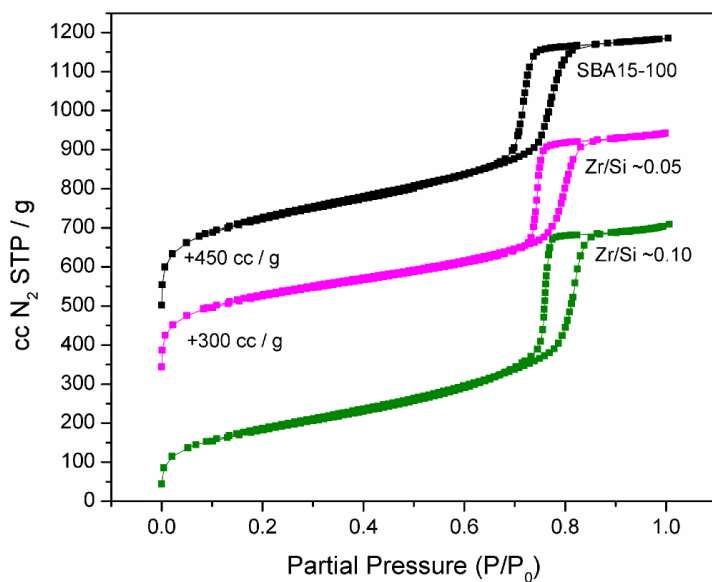Figure B.4. SEM image of synthetic Zr-SBA15-100 with modified synthesis. Materials had a Zr/Si ~ 0.1



Figure B.5. $N_2$ physisorption profiles of 'morphologically controlled' Zr-SBA-15

# APPENDIX C

## SUPPLEMENT TO CHAPTER 4

### C.1 Review of Additive Use in Supported Amine Adsorbents

In 2001, Satyapal et al reported using poly(ethylene glycol) (PEG) and PEI supported on porous poly(methylmethacrylate) (PMMA) in the removal of $CO_2$ from air in spacecraft, though in this early work the effect of PEG on the $CO_2$ capacity and amine efficiency was not directly quantified.[1] Song reported an increase in the $CO_2$ capacity of an MCM-41 silica impregnated with PEG and PEI at a weight ratio of 2:3 g PEG/g PEI and found that the capacity increased from 68.7 mg/g to 77.1 mg/g in adsorption using pure $CO_2$ at 75 $^{o}$C.[2] Additionally, Song recently found that the addition of potassium carbonate into PEI supported on fumed silica increased the capacity and breakthrough time of the sorbent adsorbing $CO_2$ from a 15% $CO_2$ stream.[3] Drage and Snape incorporated PEI and PEG onto fly ash derived carbon adsorbents and altered the PEI weight percent of the sorbents while keeping the PEG weight percent constant at 20. They reported $CO_2$ adsorption profiles collected at 75 $^{o}$C with pure $CO_2$ from TGA experiments for PEG/PEI sorbents at PEI weight percents of 20, 40 and 60 and found that the addition of PEG increased the uptake, reported in weight percent, in each case, though to a lesser extent at higher PEI loadings.[4] Olah's group has studied the effect of PEG on PEI impregnated fumed silica sorbents. In one study they reported decreases in the per gram $CO_2$ capacity of sorbents with PEG incorporated at a PEG/PEI ratio of 0.5, but enhanced isothermal desorption of the $CO_2$ from the material using vacuum.[5] In another study they reported increases in the per gram $CO_2$ capacity as well as the amine efficiency for mixtures of PEG and PEI

supported on silica nanoparticles when the percentage of PEG in the sorbent ranged from 0-12.5.[6] Here, the sorbents were prepared in a two-step process of addition of PEG followed by addition of PEI to the silica. They reported an amine efficiency as high as 62% for adsorption of pure $CO_2$ in a 'static procedure' in the optimal material. Wang explored the incorporation of a wide range of additive molecules into PEI impregnated in hierarchical porous silica monoliths and found that all of the additives increased the $CO_2$ capacity of the sorbent compared to the sorbent with just PEI when adsorbing pure $CO_2$ at ambient pressure and varying temperatures.[7] The same group reported similar results when incorporating additive molecules into silica templated mesoporous carbons with large pore volumes.[8]

Chuang's group has studied the use of PEG as an additive to silica supported tetraethylenepentamine (TEPA) and found that the addition of PEG to the sorbents reduced the extent of oxidative degradation of the materials because of hydrogen bonds formed between the oxygen and alcohol groups on PEG and amine groups on TEPA.[9–11] Sayari's group incorporated the hydrocarbon chains of CTAB into a supported amine material by not removing them after formation of MCM41 silica, and subsequently impregnating the material with PEI. [12,13] Similarly, Zhu $et\ al$ reported adsorbents prepared via impregnation of TEPA into SBA-15 with and without removal of the P123 template and found that this the CO2 capacities of the samples containing template and TEPA were improved over those with just TEPA[14]. Materials modified with organosilanes and subsequently impregnated with PEI have shown similarly enhanced performance as well.[15–18]

193

## C.2   FTIR Characterization



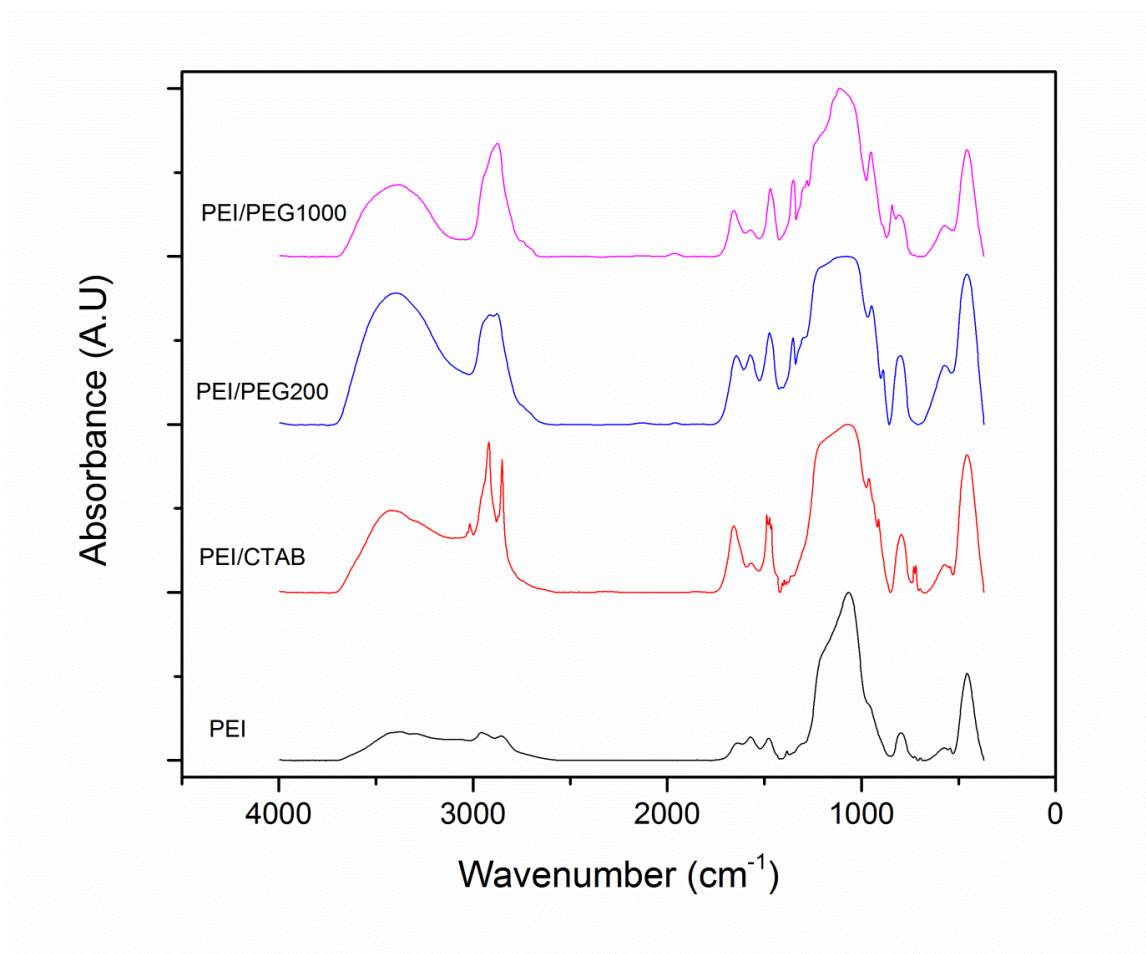Figure C.1 FTIR spectra of co-impregnated additive and PEI into SBA-15 at ~ 2g additive / g PEI
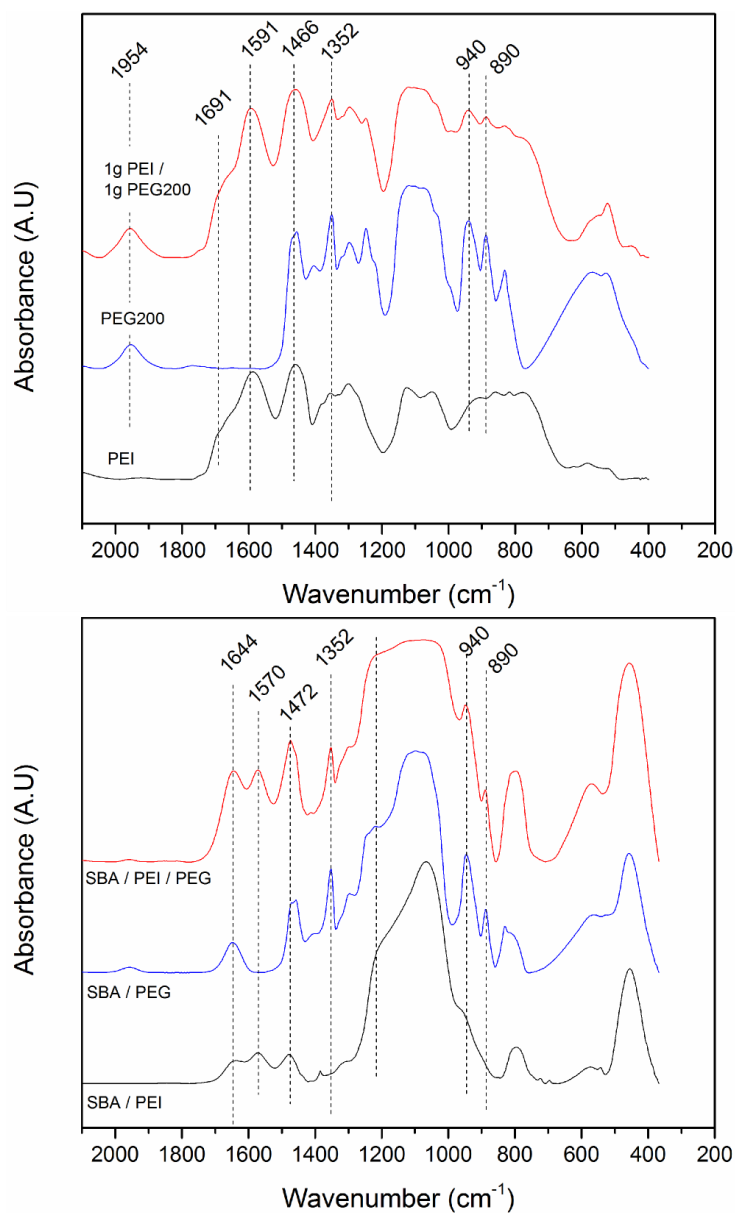
Figure C.2 FTIR spectra of PEI, PEG200 and a mixture of the two as liquids (unsupported) (top) and supported on SBA-15 (bottom).

Characteristic PEG bands not overlapping with the strong bands associated with the silica or the PEI at 1350 cm$^{-1}$ associated with $CH_2$ bending, and 940 and 890 cm$^{-1}$ associated with $CH_2$ rocking motions[19–21] confirmed that PEG was incorporated into the samples. Additional bands are observed at 1472, 1570 and 1644 cm$^{-1}$ in the supported

195

materials, with the exception of that at 1570 cm$^{-1}$, which was not present in the spectrum of supported PEG. Interestingly, these bands are slightly red shifted relative to the apparently analogous set of bands in the spectra of the liquid samples, which appear at 1466, 1591 and1691 cm$^{-1}$. Again in this case, the peak at 1591 cm$^{-1}$ is not present in the PEG, while the peak at 1691 cm$^{-1}$ is also absent in the PEG. In the liquid PEG and PEG/PEI mixture there is an additional band at 1954 cm$^{-1}$, which is also present, but much weaker, in the supported samples. The band at 1470 is associated with $CH_2$ motions, and is thus present in both PEG and PEI. The band at 1570 cm$^{-1}$ is associated with the asymmetric COO stretch of carbamate, the adsorption product of $CO_2$ with amines. 1691 has been associated with carbamic acid, which is has also been shown to be enhanced in polymeric amines in the presence of PEG.[9]
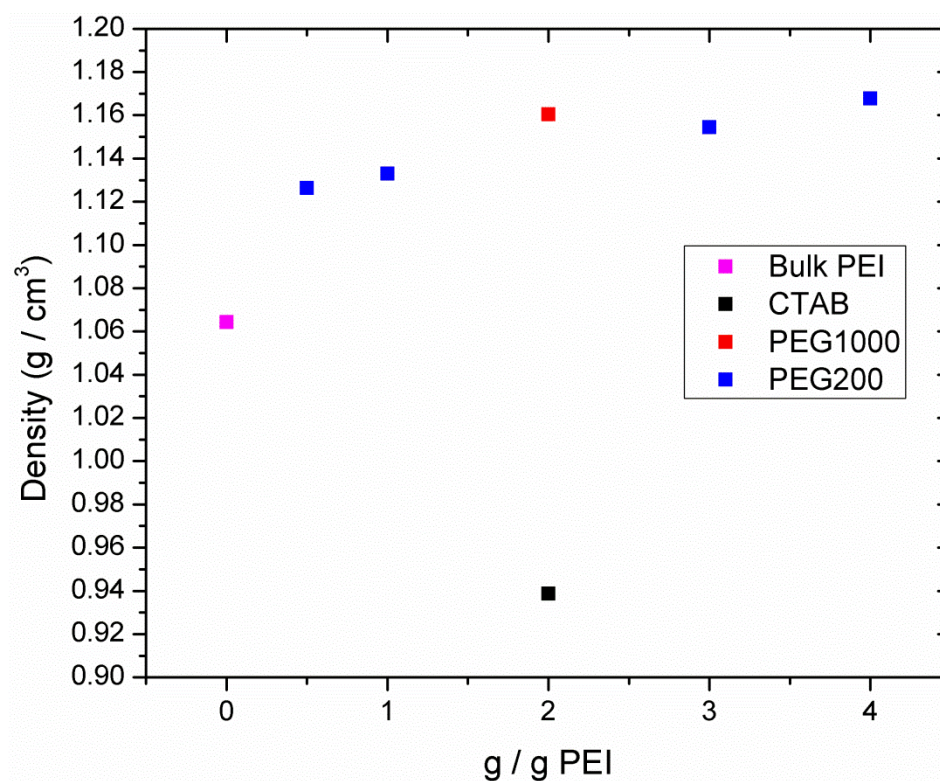
196

## C.3   Bulk Density of Additive/PEI Mixtures



Figure C.3 Measured bulk density of PEI (magenta), mixtures of PEI with CTAB (black) and PEG1000 (red) at a mass ratio of 2 g additive / 1 g PEI, and various mass ratios of PEG200 to PEI (blue). Data collected in bulk (no support used).
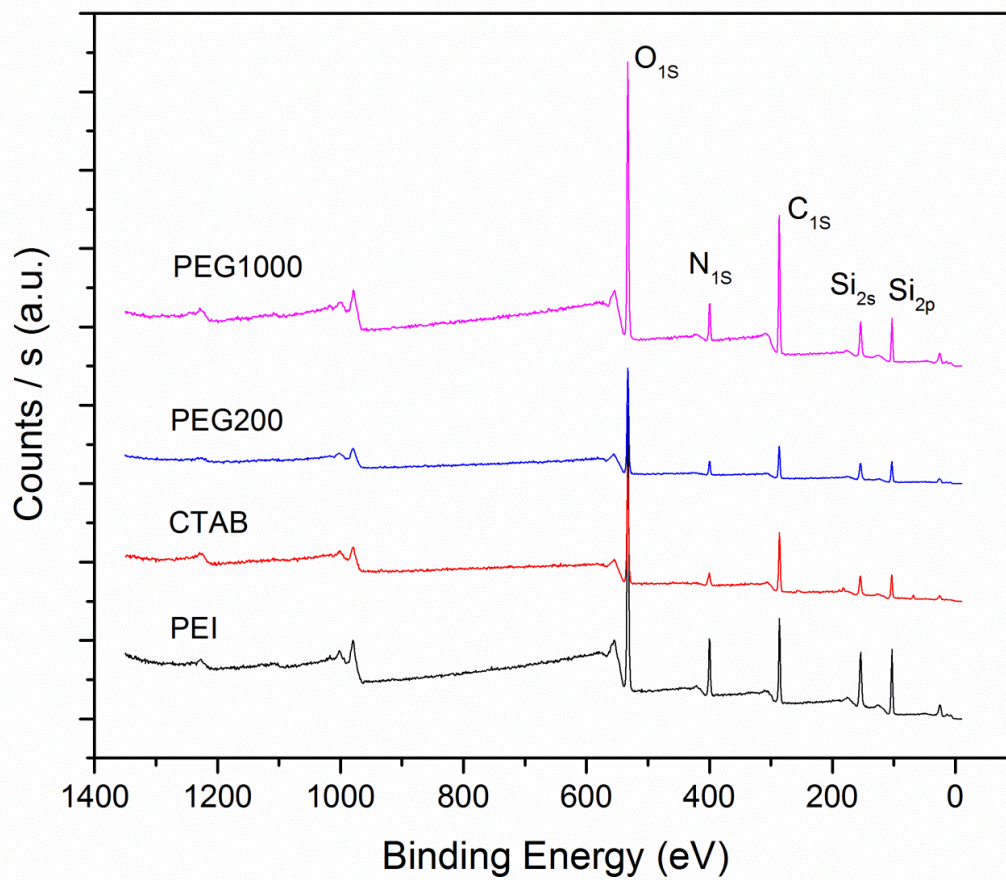
## C.4   XPS Spectra



Figure C.4 Raw XPS data of co-impregnated sorbents containing PEG1000, PEG200, or CTAB or no additive co-impregnated with PEI into SBA-15

## C.5  Properties of SBA-15/PEI/PEI200 Adsorbents

Table C.1 Physical and textural properties of SBA-15 co-impregnated with PEI and PEG200 at varying PEG loadings for three PEI loadings

| Additive | Organic / Silica Ratio[a] | Carbon / Nitrogen[b] | Additive / PEI[c] | BET Surface Area[d] | Pore Volume[d] | Amine content[b] | $CO_2$ capacity[e] |
|---|---|---|---|---|---|---|---|
| | ($g\ Org/g\ SiO_2$) | ($mol\ C/ mol\ N$) | $g / g$ | $m^2 / g\ SiO_2$ | $cm^3 / g\ SiO_2$ | $mmol\ N / g\ sorbent$ | $mmol\ CO_2 / g\ sorbent$ |
| *40% PEI Pore Filling (0.43 g PEI / g $SiO_2$ Basis)* | | | | | | | |
| PEI (none) | 0.51 | 2.2 | 0.1 | 317 | 0.67 | 6.36 | 0.63 |
| PEG200 | 0.54 | 2.6 | 0.3 | 236 | 0.50 | 5.75 | 0.79 |
| PEG200 | 0.66 | 3.2 | 0.6 | 263 | 0.54 | 4.97 | 0.73 |
| PEG200 | 1.32 | 5.6 | 1.8 | 147 | 0.33 | 3.88 | 0.64 |
| PEG200 | 2.13 | 8.8 | 3.4 | 1 | 0 | 3.42 | 0.49 |
| *70% PEI Pore Filling (0.8 g PEI / g $SiO_2$)* | | | | | | | |
| PEI (none) | 0.83 | 2.0 | 0 | 142 | 0.32 | 9.62 | 1.26 |
| PEG200 | 0.79 | 2.4 | 0.2 | 126 | 0.28 | 8.30 | 1.31 |
| PEG200 | 1.00 | 2.5 | 0.2 | 15 | 0.18 | 7.99 | 1.41 |
| PEG200 | 1.35 | 3.7 | 0.9 | 9 | .03 | 6.23 | 1.23 |
| PEG200 | 2.13 | 5.4 | 1.7 | 0 | 0 | 5.15 | 0.90 |
| *90% PEI Pore Filling (1 g PEI / g $SiO_2$)* | | | | | | | |
| PEI (none) | 1.04 | 2.0 | 0 | 127 | 0.24 | 10.45 | 1.36 |
| PEG200 | 1.41 | 2.9 | 0.5 | 1 | 0 | 8.50 | 1.59 |
| PEG200 | 1.50 | 3.1 | 0.5 | 2 | 0 | 8.38 | 1.64 |
| PEG200 | 2.52 | 4.8 | 1.4 | 0 | 0 | 6.21 | 1.15 |

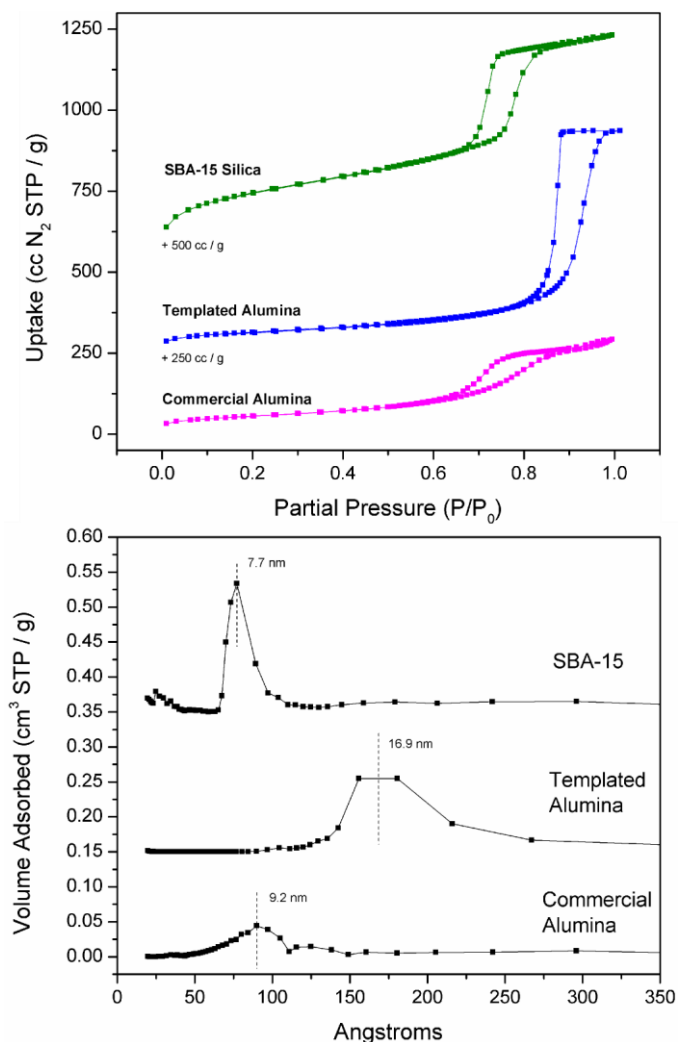## C.6    Characterization of Alumina Adsorbents



Figure C.5 N$_2$ physisorption profiles (top) and BdB-FHH pore size distributions of SBA-15 and alumina supports. Templated alumina and SBA-15 offset by 250 and 500 cc/g, respectively

The presence of hysteresis in the capillary condensation region of the N$_2$ physisorption isotherms confirmed the presence of mesopores in each of the three materials; however other textural properties differed. The pore volumes of the micelle templated SBA-15 and alumina were similar at around 1.1 cm$^3$/g, while that of the

Corning alumina was much lower at 0.45 cm$^3$/g. The BET surface area of the SBA-15 was nearly a factor of 4 higher than those of both aluminas, which were similar at ~200 m$^2$/g.  The average pore size of the materials increased from the SBA-15 (~7.7 nm) to the commercial alumina (~9.2 nm) to the templated alumina (~16.9 nm), and the distribution of pore sizes followed the same trend from small to large.
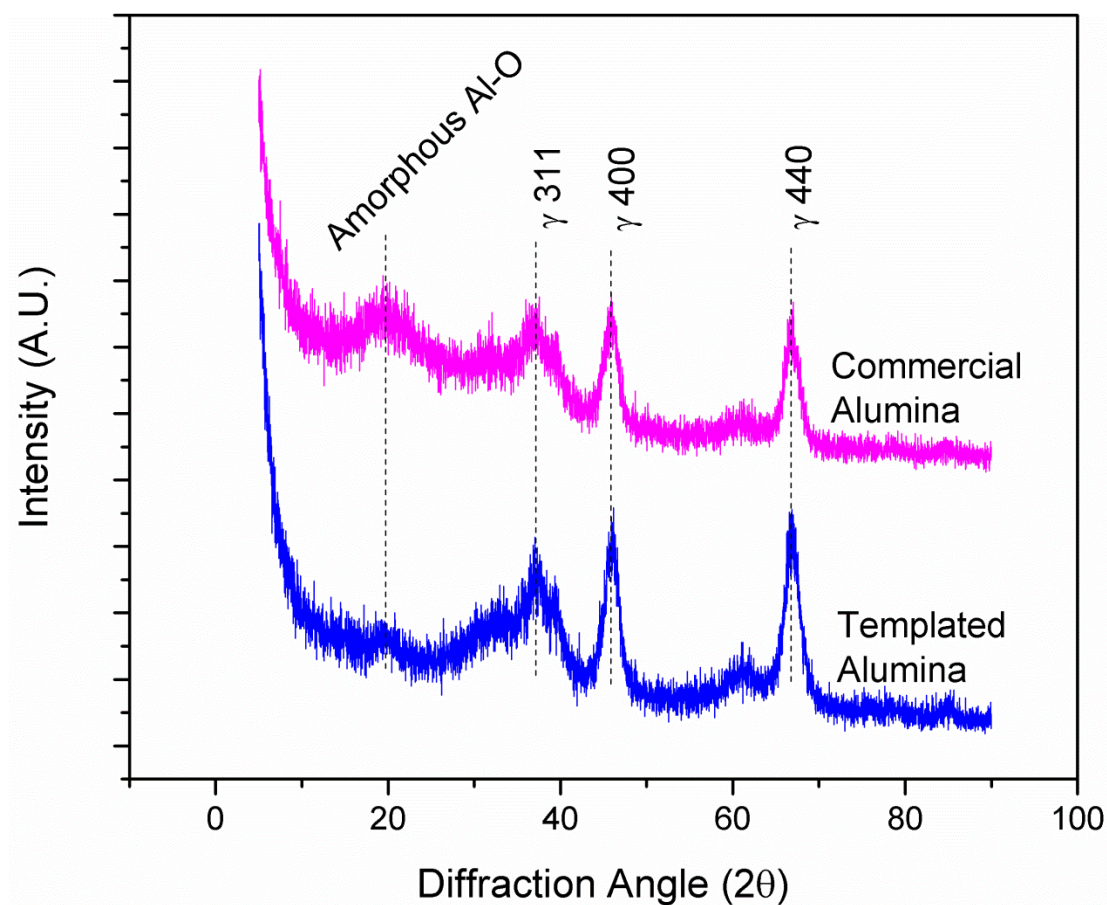


Figure C.6 XRD patterns of alumina supports

## C.7 Properties of Alumina/PEI/PEG200 Adsorbents

Table C.2 Physical and textural properties of alumina supports co-impregnated with PEI and PEG200 at varying PEG loadings

| Additive | Organic / Silica Ratio[a] | Carbon / Nitrogen[b] | Additive / PEI[c] | BET Surface Area[d] | Pore Volume[d] | Amine content[b] | $CO_2$ capacity[e] |
|---|---|---|---|---|---|---|---|
| | (g Org/g $SiO_2$) | (mol C/ mol N) | g / g | $m^2$ / g $SiO_2$ | $cm^3$ / g $SiO_2$ | mmol N / g sorbent | mmol $CO_2$ / g sorbent |
| *Templated Alumina* | | | | | | | |
| Bare Support | - | - | - | 231 | 1.06 | - | - |
| PEI (none) | 0.43 | 2.00 | 0.00 | 162 | 0.74 | 6.86 | 1.16 |
| PEG200 | 0.53 | 2.15 | 0.07 | 113 | 0.56 | 6.19 | 1.07 |
| PEG200 | 0.73 | 2.80 | 0.40 | 81 | 0.41 | 5.98 | 1.29 |
| PEG200 | 0.80 | 3.35 | 0.67 | 82 | 0.48 | 5.34 | 1.17 |
| PEG200 | 0.96 | 3.60 | 0.80 | 71 | 0.41 | 5.26 | 1.12 |
| PEG200 | 1.54 | 5.65 | 1.82 | 0 | 0.00 | 4.26 | 0.88 |
| *Commercial Alumina* | | | | | | | |
| Bare Support | - | - | - | 201 | 0.45 | - | - |
| PEI (none) | 0.43 | 2.00 | 0.00 | 15 | 0.05 | 6.08 | 0.71 |
| PEG200 | 0.53 | 2.15 | 0.07 | 0 | 0.02 | 5.54 | 0.76 |
| PEG200 | 0.73 | 2.80 | 0.40 | 1 | 0.04 | 5.94 | 0.89 |
| PEG200 | 0.80 | 3.35 | 0.67 | 2 | 0.07 | 5.57 | 0.90 |
| PEG200 | 0.96 | 3.60 | 0.80 | 1 | 0.05 | 5.39 | 0.98 |
| PEG200 | 0.70 | 3.77 | 0.88 | 0 | 0.00 | 5.07 | 1.06 |

## C.8 References

(1)     Satyapal, S.; Filburn, T.; Trela, J.; Strange, J. Performance and Properties of a Solid Amine Sorbent for Carbon Dioxide Removal in Space Life Support Applications. *Energy & Fuels* **2001**, *15* (2), 250–255.

(2)     Xu, X.; Song, C.; Andrésen, J. M.; Miller, B. G.; Scaroni, A. W. Preparation and Characterization of Novel CO2 "molecular Basket" Adsorbents Based on Polymer-Modified Mesoporous Molecular Sieve MCM-41. *Microporous Mesoporous Mater.* **2003**, *62* (1-2), 29–45.

(3)     Wang, X.; Song, C. New Strategy To Enhance CO 2 Capture over a Nanoporous Polyethylenimine Sorbent. *Energy & Fuels* **2014**, *28*, 7742–7745.

(4)     Arenillas, a.; Smith, K. M.; Drage, T. C.; Snape, C. E. CO2 Capture Using Some Fly Ash-Derived Carbon Materials. *Fuel* **2005**, *84* (17), 2204–2210.

(5)     Goeppert, A.; Meth, S.; Prakash, G. K. S.; Olah, G. a. Nanostructured Silica as a Support for Regenerable High-Capacity Organoamine-Based CO2 Sorbents. *Energy Environ. Sci.* **2010**, *3* (12), 1949–1960.

(6)     Meth, S.; Goeppert, A.; Prakash, G. K. S.; Olah, G. A. Silica Nanoparticles as Supports for Regenerable CO 2 Sorbents. *Energy & Fuels* **2012**, *26*, 3082–1090.

(7)     Wang, J.; Long, D.; Zhou, H.; Chen, Q.; Liu, X.; Ling, L. Surfactant Promoted Solid Amine Sorbents for CO2 Capture. *Energy Environ. Sci.* **2012**, *5* (2), 5742–5749.

(8)     Wang, J.; Wang, M.; Zhao, B.; Qiao, W.; Long, D.; Ling, L. Mesoporous Carbon-Supported Solid Amine Sorbents for Low- Temperature Carbon Dioxide Capture. *Ind. Eng. Chem. Res.* **2013**, *52*, 5437–5444.

(9)    Tanthana, J.; Chuang, S. S. C. In Situ Infrared Study of the Role of PEG in Stabilizing Silica-Supported Amines for CO(2) Capture. *ChemSusChem* **2010**, *3* (8), 957–964.

(10)   Srikanth, C. S.; Chuang, S. S. C. Spectroscopic Investigation into Oxidative Degradation of Silica-Supported Amine Sorbents for CO(2) Capture. *ChemSusChem* **2012**, *5* (8), 1435–1442.

(11)   Srikanth, C. S.; Chuang, S. S. C. Infrared Study of Strongly and Weakly Adsorbed CO 2 on Fresh and Oxidatively Degraded Amine Sorbents. *J. Phys. Chem. C* **2013**, *117*, 9196–9205.

(12)   Heydari-Gorji, A.; Sayari, A. CO2 Capture on Polyethylenimine-Impregnated Hydrophobic Mesoporous Silica: Experimental and Kinetic Modeling. *Chem. Eng. J.* **2011**, *173* (1), 72–79.

(13)   Heydari-Gorji, A.; Belmabkhout, Y.; Sayari, A. Polyethylenimine-Impregnated Mesoporous Silica : Effect of Amine Loading and Surface Alkyl Chains on CO 2 Adsorption. *Langmuir* **2011**, *27*, 12411–12416.

(14)   Yue, M. B.; Chun, Y.; Cao, Y.; Dong, X.; Zhu, J. H. CO2 Capture by As-Prepared SBA-15 with an Occluded Organic Template. *Adv. Funct. Mater.* **2006**, *16* (13), 1717–1722.

(15)  Fauth, D. J.; Gray, M. L.; Pennline, H. W.; Krutka, H. M.; Sjostrom, S.; Ault, A. M. Investigation of Porous Silica Supported Mixed-Amine Sorbents for Post-Combustion CO2 Capture. *Energy & Fuels* **2012**, *26*, 2483–2496.

(16)  Sanz, R.; Calleja, G.; Arencibia, A.; Sanz-Pérez, E. S. CO 2 Uptake and Adsorption Kinetics of Pore-Expanded SBA-15 Double-Functionalized with Amino Groups Rau L. *Energy & Fuels* **2013**, *27*, 7637–7644.

(17)  Liu, J.; Cheng, D.; Liu, Y.; Wu, Z. Adsorptive Removal of Carbon Dioxide Using Polyethyleneimine Supported on Propanesulfonic-Acid-Functionalized Mesoporous. *Energy & Fuels* **2013**, *27*, 5416–5422.

(18)  Sanz, R.; Calleja, G.; Arencibia, A.; Sanz-Pérez, E. S. Development of High Efficiency Adsorbents for CO2 Capture Based on a Double-Functionalization Method of Grafting and Impregnation. *J. Mater. Chem. A* **2013**, *1* (6), 1956–1962.

(19)  Davison, W. H. T. Davisofi : Infyared Spectra An.d Crystallinity. Part III. Infrared Spectra and Crystallinity. Part III. * Poly( Ethylene Glycol). *J. Chem. Soc.* **1955**, No. 2431, 3270–3274.

(20)  Papke, B. L.; Ratner, M. A.; Shriver, D. F. Vibrational Spectroscopy and Structure of Polymer Electrolytes, Poly(ethylene Oxide) Complexes of Alkali Metal Salts. *J. Phys. Chem. Solids* **1981**, *42*, 493–500.

(21)    Kang-Jen, L.; Parsons, J. L. Solvent Effects on the Preferred Conformation of Poly
(ethylene Glycols). *Macromolecules* **1969**, *2* (5), 529–533.

# APPENDIX D

## SUPPLEMENT TO CHAPTER 5

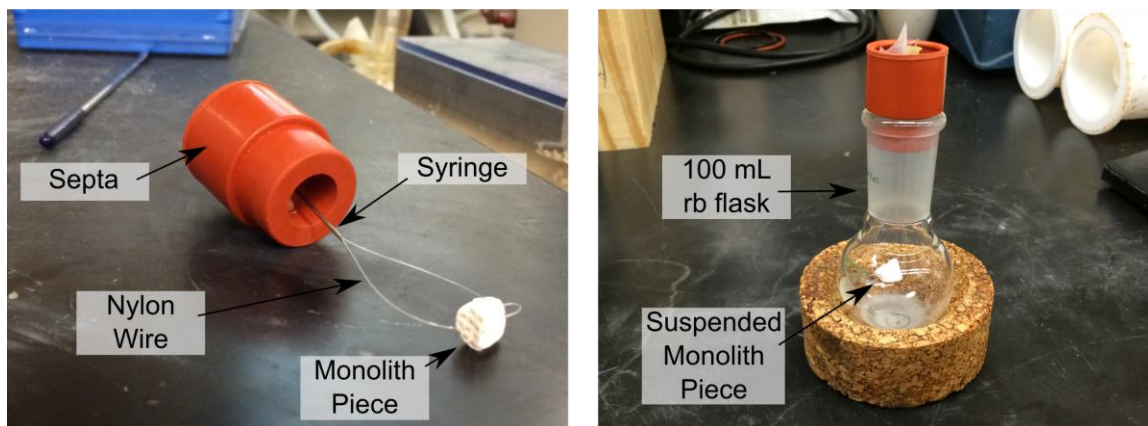### D.1   Picture of Monolith Dipping Setup



Figure D.1 Picture of typical monolith dipping setup
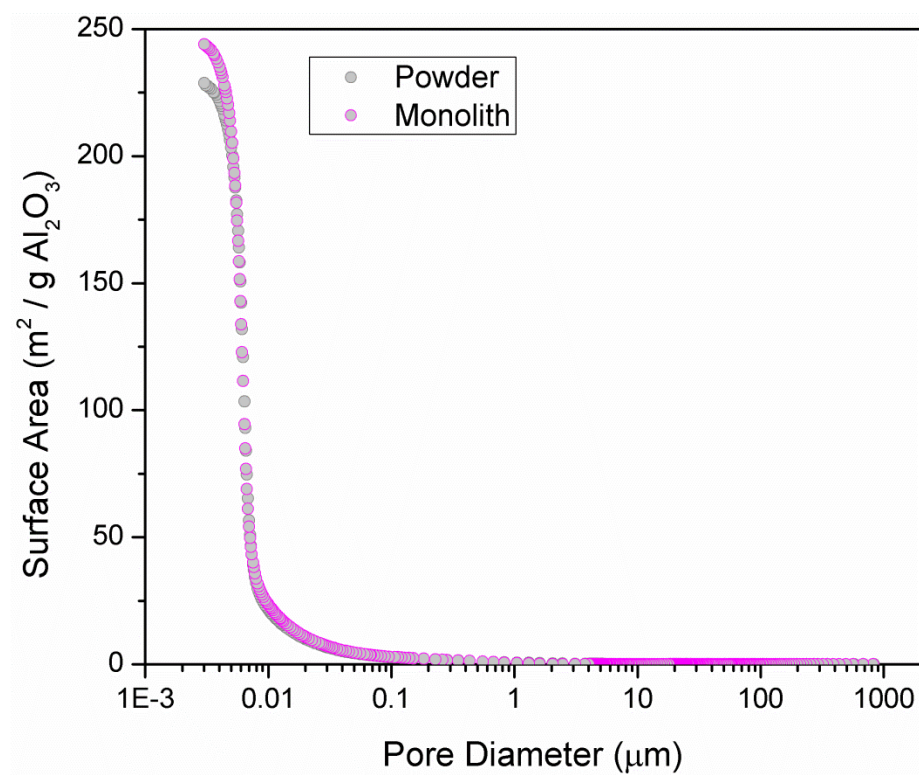
## D.2   Additional Porosity Analysis



Figure D.2. Cumulative surface area as a function of pore diameter measured from mercury porosimetry.
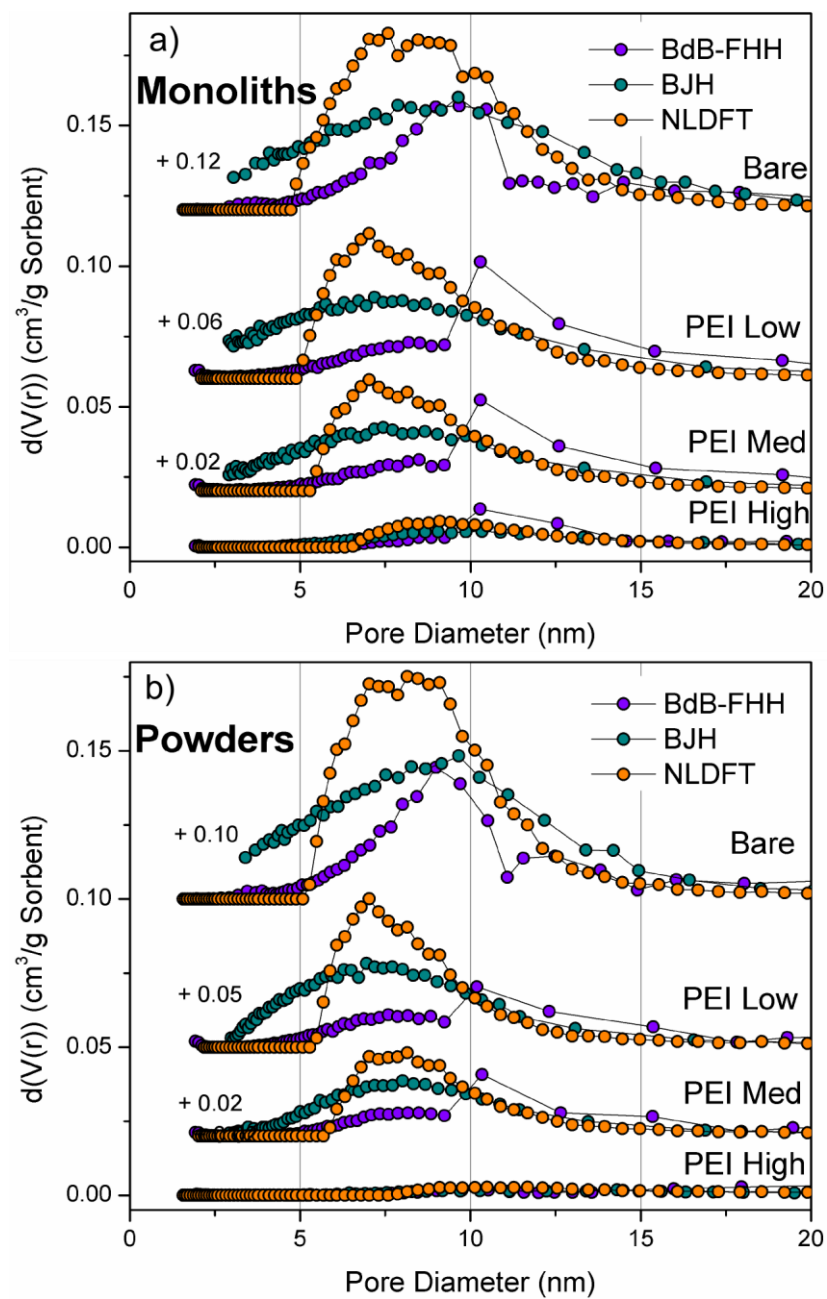
Figure D.3 Pore size distributions for monoliths (a) and powders (b) derived using $N_2$ physisorption data and either the BdB-FHH (purple), BJH (green) or NLDFT (orange) models.

### D.3  Properties of Monolith Sorbents with Similar Compositions

Table D.1 Properties of monolith sorbents prepared with similar composition but different preparation time and textural properties. Each sample prepared using 'capillary' method.

| Immersion time | Amine content | Remaining PV | Deviation in PV | $CO_2$ capacity | Amine efficiency |
|---|---|---|---|---|---|
| | g PEI / g $Al_2O_3$ | $cm^3$ / g $Al_2O_3$ | % | mmol / g | mol $CO_2$ / mol N |
| 1h | 0.50 | 0.07 | 27 | 0.63 | 0.09 |
| 1h | 0.44 | 0.10 | 28 | 0.75 | 0.11 |
| 6h | 0.43 | 0.13 | 31 | 0.54 | 0.08 |
| 6h | 0.49 | 0.10 | 33 | 0.71 | 0.10 |

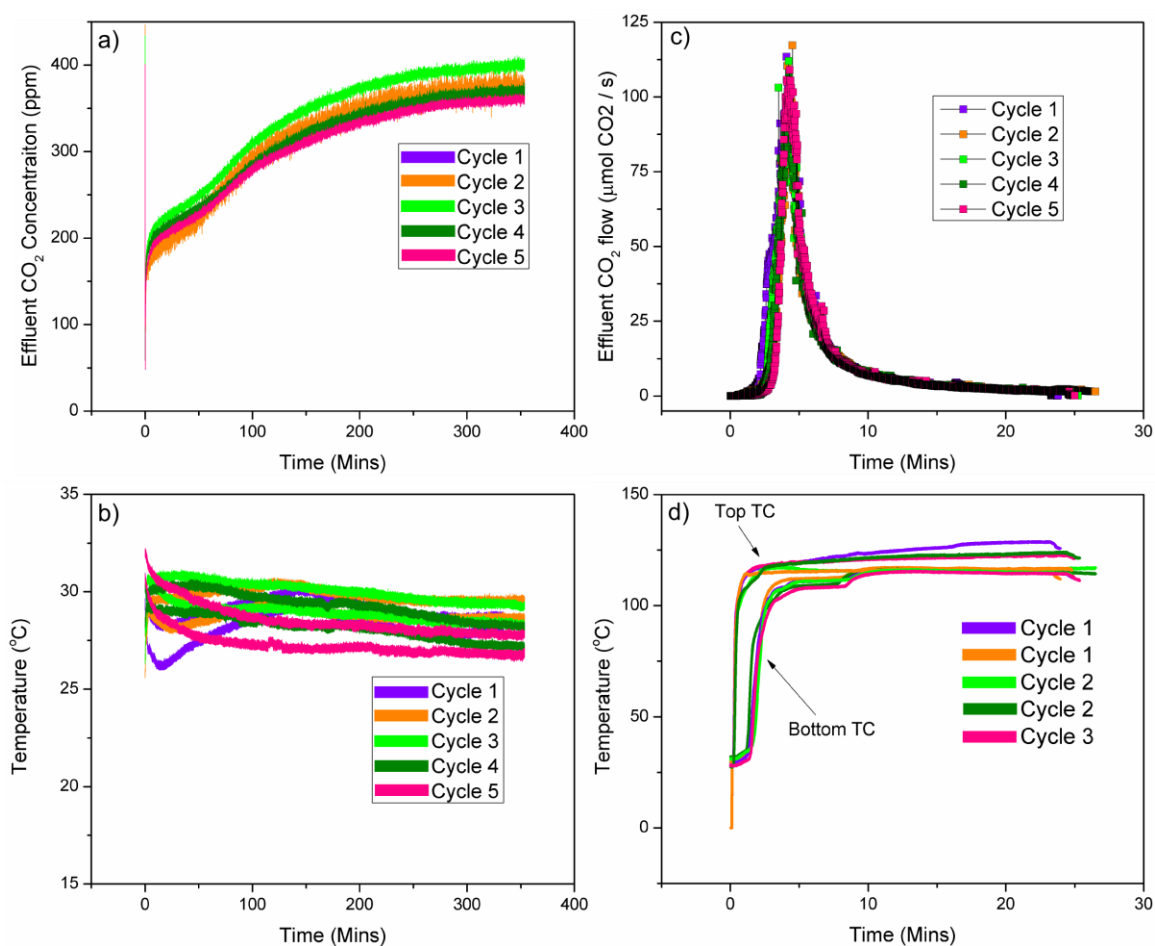## D.4  Transient Data Collected from Flow Adsorption Experiment



Figure D.4 Data collected from flow adsorption experiments on monolithic sorbent. Adsorption cycle step $CO_2$ (a) and temperature (b) profiles and steam desorption step effluent $CO_2$ (c) and temperature (d) profiles.